The Measurement of the Photoionization Cross Sections of the Atomic Gases

JAMES A. R. SAMSON

Space Sciences Laboratory, GCA Corporation, Bedford, Massachusetts

I. Introduction

The interaction of radiation of wavelengths shorter than 1000 Å with a gas will in general produce ionization in the gas. The cross sections for the ionizing process are important parameters in many fields of science. For example, they are used in determining the photoionization rates produced in the ionosphere owing to the interaction of the extreme ultraviolet radiation from the sun with the earth's atmosphere. The various layers of the ionosphere are partially produced by different regions of the extreme ultraviolet extending down to the X-ray region. Other examples can be found in gaseous discharges including thermonuclear devices. Here radiation created by the discharge can be reabsorbed by the neutral and ionized atoms. Any serious investigation of such devices must include knowledge of the photoionization cross sections of the gases involved. An important practical application of the knowledge of photoionization cross sections of the rare gases is found in the rare gas ionization chambers. These ion chambers are used as absolute standards in determining the intensity of radiation below 1000 Å and for the absolute calibration of thermopiles (Samson, 1964a). For accurate intensity measurements it is necessary to make measurements in spectral regions free from discrete structure and preferably in regions where the photoionization cross sections are not varying too rapidly. Until recently the position and even the existence of discrete structure within the ionization continuum of the rare gases was unknown (Samson, 1963; Madden and Codling, 1963).

In the theoretical field experimental data are required to check the validity of the various models for the photoionization process. This is extremely important since in many cases experimental data are unavailable and one must rely on theoretical values.

The absorption of radiation by a gas is defined by the Lambert–Beer Law which is given by

$$I = I_0 \exp(-\sigma_t n L), \tag{1}$$

where I_0 is the intensity of the incident radiation, I the intensity after passing through a layer of gas of thickness L, σ_t is the total absorption cross section, and n is the number of atoms/cc. The number of atoms/cc measured at a pressure p and temperature T is given by

$$n = n_0\left(\frac{pT_0}{p_0T}\right), \tag{2}$$

where n_0 is Loschmidt's number equal to 2.69×10^{19} atoms/cc, while p_0 and T_0 are, respectively, the pressure and temperature at STP.

The total absorption cross section is given by $\sigma_t = \sigma_s + \sigma_a$, where σ_s and σ_a are the scattering and true absorption cross sections, respectively. The scattering of radiation in the vacuum ultraviolet region below 1000 Å is extremely small compared to the true absorption of the radiation and so far has not been detected. Unless explicitly stated the scattering cross section will be assumed to be zero with $\sigma_t = \sigma_a = \sigma$. Some theoretical scattering cross sections are tabulated for the rare gases and atomic oxygen for wavelengths below 10 Å.

The total absorption coefficient k is given by

$$k = n_0\sigma. \tag{3}$$

The photoionization cross section σ_i is defined as

$$\sigma_i = \gamma\sigma, \tag{4}$$

where γ is the photoionization yield, or efficiency, and is defined as the number of ions produced per photon absorbed. For atoms the yield is generally considered to be unity at wavelengths shorter than the ionization threshold with the reservation that discrete structure may or may not have yields of unity. Watanabe (1964) has measured the yield of Xe using a thermopile and found it to be unity from threshold to 900 Å. Other experimental evidence showing that the yields of the rare gases are unity has been given by Samson (1964a).

The units of absorption are sometimes expressed in terms of the absorption coefficient k measured in cm^{-1}, and sometimes in terms of the absorption cross section σ measured in cm^2 or in megabarns (Mb), where 1 Mb = 10^{-18} cm^2.

The ionization onset potential of an atom is variously referred to as "threshold," "spectral head," or "series limit." All four expressions are used throughout this review.

The photoionization cross sections of the rare gases have been measured from threshold to 80 Å from the long wavelength side (optical radiation), and from 0.01 to 50 Å from the short wavelength side (X-radiation). Although detailed gaps still exist, essentially a complete picture of the continuum absorption of these gases has emerged. This is not the case for any other atom. The alkali metals have been studied only from threshold to 1100 Å, however, work is in progress to extend these measurements down to 500 Å (Hudson, 1965). Calcium, indium, magnesium, and thallium have been studied from threshold to 1600 Å.

At present, work is underway to measure the cross sections of atomic oxygen, nitrogen, and hydrogen. The problem of dissociating the parent molecules to produce these atoms and measuring the atom concentrations adds to the difficulties already involved in cross section measurements. Thus direct

measurements have been limited in their spectral range. An approximate measure of the atomic cross section can be obtained in the soft X-ray region by considering a molecule to be equivalent to two atoms. Cross sections have been inferred from molecular cross section data measured from 0.01 to 68 Å and from 200 to 500 Å.

The experimental cross sections are discussed in Section II–V; the subdivision of the discussion being dictated in part by the various methods used in the cross section measurements.

In the case of the rare gases discrete structure is discussed due to excitation of inner shell electrons and their energy levels predicted where they have not yet been observed. A table of critical absorption energies has been compiled from the literature since no such table exists. Finally, a discussion of the oscillator strengths for transitions to the photoionization continuum is given for each of the rare gases.

II. The Rare Gases

A. Experimental Procedure

Absorption coefficients were measured by the double ion chamber technique. Figure 1 shows the ion chamber in detail. A complete discussion of this ion chamber has been given by Samson (1964a). Briefly, however, the essentials are that the two collector plates must be identical in length, and the slits must be held at a positive potential to drive all ions formed in the vicinity of the slit over to plate i_1. A guard ring at the end of the ion chamber provides a uniform field at the end of the second plate. Thus, all ions formed are collected by their respective collector plates. The absorption coefficient k is then given by

$$k = (1/x) \ln(i_1/i_2),$$

where x is the length of one collector plate reduced to STP, i.e., $x = L(p/760)(273/T)$ where L is the actual pathlength in centimeters, p is the pressure in millimeters, and T the temperature in degrees Kelvin.

Two major advantages of this technique are: (*a*) that the ion currents i_1 and i_2 are measured simultaneously and thus there is no demand that the light source intensity remains constant, and (*b*) since the gas itself is the detector of the incident radiation it is insensitive to scattered radiation of wavelengths longer than its ionization threshold. Some precautions, however, do have to be considered. For instance there is a danger of collecting electrons as well as ions. This occurs when the incident radiation can eject a photoelectron of sufficient energy to overcome the retarding potential of the collector plates. Thus sufficient voltage between the plates must be used to retard the

most energetic electrons likely to be encountered. Secondary ionization by these energetic electrons also occurs and at first may appear to be a source of error. However, it can be shown (Townsend, 1903) that the total ion current is proportional to $i_0 e^{\alpha d}$, where i_0 is the ion current when these secondary effects are absent, α, the first Townsend coefficient, is the number of ions created per centimeter/electron, and d is the separation between the repeller

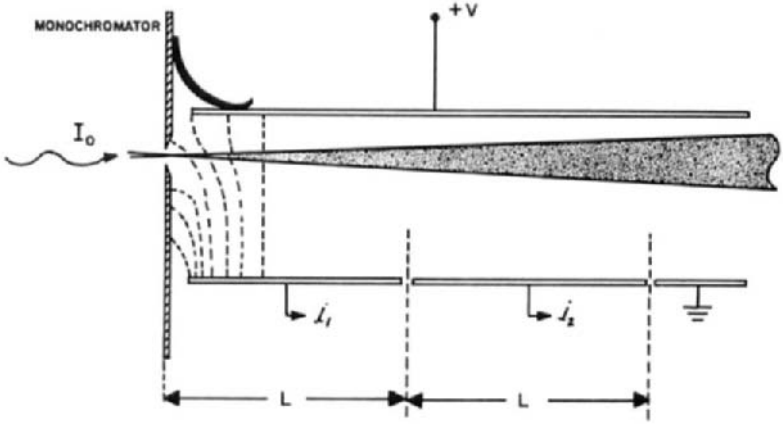

FIG. 1. Double ion chamber absorption cell. The exit slit of the monochromator is held at the same potential as the repeller plate while a grounded guard plate at the end of the ion chamber provides a uniform field at the end of the second collector plate. Thus, all the ions formed under a given plate will be collected by that plate.

plate and the ion plates. Thus, $e^{\alpha d}$ is a constant for any given gas, pressure, and wavelength. The ratio of the two currents i_1/i_2 should therefore remain constant, and indeed this is found to be the case over quite a considerable voltage range. Figure 2 shows a typical curve of ion current vs voltage. The insert shows that i_1/i_2 varies little, not only in the region where secondary ionization takes place but also in the region where electrons are being collected.

The vertical arrows *a*, *b*, and *c* represent, respectively, the ion chamber voltage necessary to start the retardation of the electrons, the voltage necessary to complete retardation, and the minimum voltage at which secondary ionization by electron collision is possible. In all runs, however, measurements were made within the plateau region of the ion current vs voltage curve, or as near to it as was possible.

The ion chamber was mounted on the exit arm of a Seya-monochromator, which was equipped with two interchangeable gratings. The gratings were both Bausch and Lomb replicas platinized to enhance their reflectivity at short wavelengths. The first-order spectrum was increased by a factor of five compared to the unplatinized condition. Wavelength separations of 2.6

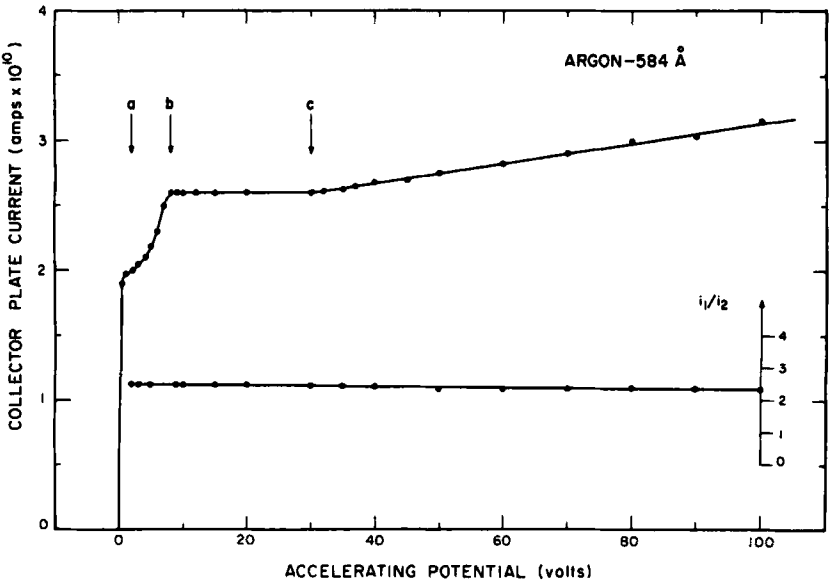

FIG. 2. Typical ion current vs voltage curve. Argon was ionized by 584-Å radiation, thereby releasing electrons with approximately 5-eV energy. For the particular dimensions of the cell used the vertical arrows *a*, *b*, and *c* represent, respectively, the voltages at which retardation of the electrons start, finish, and at which the onset of secondary ionization occurs. The insert shows the variation of the ratio i_1/i_2 with voltage. There is a maximum variation of about 4% over the entire voltage range.

and 1.3 Å were achieved with the 600- and 1200-line/mm gratings, respectively. The exit slit of the monochromator was 37 μ wide by 7 mm high. This small opening was used not only to provide maximum resolution but to reduce the flow rate of the gas within the ion chamber allowing accurate pressure measurements to be made. Figure 3 illustrates the complete experimental arrangement.

The light source consisted of a high-voltage condensed spark discharge through a ceramic capillary. This produced a line spectrum characteristic of the gas used, which in this case was argon at approximately 0.1 Torr. The light source was separated from the monochromator by a two-stage differential pumping unit. The first stage was evacuated by a 15 ft^3/min Welch mechanical pump, while in the second stage a 4-in. diffusion pump was used. The main monochromator was also evacuated by a 4-in. diffusion pump. With this arrangement a negligible amount of the light source gas found its way into the ion chamber.

The all-metal ion chamber had its own 2-in. diffusion pump which evacuated the chamber down to 1×10^{-5} Torr. After thorough pumping the 2-in.

system was valved off. The ion chamber was then pumped on by the main monochromator pumps via the exit slit. An equilibrium pressure of 1×10^{-4} Torr was then obtained. The gas under investigation was passed through a leak valve, then through a cold trap, and finally into the rear of the ion chamber. The minimum pressure of the gas in all experiments was about 0.1 Torr. Thus, even if we assume that the dynamical flow of gas did *not* remove any of the residual impurities, we still have a purity ratio of 1000:1 at the minimum pressure.

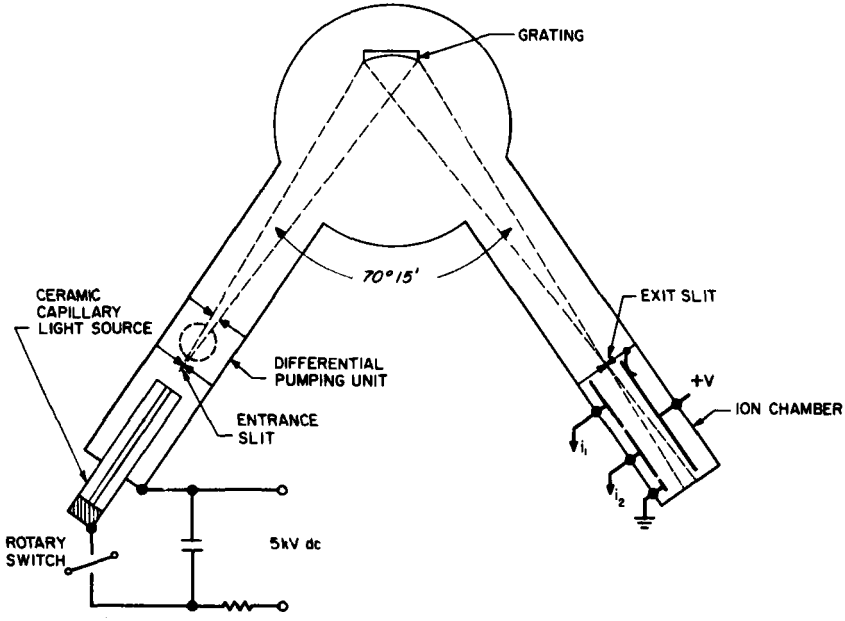

FIG. 3. 1/2M Seya-monochromator showing the experimental arrangement of light source, vacuum monochromator, and absorption cell.

Research grade gas from the Matheson Company was used in the case of Ne, Kr, and Xe. Argon and helium were also obtained from the Matheson Company, with a quoted purity of 99.9%. Neon and helium were further purified by passing them through a liquid nitrogen–cooled charcoal trap. The remaining gases were all passed through dry ice traps.

The two micromicroammeters used to measure i_1 and i_2 were calibrated to an accuracy of 1%. This was achieved by making a high impedance current source using a standard cell and Victoreen high-megohm resistors quoted to be accurate to within 1%. The micromicroammeters were used to drive two Leeds and Northrop recorders, each of which had an accuracy of $\frac{1}{4}$% for full-scale deflection.

Only radiation below the ionization threshold could contribute to the detectable scattered radiation. This scattered radiation was troublesome only below 400 Å since in this region the line spectrum was much less intense than at the longer wavelengths. Correction for the scattered radiation was performed as follows: A measure of the scattered light was made between 50–150 Å and was found to be constant. Since the monochromator produced no spectrum in this region the signal must be due entirely to scattered light. The constancy of the scattered light was assumed to hold up to 400 Å. This constant signal was then subtracted from the measured ion currents.

The ratio of the ion currents could be measured with considerable precision. The main source of error left was in measuring the absolute pressure of the gas. This error was estimated to be 3% maximum. Although the gas flow was dynamic, no serious pressure gradients existed in the ion chamber. Measurements of k with different techniques yielded values within a few percent of each other. A McLeod gauge was used in all pressure measurements to eliminate accumulative errors due to the calibration of secondary pressure sensitive devices. However, a thermocouple pressure gauge was used to insure that the pressure of the gas remained constant during a run.

The absolute values of the absorption coefficients thus determined were estimated to have an error spread of $\pm 5\%$ except where discrete structure existed and also for the weakest lines where the error was somewhat more. The error in the spectral shape of the absorption curves was dependent only on the error in the logarithm of i_1/i_2. Since the ratio of i_1/i_2 was always adjusted to be greater than 2, the error in i_1/i_2 was not magnified by taking the logarithm of the ratio. The error was estimated to be within $\pm 3\%$.

B. Helium

The photoionization cross sections of helium were first calculated by Vinti (1933) and Wheeler (1933) using a hydrogenic approximation. In this approximation the inner electron is regarded as moving in a field of charge two while the outer electron, excited into the continuum, is assumed to be in a field of charge one. Later, calculations were performed by many investigators (Köwien, 1934; Huang, 1948; Dalgarno and Lynn, 1957; Dalgarno and Stewart, 1960; Salpeter and Zaidi, 1962; Stewart and Wilkinson, 1960; Stewart and Webb, 1963; Cooper, 1962). These calculations included the use of the more sophisticated Hartree and Hartree–Fock wavefunctions.

Available experimental cross sections (Lee and Weissler, 1955; Axelrod and Givens, 1959; Baker *et al.*, 1961) agreed with the theoretical values within their experimental errors; however, it was not possible to say which theoretical approach was the most satisfactory. The present work (Samson, 1964b) has endeavored to reduce the scatter in the experimental points and to

improve the over-all accuracy of the cross section measurements to enable a choice between the various calculations to be made.

All previous experimental cross section measurements have been made using the photographic plate as a detector of radiation, and all depended on the incident radiation intensity remaining constant during the exposures taken with the absorption cell empty and then filled with helium. The difficulties and errors inherent in the above method were removed by using two ionization chambers in series as discussed in the last section. This is the first time this method has been applied to helium. The cross sections shown in Fig. 4 represent the average of four different determinations with the gas pressure varying from 0.5 to 1.0 Torr. The scatter of points lies within $\pm 2.5\%$ of the average curve.

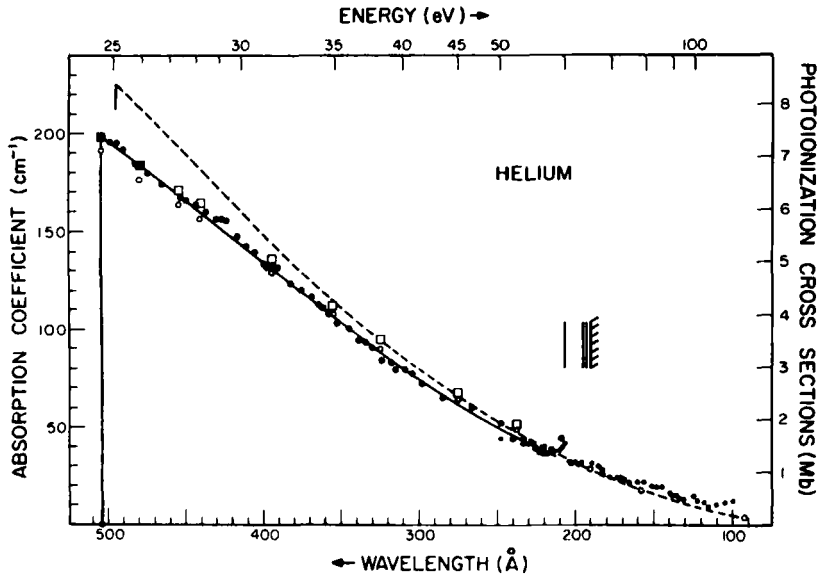

FIG. 4. Photoionization cross sections of helium compared to theoretical values. Stewart and Webb: □ dipole length, O dipole velocity; Cooper, - - - -; Lowry *et al.*, •; present data, ●.

The vertical lines in Fig. 4 represent the positions of absorption lines discovered by Madden and Codling (1963, 1965a) using the continuum radiation from a 180-MeV synchrotron. They account for the series as being due to a double-electron excitation process of the type $1s^2 - 2s,np$ and $1s^2 - 2p,ns$. The first member of the series, appearing at 260.21 Å, is common to the two series and represents the transition $1s^2\ ^1S_0 - 2s,\ 2p\ ^1P^0$. The second series was observed to be extremely weak.

The data are compared with the theoretical calculations of Cooper (1962), who used a one electron model, and with that of Stewart and Webb (1963), using the Hartree–Fock wavefunction. The experimental points of Lowry *et al.* (1965) are included to extend the range of comparison down to 100 Å. The recent work of Stewart and Webb is felt to be the most sophisticated calculation of the helium cross sections available. They have computed the cross sections using the Coulomb, Hartree, and Hartree–Fock approximations, and for each approximation they quote values using the dipole length, velocity, and acceleration formulations. We have selected the values obtained by the Hartree–Fock approximation as the ones which best fit our experimental data. It can be seen that the dipole length formulation is the best fit at the spectral head, but at the shorter wavelengths the velocity formulation appears superior. This is in agreement with the conclusion reached by Stewart and Webb.

It should be mentioned that the selected cross section values of Dalgarno and Stewart (1960) are very close to those calculated by Stewart and Webb. The selected values were obtained from the data of Stewart and Wilkinson (1960) for energies up to 1 Ry (1 Ry = 13.6 eV) and Huang's (1948) acceleration values for energies greater than 1 Ry; these values were then adjusted to provide good agreement with the various sum rules involving the oscillator strengths.

The experimental oscillator strength f for excitation into the continuum was obtained by using the relation

$$f = \frac{mc^2}{e^2 \pi n_0} \int k(\nu)\, d\nu,$$

where k is the absorption coefficient and ν is the wave number, both expressed in cm^{-1}, and m, e, and c have their usual meaning. n_0 is Loschmidt's number. The numerical value of $(mc^2)/(e^2\pi n_0)$ is 4.19×10^{-8}.

The integral was evaluated graphically from the ionization threshold to 0.01 Å using the k values tabulated in Tables I–III. A value of $f = 1.54$ was obtained. Since the contribution between 0.01 and 4.0 Å amounts to only 0.0001, the contribution below 0.01 is assumed to be negligible. The Thomas–Kuhn sum rule requires that the total oscillator strength be equal to the number of electrons in the atom, that is two for helium. Thus, the contribution to the oscillator strength due to discrete structure must be equal to 0.46. Theoretical values for the discrete transitions have been calculated by several investigators (Vinti, 1932, 1933; Wheeler, 1933; Köwien, 1934; Huang, 1948; Dalgarno and Lynn, 1957; Dalgarno and Stewart, 1960; Salpeter and Zaidi, 1962; Hylleraas, 1937; Trefftz *et al.*, 1957). A value of 0.45 was obtained by both Dalgarno and Stewart (1960) and by Salpeter and Zaidi (1962). The

calculations included the f values for the doubly excited transitions as well as those for the resonance series. Since Dalgarno and Stewart quote f values only for $n = 2$ to 6, the remainder of the sum for $n = 7$ to∞ was obtained from the earlier paper (Dalgarno and Lynn, 1957).

TABLE I

HELIUM ABSORPTION COEFFICIENTS FROM 0.01 TO 44.6 Å

Shell	λ (Å)	Experimental,[a] k (cm^{-1})	Semiempirical, k (cm^{-1})
K	0.010	—	0.0102×10^{-3} [b]
	0.015	—	0.0124×10^{-3} [b]
	0.020	—	0.0141×10^{-3} [b]
	0.030	—	0.0167×10^{-3} [b]
	0.04	—	0.0187×10^{-3} [b]
	0.05	—	0.0202×10^{-3} [b]
	0.10	—	0.0250×10^{-3} [b]
	0.15	—	0.0276×10^{-3} [b]
	0.20	—	0.0293×10^{-3} [b]
	0.50	—	0.0338×10^{-3} [b]
	0.80	—	0.0386×10^{-3} [b]
	1.00	0.045×10^{-3}	0.0433×10^{-3} [b]
	3.57	0.463×10^{-3}	—
	4.36	0.819×10^{-3}	—
	5.17	1.34×10^{-3}	—
	6.97	3.20×10^{-3}	—
	8.32	5.87×10^{-3}	5.34×10^{-3} [c]
	9.87	9.97×10^{-3}	—
	13.37	22.43×10^{-3}	21.36×10^{-3} [c]
	17.67	50.91×10^{-3}	48.95×10^{-3} [c]
	21.7	—	89.00×10^{-3} [c]
	23.7	—	117.48×10^{-3} [c]
	27.4	—	178.00×10^{-3} [c]
	31.6	—	279.46×10^{-3} [c]
	36.3	—	409.40×10^{-3} [c]
	44.6	640.8	765.40×10^{-3} [c]

[a] Determined from the mass absorption coefficients compiled by Allen (1935).
[b] Victoreen (1949).
[c] Henke (1957).

Discrete transitions for large n have f values given, approximately, by $f = C/n^3$ (Hargreaves, 1928–1929), where n is the principal quantum number and C is given by twice the value of $df/d\varepsilon$ evaluated at the series limit ($k = 217$

$df/d\varepsilon$ cm^{-1}), ε being the kinetic energy of the released photoelectron measured in rydbergs. Using the present experimental data we find $C = 1.83$. Table IV compares the results of Dalgarno and Stewart with the values obtained from the above relation. As n increases we find the two results in good agreement.

TABLE II

HELIUM ABSORPTION COEFFICIENTS FROM 100 TO 247 Å[a]

Shell	λ (Å)	k (cm^{-1})	λ (Å)	k (cm^{-1})	λ (Å)	k (cm^{-1})
K	100.90	12.9	144.82	19.6	198.03	31.9
	104.81	11.6	147.27	19.0	200.68	32.1
	107.00	9.8	151.51	19.0	202.32	32.9
	110.48	9.8	153.94	22.6	203.86	32.7
	115.82	9.6	156.18	22.1	207.24	41.9
	116.38	9.9	159.36	22.5	207.79	40.2
	117.85	11.0	160.10	21.9	209.28	38.1
	118.97	11.2	162.47	22.3	213.09	37.8
	122.25	12.2	164.60	23.5	214.25	38.3
	124.58	12.8	166.17	22.3	215.20	39.4
	125.23	14.9	168.08	23.8	216.02	38.3
	126.06	13.4	170.21	24.0	220.35	40.5
	128.26	13.4	171.09	24.4	221.65	36.5
	129.83	13.3	173.01	24.7	222.77	35.4
	131.80	13.9	177.75	25.6	223.78	36.5
	132.28	14.2	181.21	26.0	225.20	38.6
	132.84	14.2	182.40	28.4	227.53	42.1
	133.35	14.4	184.04	31.6	231.20	42.7
	135.52	15.1	185.74	30.2	233.52	42.1
	138.07	15.4	188.44	32.1	246.20	44.8
	139.02	16.0	192.82	29.2	247.60	44.8
	140.07	17.4	195.95	32.7		

[a] Lowry *et al.* (1965)

An experimental determination of the oscillator strength of the 584-Å resonance line has been made by Lincke and Griem (1965). They obtained a value of 0.26 ± 0.08 in agreement with theory.

C. NEON

As in helium, the photoionization cross sections of neon were treated theoretically many years before the first experimental results were available. The early calculations by Bates (1939) gave the value of the photoionization cross section of neon at its spectral head as 5.8 Mb (1 Mb = 10^{-18} cm^2). Subsequent

TABLE III

HELIUM ABSORPTION COEFFICIENTS FROM 209 Å TO THRESHOLD[a]

Shell	λ (Å)	k (cm^{-1})	λ (Å)	k (cm^{-1})
K	209.3	45	390.6	132
	225.8	39	394.0	133
	234.8	44	397.1	133
	240.0	45	400.3	134
	247.2	53	405.7	140
	266.3	61	410.6	143
	283.6	66	416.6	148
	297.9	73	423.3	156
	303.1	78	425.5	157
	308.4	80	429.7	157
	315.0	79	436.5	160
	317.7	84	442.8	163
	323.2	85	448.8	166
	329.3	91	452.0	167
	335.4	94	464.4	174
	338.1	95	473.6	180
	345.0	101	478.0	184
	352.2	103	482.0	185
	357.5	108	489.3	191
	362.9	112	494.3	195
	364.0	113	498.4	196
	368.4	117	503.0	198
	375.7	120	504.26	Threshold
	382.1	124		

[a] Present data.

TABLE IV

HELIUM f VALUES FOR THE TRANSITION 1^1S–n^1P AS OBTAINED FROM THE RELATION $f = C/n^3$

n	Dalgarno and Stewart[a]	Present data, $f = C/n^3$
2	0.270	0.229
3	0.0746	0.0679
4	0.0304	0.0286
5	0.01530	0.0147
6	0.00878	0.00848
7	—	0.00505
8	—	0.00359
9	—	0.00251
10	—	0.00183

[a] Dalgarno and Stewart (1960).

experimental values at the spectral head varied between 4 and 6.3 Mb, providing substantial verification of the theoretical value. However, at shorter wavelengths the theoretical curve of Bates deviated considerably from the experimental curves.

Recently, Seaton (1951a, 1954), Cooper (1962), and Sewell (1965a) have published theoretical treatments, each using different assumptions and approximations. Cooper has used the Hartree–Fock orbitals for the neutral atom in computing the potential and exchange functions in the free electron equation, whereas Sewell has used the orbitals for the ionized atom. Seaton approximated the Hartree–Fock orbitals for Ne^+ by using the published values for neutral neon and Ne^{++}. The theoretical curves deviate considerably from each other, indicating the sensitivity of the calculations to the various approximate wave functions.

It is difficult to assess the relative merits of the theoretical curves from the early experimental values, owing to the spread in their data and the uncertainty of the absolute cross sections. The experimental work of Lee and Weissler (1952) and also of Ditchburn (1960) give cross sections which are from 15 to 20% lower than those presented here. Further, their curves rise more steeply from the spectral head and fall off more sharply near the L_1 edge (255.8 Å). The fall off at the L_1 edge can be understood in the light of the recent absorption spectra of the $2s - np$ transitions obtained by Madden and Codling (1963). Unlike the more familiar absorption series these resonances exhibit a large increase in absorption, relative to the continuum, on the long-wavelength side of the resonance and a large decrease in absorption on the short-wavelength side. Any emission line coinciding with the "window" will produce a low cross section and give the impression of a large jump at the L_1 edge. According to Codling and Madden (1965), the position of maximum absorption of the $2s - 3p$ transition lies at 272.21 Å; thus, the minimum will lie slightly below this value. This wavelength coincides with an O IV group of emission lines, the most intense of which lies at 272.125 Å. Most spark discharge light sources will produce this line, and consequently any cross section measurement in neon made with this line will produce a very low value. This is illustrated in the present results shown in Fig. 5. Since the other members of the O IV group were unresolved in this measurement the cross section is not as low as it might be.

The recent work by Ederer and Tomboulian (1964a) provides the only other detailed experimental data available. They used, as did earlier workers, the photographic method for recording the incident radiation intensity with the exception, however, of using a Geiger counter at several selected wavelengths. Instead of filling the spectrograph with neon, as was done by the previous investigators, they used a small absorption cell with thin Zapon windows. The cell was located between the entrance slit and the grating.

They obtained a cross section of 6.3 Mb at the spectral head in agreement with the present results. Below 450 Å their data tend to be about 10% high. However, they do lie just within the respective error limits of the two results. Some low points again in the vicinity of the L_1 edge give their data the appearance of an absorption jump; however, if these points are ignored a rather smooth continuation of the cross sections across the L_1 edge is obtained. In the present data no sign of an absorption discontinuity can be observed. If an edge exists it would have to be less than a 5% jump since this is the maximum spread in the data. Recent theoretical work by Fano and Cooper (1965) indicates that the absorption jumps can be zero, negative, or positive.

Comes and Elzer (1964) have measured neon cross sections with the aid of a mass spectrometer. The principle of this method is that for a small attenuation of the incident photon beam the ratio of the ions produced to the absolute intensity of the incident beam is proportional to the photoionization cross section of the gas (Samson, 1958). The real advantage in using this method is to determine the cross sections for dissociative ionization processes such as

$$0_2 + h\nu \rightarrow 0 + 0^+ + e,$$

where a mass spectrometer is essential to identify the ionized fragments. It is necessary to know the transmission of the mass spectrometer for the given ion and also to provide a calibrated detector to measure the absolute intensity of the incident photon beam. Normally the instrument can be calibrated using a rare gas of known cross section.

The present experimental techniques differ in many ways from all the previous methods. The simultaneous measurement of the incident and transmitted radiation, using the double ion chamber as a detector of the radiation, is mainly responsible for reducing the scatter in the experimental points. As in the case of helium, the reagent grade neon was passed through a liquid nitrogen–cooled activated charcoal trap for further purification before it entered the absorption chamber.

The experimental results are shown in Fig. 5. Sewell's theoretical curves are also shown in the figure since they were obtained using more accurate wavefunctions and show the closest agreement with the experimental data. The good agreement with the experimental data does favor Sewell's suggestion that the orbitals for the ionized atom should be used in computing the potential and exchange functions.

The dipole velocity approximation (lower curve) seems to be superior beyond the threshold, especially since it predicts an absorption jump of only 4% at the L_1 edge.

Seaton's dipole length approximation agrees well with the experimental results at the spectral head, while his dipole velocity approximation, although

lower in magnitude, faithfully reproduces the spectral shape of the experimental absorption curve. His calculations, however, predict an 18% jump at the L_1 edge. Cooper's one-electron model deviates somewhat more in magnitude and in its spectral shape. His curve agrees with the general experimental shape by increasing to a maximum and then decreasing; however, the position of the maximum is located at shorter wavelengths.

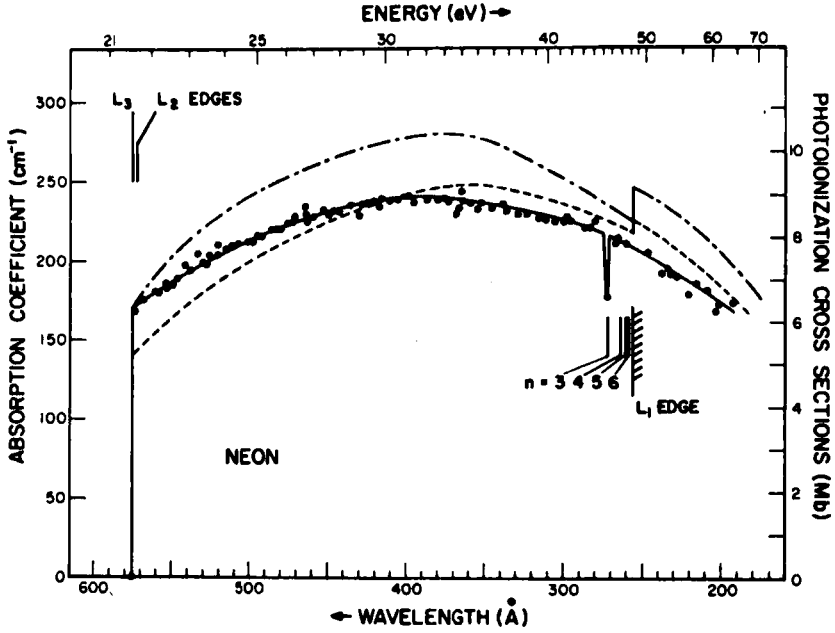

FIG. 5. Photoionization cross sections of neon compared to theoretical values. Sewell: — — — dipole length, - - - - dipole velocity; present data, ●.

The vertical lines shown in Fig. 5 indicate the position of the absorption series due to the transition $2s^2\,2p^6\,{}^1S_0 - 2s\,2p^6\,np\,{}^1P_1{}^0$ as observed by Madden and Codling (1963).

The oscillator strength for transitions into the continuum was measured graphically from threshold to 0.01 Å using the data given in Tables V and VII. A continuum f value $f_c = 9.4$ was obtained.

The data between 40 and 190 Å in Table VII were interpolated between the present data and those of Table V. The results of Ederer and Tomboulian provided the general shape of the curve in the region down to 100 Å; their cross sections were reduced, however, by 10%. This was done since their data are approximately 10% higher in the region where they overlap the present results.

TABLE V

NEON ABSORPTION COEFFICIENTS FROM 0.01 TO 44.6 Å

Shell	λ (Å)	Experimental,[a] k (cm^{-1})	Semiempirical, k (cm^{-1})	Shell	λ (Å)	Experimental,[a] k (cm^{-1})	Semiempirical, k (cm^{-1})
K	0.01	—	0.051×10^{-3} [b]	*K (cont.)*	1.934	44.1×10^{-3}	—
	0.02	—	0.071×10^{-3} [b]		2.500	90×10^{-3}	—
	0.03	—	0.084×10^{-3} [b]		3.57	247×10^{-3}	—
	0.05	—	0.102×10^{-3} [b]		4.36	430×10^{-3}	—
	0.08	—	0.121×10^{-3} [b]		5.17	687×10^{-3}	—
	0.098	0.133×10^{-3}	—		6.97	1554×10^{-3}	—
	0.100	—	0.131×10^{-3} [b]		8.32	2475×10^{-3}	2487×10^{-3} [c]
	0.130	0.143×10^{-3}	—		9.87	3879×10^{-3}	—
	0.175	0.166×10^{-3}	—		13.37	7650×10^{-3}	7416×10^{-3} [c]
	0.200	0.189×10^{-3}	—		14.298	—	—
	0.260	0.243×10^{-3}	—				
	0.417	0.522×10^{-3}	—	*L*	14.298	—	—
	0.497	0.837×10^{-3}	—		17.6	—	971×10^{-3} [c]
	0.631	1.62×10^{-3}	—		21.7	—	1677×10^{-3} [c]
	0.710	2.25×10^{-3}	—		23.7	—	2141×10^{-3} [c]
	0.880	4.09×10^{-3}	—		27.4	—	3218×10^{-3} [c]
	1.00	5.85×10^{-3}	—		31.6	—	4725×10^{-3} [c]
	1.235	11.16×10^{-3}	—		36.3	—	6876×10^{-3} [c]
	1.389	15.3×10^{-3}	—		44.6	11790×10^{-3}	11860×10^{-3} [c]
	1.54	21.6×10^{-3}	—				

[a] Determined from the mass absorption coefficients compiled by Allen (1935).
[b] Victoreen (1949).
[c] Hencke (1957).

TABLE VI

NEON ABSORPTION COEFFICIENTS FROM 80 TO 283 Å[a]

Shell	λ (Å)	k (cm^{-1})	λ (Å)	k (cm^{-1})
L	80.6	67.2	196.0	195.8
	83.5	68.0	202.3	203.3
	85.3	74.3	203.9	200.1
	90.4	81.3	207.2	206.3
	96.6	71.3	209.3	204.7
	99.6	77.8	214.3	209.0
	104.8	91.3	215.2	207.6
	110.5	100.4	218.5	207.0
	115.8	99.9	220.4	217.6
	117.9	102.3	227.5	220.9
	119.0	104.8	228.0	213.0
	129.8	118.8	231.2	221.7
	133.5	127.2	233.5	221.4
	135.5	129.1	238.5	222.2
	138.1	133.7	241.5	212.0
	150.0	152.6	243.0	220.0
	151.5	151.7	246.2	231.9
	159.4	160.9	247.6	230.9
	162.5	164.4	248.6	240.0
	164.6	164.2	251.5	225.0
	166.2	168.2	256.3	230.0
	168.1	170.1	260.5	236.0
	172.2	177.7	263.5	237.6
	173.0	183.1	267.0	230.0
	184.0	182.5	267.5	212.0
	185 ± 5	187.0	277.3	206.6
	185.7	191.7	283.5	216.0
	192.8	191.2	282.3	215.7
	194.6	182.8		

[a] Ederer and Tomboulian (1964a).

The individual contributions of f_c were as follows:

threshold to L_1 *edge*	$= 2.04$
L_1 *edge to* K *edge*	$= 5.55$
K *edge to* 0.01 *Å*	$= 1.81$
Total	$= 9.4$

Using the sum rule, f for the continuum and discrete absorption lines must be equal to ten. If an error of $\pm 5\%$ is assigned to f_c from threshold to the K edge and an arbitrary $\pm 10\%$ below the K edge, then the total discrete oscillator strengths must be ≤ 1.16.

TABLE VII

NEON ABSORPTION COEFFICIENTS FROM THRESHOLD TO 40 Å[a]

Shell	λ (Å)	k (cm^{-1})	λ (Å)	k (cm^{-1})
L	40	(9)	374.1	238
	50	(16)	374.7	239
	60	(25)	380.0	239
	70	(36)	387.5	239
	80	(47)	395.4	237
	90	(60)	398.7	242
	100	(72)	405.0	240
	110	(87)	410.6	238
	120	(100)	416.6	240
	130	(110)	418.7	235
	140	122)	420.7	238
	150	(132)	425.0	237
	160	(142)	428.2	236
	170	(150)	430.0	229
	180	(157)	435.0	236
	190	(170)	442.8	232
	192.9	178	447.0	232
	202.4	172	449.0	230
	203.9	169	452.0	233
	207.7	190	457.5	230
	209.3	182	459.5	228
	215.2	187	462.0	226
	220.4	179	463.5	230
	228.3	190	464.3	235
	232.0	192	471.4	228
	234.3	195	472.4	225
	238.9	192	476.0	224
	247.2	206	479.8	220
	260.5	211	481.5	220
	266.3	215	486.0	220
	267.0	212	492.5	216
	272.1	178	495.2	216
	279.9	225	498.7	212
	283.6	223	501.5	212
	286.2	222	508.0	211
	295.0	226	512.0	210
	297.6	228	516.0	208
	299.1	226	520.0	210
	303.0	226	521.6	203
	305.0	225	526.5	204
	311.0	226	528.7	197
	315.0	227	530.5	199
	323.0	230	534.0	205
	328.4	230	538.7	194

TABLE VII (CONTINUED)

NEON ABSORPTION COEFFICIENTS FROM THRESHOLD TO 40 Å[a]

Shell	λ(Å)	$k(cm^{-1})$	λ(Å)	$k(cm^{-1})$
	335.4	231	541.4	198
	338.1	238	546.9	189
	345.0	234	549.2	185
	352.0	237	553.5	183
	354.6	233	554.7	186
	358.5	237	558.0	180
	363.0	238	561.6	180
	364.0	245	567.5	176
	365.0	233	573.5	168
	367.3	230	574.9	Threshold

[a] Present data. The coefficients in parentheses represent interpolated data between the present values and those of Table V.

Theoretical calculations have been made on the values of the discrete oscillator strengths by Cooper (1962) and by Gold and Knox (1959). Gold and Knox obtained an f value of 0.11 for the 736-Å line and 0.011 for the 742-Å line. From Cooper's calculations the $2p$-nd and the $2p$-ns transitions were estimated to contribute 0.3 to the discrete oscillator strengths. An experimental value $f = 0.2$ for the 736-Å line is quoted by Landolt and Börnstein (1950), while Korolev *et al.* (1964) obtain a value of 0.16 ± 0.014. From all the above considerations, if we estimate a total discrete oscillator strength of 0.3 due to both the $2p$ and $2s$ electrons, we then get a total f value of 9.7, which certainly verifies the sum rule within the experimental error. It is interesting to note that if the L-shell electrons are assumed to contribute 0.3 to the discrete oscillator strengths then the total contribution of these electrons is eight, assuming that they contribute ~ 0.1 below the K edge. Thus, it would appear that the eight electrons in the L shell contribute an oscillator strength of eight to the whole atom. Carrying this picture further into the sub shells we might expect the p electrons to contribute six to the oscillator strength. If this is the case, more than half of their contribution must come from energies greater than the L_1 edge since the f value from threshold to the L_1 edge is only two. This implies that the major contribution to the photoionization cross section just below the L_1 edge is due to the ejection of a p electron, which is the case according to Sewell's dipole velocity calculations. The theoretical cross sections for the ejection of the s and p electrons have been kindly supplied by Dr. Sewell and are tabulated in Table VIII.

It would be interesting to measure the individual cross sections for the ejection of s and p electrons below the L_1 edge. This could be achieved by

TABLE VIII

THEORETICAL PHOTOIONIZATION CROSS SECTIONS FOR NEON[a]

Photon energy		Cross sections (Mb)					
		2p electron		2s electron		Total	
Ry	λ (Å)	σ_{DL}	σ_{DV}	σ_{DL}	σ_{DV}	σ_{DL}	σ_{DV}
1.585	574.93	6.2	5.2	—	—	6.2	5.2
1.75	520.7	8.5	6.9	—	—	8.5	6.9
2.00	455.6	9.7	8.3	—	—	9.7	8.3
2.25	405.0	10.3	9.0	—	—	10.3	9.0
2.50	364.5	10.4	9.2	—	—	10.4	9.2
2.75	331.4	10.0	9.1	—	—	10.0	9.1
3.00	303.8	9.4	8.9	—	—	9.4	8.9
3.50	260.4	8.5	8.2	—	—	8.5	8.2
3.562	255.77	8.4	8.1	0.73	0.29	9,1	8.4
4.00	227.9	7.7	7.4	0.81	0.34	8.5	7.7
4.50	202.5	6.9	6.6	0.81	0.39	7.7	7.0
5.00	182.3	6.1	5.8	0.78	0.41	6.9	6.2
5.50	165.7	5.4	5.0	0.74	0.42	6.1	5.4
6.00	151.9	4.7	4.4	0.71	0.43	5.4	4.8
6.50	140.2	4.1	3.8	0.67	0.43	4.8	4.2
7.00	130.2	3.6	3.3	0.63	0.42	4.2	3.7
7.50	121.5	3.1	2.9	0.60	0.41	3.7	3.3
8.00	113.9	2.7	2.6	0.56	0.40	3.3	3.0
8.50	107.2	2.4	2.3	0.53	0.38	2.9	2.6
9.00	101.3	2.1	2.0	0.50	0.37	2.6	2.4
9.50	95.9	1.9	1.8	0.47	0.35	2.4	2.1
10.00	91.1	1.7	1.6	0.44	0.33	2.1	1.9
10.50	86.8	1.5	1.4	0.42	0.32	1.9	1.7
11.00	82.8	1.4	1.2	0.39	0.30	1.8	1.5

[a] Sewell (1965b).

measuring the relative number of electrons ejected with energies equal to $h\nu - E(L_1 \text{ edge})$ and $h\nu - E(L_{2,3} \text{ edge})$, where $h\nu$ is the energy of the incident photon and E is the minimum energy necessary to eject the appropriate electron.

The absorption of radiation in the extreme ultraviolet is due primarily to the photoionization process. Scattering becomes important only at wavelengths below 1 Å. Table IX presents theoretical data by Woo and Sun (1937–1947) of the scattering cross sections for radiation between 1.54 and 0.098 Å. It can be seen that scattering contributes about 7% to the total cross section at 1 Å and increases rapidly at shorter wavelengths.

TABLE IX

NEON: TOTAL ABSORPTION (σ_t) AND SCATTERING (σ_s) CROSS SECTIONS[a]

Shell	λ (Å)	σ_t(cm^2) ($\times 10^{-23}$)	σ_s(cm^2) ($\times 10^{-23}$)
K	0.098	0.47	0.46
	0.130	0.54	0.50
	0.175	0.64	0.56
	0.200	0.71	0.59
	0.260	0.92	0.64
	0.417	1.98	0.77
	0.497	2.94	0.84
	0.631	5.37	0.96
	0.710	7.42	1.04
	1.000	19.74	1.32
	1.235	36.81	1.57
	1.540	70.90	1.87

[a] Woo and Sun (1937–1947).

D. ARGON

The photoionization cross sections of argon have been measured from threshold (786.72 Å) to 0.01 Å giving a complete picture of the continuous absorption spectrum.

Details of the cross sections between the $^2P_{1/2}$ and $^2P_{3/2}$ thresholds have been measured by Huffman *et al.* (1963a), see Section H, and by G. R. Cook and Metzger (1964) using continuum light sources. Although these data differ by about 15%, they represent the only detailed measurements of the absolute cross sections within this autoionizing region.

Between the $^2P_{1/2}$ threshold (M_2 edge) and 200 Å the cross sections have been measured by Wainfan *et al.* (1955), Lee and Weissler (1955), Rustgi (1964), and Samson (1964c). Where the data overlap, very good agreement is obtained between the present work and that of Rustgi. In general the results of other investigators lie within 10–20% of the present work.

The gap between 200 Å and the *L* edge has recently been closed by the work of Lukirskii and Zimkina (1963). From the plot in Fig. 6 it can be seen that the present data join smoothly onto those of Lukirskii and Zimkina.

Dalgarno (1952) has calculated the cross section for argon at its spectral head and obtained a value of 30 Mb in agreement with the present value of 31 Mb. Cooper's (1962) theoretical model provides k values of the correct order of magnitude; however, the spectral shape of the absorption curve

shows an immediate decrease in the absorption coefficients to wavelengths shorter than the $^2P_{1/2}$ edge in contradiction to the present experimental data.

Discrete absorption structure due to excitation of the inner s electrons can be seen starting at 465.5 Å and ending with the removal of the s electron at 424 Å. The unusual decrease in absorption for excitation of the $3s$ electrons

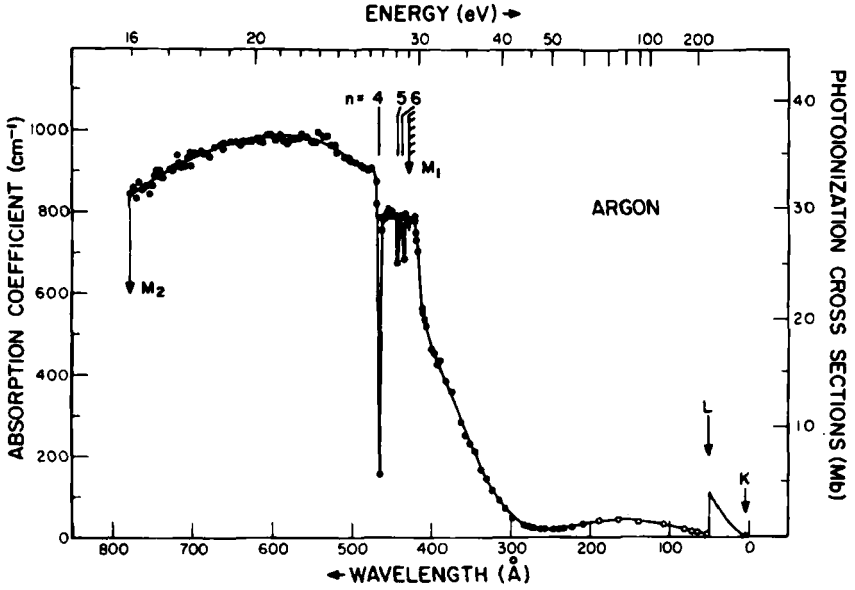

FIG. 6. Photoionization cross sections of argon. Present data, ●; Lukirskii and Zimkina, O.

is due to configuration interaction between the discrete states and the underlying continuum (Fano, 1961). An excellent photograph of this series has been given by Madden and Codling (1963), while a discussion of the Rydberg series has been given by Samson (1963). Unlike helium and neon these resonances are not of the asymmetrical type; rather they show a simple reduction in cross section relative to that of the continuum. From the spectra obtained by Madden and Codling this series is shown to be rather diffuse with the $3s - 4p$ transition line having a width of approximately 1 Å. Fortunately, this resonance coincides with the 465.586 Å argon VI emission line from the spark light source enabling the continuum cross section to be measured within the resonance. This was done as follows: The pressure of argon in the absorption cell was increased until no radiation other than the 465.5-Å line was transmitted; after noting this intensity, the pressure was increased further

TABLE X

ARGON ABSORPTION COEFFICIENTS FROM 0.01 TO 44.6 Å

Shell	λ (Å)	Experimental,[a] k (cm^{-1})	Semiempirical, k (cm^{-1})	Shell	λ (Å)	Experimental[a] k (cm^{-1})	Semiempirical k (cm^{-1})
K	0.01	—	0.092×10^{-3} [b]	*K (cont.)*	3.570	2160.0×10^{-3}	—
	0.02	—	0.128×10^{-3} [b]		3.870	2610.0×10^{-3}	—
	0.03	—	0.153×10^{-3} [b]				
	0.05	—	0.190×10^{-3} [b]	*L*	3.870	263.0×10^{-3}	—
	0.08	—	0.247×10^{-3} [b]		4.360	360.0×10^{-3}	—
	0.098	0.328×10^{-3}	—		5.170	578.0×10^{-3}	—
	0.100	—	0.293×10^{-3} [b]		6.970	1335.0×10^{-3}	—
	0.130	0.437×10^{-3}	—		8.320	2070.0×10^{-3}	2076×10^{-3} [c]
	0.175	0.714×10^{-3}	—		9.870	3320.0×10^{-3}	—
	0.200	0.794×10^{-3}	—		11.90	5360.0×10^{-3}	—
	0.260	1.510×10^{-3}	—		13.3	—	6760×10^{-3} [c]
	0.417	5.260×10^{-3}	—		17.6	—	12680×10^{-3} [c]
	0.497	8.93×10^{-3}	—		21.7	—	19720×10^{-3} [c]
	0.631	17.45×10^{-3}	—		23.7	—	24150×10^{-3} [c]
	0.710	23.2×10^{-3}	—		27.4	—	33700×10^{-3} [c]
	0.880	42.9×10^{-3}	—		31.6	—	45800×10^{-3} [c]
	1.000	62.5×10^{-3}	—		36.3	—	61950×10^{-3} [c]
	1.235	111.0×10^{-3}	—		44.6	81600.0×10^{-3}	—
	1.389	153.0×10^{-3}	—		50.6	—	—
	1.540	211.0×10^{-3}	—				
	1.934	420.0×10^{-3}	—	*M*	50.6	—	—
	2.500	846.0×10^{-3}	—				

[a] Determined from the mass absorption coefficients compiled by Allen (1935).
[b] Victoreen (1949).
[c] Henke (1957).

reducing the intensity by about a factor of four. The logarithm of this ratio is then related to the absorption coefficient. A value of 158 cm^{-1} was obtained. It is not known if this value represents the minimum in the resonance line, but it certainly provides an upper limit to the k value. In the case of helium Madden and Codling (1965) found that the minimum of the $2s\ 2p\ ^1P_1^0$ line was zero.

Recently, Schönheit (1961) published a detailed curve of the relative cross sections using a mass spectrometer and a line emission light source similar to that used here. His very low relative cross section value at 466 Å is undoubtedly due to the $3s - 4p$ excitation.

Comes and Lessmann (1961), also using a mass spectrometer, studied the relative cross sections down to 685 Å. They observed considerable apparent structure to the short wavelength side of the $^2P_{1/2}$ edge. This structure is not apparent in the present work nor in any work using the conventional absorption techniques. Although some scatter of points is observed above the $^2P_{1/2}$ edge in Fig. 6, no significance is placed on them at this time. It may be possible that weak excitations in a strong ionization continuum are more easily observed at the low pressures used in the relative cross section measurements.

A second maximum in the M-shell absorption curve occurs between 350 Å and the L edge. This maximum was predicted by Cooper (1964) using the one

TABLE XI

ARGON ABSORPTION COEFFICIENTS FROM 4 TO 250 Å[a]

Shell	λ (Å)	k (cm^{-1})	Shell	λ (Å)	k (cm^{-1})
L	3.87	—	M	50.6	—
	4.0	0.27		53.0	9.3
	5.0	0.51		64.5	13.1
	7.0	1.22		72.5	16.1
	9.0	2.35		82.0	19.8
	12.0	4.86		108.5	31.4
	15.0	8.44		139.5	39.0
	20.0	17.6		164.5	41.3
	25.0	28.9		190.7	40.0
	30.0	44.2		230.0	35.6
	35.0	64.8		251.5	31.7
	44.0	72.7			
	46.5	83.5			
	48.5	94.7			
	50.6	—			

[a] Lukirskii and Zimkina (1963).

electron nonhydrogenic central field model. His calculations showed that the photoionization cross sections for the ejection of a p electron should have two maxima, one at threshold and a second one at approximately 100 eV higher in energy. The theoretical data are compared to the experimental results in Fig. 7. The experimental results represent the total cross section, that is, ionization of both the s and p electrons; however, the good agreement with the theoretical results suggests that the major contribution to the cross section in this region is due to ejection of a p electron. This could be verified by measuring the energies of the ejected electrons and their relative abundance.

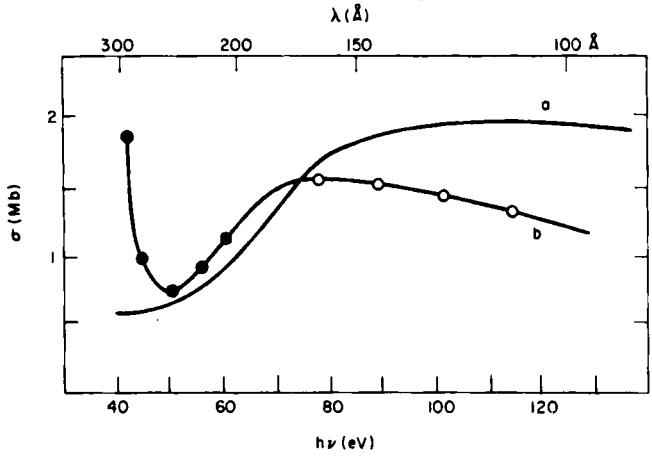

FIG. 7. Theoretical cross sections for ionization of the $3p^6$ electrons in argon (Cooper, curve *a*) compared to the measurements of the total cross section (curve *b*). Present data, ●; Lukirskii and Zimkina, O.

Table X lists the absorption coefficients from 44 to 0.01 Å, as obtained from the data compiled by Allen (1935), and the semiempirical values determined by Henke (1957) and Victoreen (1949). The values obtained by Lukirskii and Zimkina (1963) between 4 and 250 Å are given in Table XI, while the present data from threshold to 209 Å are tabulated in Table XII. The theoretical absorption and scattering cross sections by Woo and Sun (1937–1947) are given in Table XIII for the range 0.1–11.9 Å.From their results it can be seen that scattering is not important for wavelengths longer than about 0.5 Å.

Using the coefficients tabulated in Tables X–XII, the continuum oscillator strength is found to be 16.2. This value includes the contribution of the autoionizing region between the $^2P_{3/2}$ and $^2P_{1/2}$ thresholds. A value of 0.043 is taken for this region since this is the average of the values quoted by G. R. Cook and Metzger (1964) and by Huffman *et al.* (1963a).

TABLE XII

ARGON ABSORPTION COEFFICIENTS FROM THRESHOLD TO 209 Å[a]

λ (Å)	k (cm^{-1})	λ (Å)	k (cm^{-1})	λ (Å)	k (cm^{-1})	λ (Å)	k (cm^{-1})
209.3	30	430.9	798	467.6	822	614.8	991
225.8	25	431.5	789	468.2	882	616.7	973
234.8	23	432.2	787	468.7	900	618.8	981
240.0	21	432.9	804	468.8	897	625.2	978
247.2	20	433.7	782	469.5	900	629.8	973
260.6	23	434.2	747	470.1	897	634.0	978
266.3	22	434.5	692	470.8	900	637.0	964
271.0	25	435.0	703	471.3	900	641.0	971
279.0	27	436.0	742	474.0	912	644.1	971
282.8	23	436.5	766	475.7	909	649.0	971
283.6	32	436.7	770	479.4	900	651.0	973
297.8	52	436.9	768	484.2	912	660.0	952
300.2	58	437.5	770	486.8	912	662.7	971
303.1	68	438.1	796	487.9	915	664.8	968
308.0	72	438.8	794	492.5	915	668.3	956
315.0	94	439.4	780	496.5	924	670.2	960
317.3	98	440.0	768	499.4	926	675.2	924
323.0	115	440.7	763	501.3	924	677.1	936
329.0	143	441.3	757	505.8	936	680.5	945
335.4	161	441.9	731	509.3	936	683.0	945
337.6	167	442.1	712	512.1	945	684.8	945
345.0	213	442.6	695	514.3	945	688.4	950
351.0	233	443.2	673	517.5	952	692.8	940
357.6	253	443.8	720	519.5	945	694.9	945
363.8	285	444.2	773	521.9	964	700.0	915
375.2	360	444.5	778	524.2	964	703.0	945
381.6	382	445.1	796	526.7	964	705.4	934
389.9	434	445.7	796	529.3	991	709.2	915
393.3	426	446.4	796	532.0	978	713.7	912
396.5	454	447.9	788	536.0	985	715.5	920
399.3	466	449.8	787	539.3	971	718.4	940
405.2	535	450.2	790	541.8	999	721.0	915
405.7	520	450.8	808	544.9	973	724.8	900
410.0	558	451.4	800	549.3	973	727.2	900
411.5	562	452.1	808	551.4	985	735.6	883
416.9	709	452.7	798	555.1	985	737.0	887
417.6	734	453.3	817	558.8	985	739.9	906
418.2	750	453.9	810	562.1	995	742.4	905
418.8	769	454.5	810	564.6	981	744.6	890
419.4	781	455.2	800	567.9	981	747.5	865
420.0	790	455.8	790	570.4	981	751.1	845
420.7	800	457.0	783	573.7	971	755.1	866
421.3	767	457.6	780	577.0	978	760.6	856
421.8	760	459.8	778	580.0	964	765.3	876
422.4	738	462.2	768	583.0	978	767.3	830
425.2	762	462.5	768	585.5	973	772.4	860
425.8	767	463.1	780	588.9	990	774.6	852
426.4	767	463.7	723	594.1	978	776.8	845
427.0	790	464.4	669	596.7	978	779.7	627
427.7	712	465.0	579	599.5	991	783.2	671
428.3	764	465.6	158	603.4	991	786.72	Threshold
428.9	760	466.3	536	608.5	964		
429.5	752	466.6	619	610.0	973		
430.1	773	466.9	695	613.0	998		

[a] Present data.

TABLE XIII

ARGON: TOTAL ABSORPTION (σ_t) AND SCATTERING (σ_s) CROSS SECTIONS[a]

Shell	λ (Å)	σ_t (cm²) ($\times 10^{-23}$)	σ_s (cm²) ($\times 10^{-23}$)	Shell	λ (Å)	σ_t (cm²) ($\times 10^{-23}$)	σ_s (cm²) ($\times 10^{-23}$)
K	0.098	1.1	0.86	*K (cont.)*	2.50	2840.0	9.50
	0.130	1.5	0.98		2.91	4270.0	10.51
	0.175	2.4	1.13		3.25	5750.0	11.30
	0.200	3.1	1.21		3.55	7280.0	11.90
	0.260	5.5	1.41		3.87	9180.0	12.56
	0.417	18.2	1.92				
	0.497	30.3	2.23	*L*	3.87	610.0	12.56
	0.631	59.5	2.72		4.36	860.0	13.48
	0.710	83.3	3.03		5.17	1410.0	14.65
	1.000	225.0	4.28		6.97	3350.0	16.68
	1.235	404.0	5.25		8.32	5590.0	17.67
	1.540	753.0	6.40		9.87	9140.0	18.46
	1.934	1390.0	7.80		11.90	15740.0	19.22

[a] Woo and Sun (1937–1947).

The individual contributions to f_c are as follows:

$$
\begin{aligned}
{}^2P_{3/2} \textit{ threshold to } M_1 \textit{ edge} &= 4.14 \\
M_1 \textit{ edge to } L \textit{ edge} &= 2.73 \\
L \textit{ edge to } K \textit{ edge} &= 7.51 \\
K \textit{ edge to } 0.01\ \textit{Å} &= 1.77 \\
\textit{Total} &= 16.15
\end{aligned}
$$

If an error of $\pm 5\%$ is assigned to f_c, then the total discrete oscillator strengths must lie between 1.0 and 2.7 if the total oscillator strength is to equal $Z = 18$.

The f values for the first resonance lines have been computed by Knox (1958) yielding 0.2 (1048 Å) and 0.05 (1067 Å). These values are consistent with the recent experimental results of Stacey and Vaughan (1964) who found corresponding values of 0.275 and 0.036. Some unpublished results by Geiger (1962) give a total of 0.23 for the two lines. It is difficult to estimate the contribution from the remaining discrete lines; however, it is not too unreasonable to expect that their total contribution could be of the order of one. Thus, depending on the value of the total discrete oscillator strengths, it appears as if the results in argon also verify the Thomas–Kuhn sum rule.

E. KRYPTON

The only theoretical treatment of krypton available is that by Cooper (1962). As in argon, however, the theoretical absorption curve shows an

immediate decrease from the $^2P_{1/2}$ spectral head, continuing down to the shortest wavelengths.

The experimental results, illustrated in Fig. 8, show an initial increase in the cross sections from the $^2P_{1/2}$ threshold, rising to a maximum about 780 Å and then decreasing to the N_1 edge. Prior to the N_1 edge, discrete absorption dips are observed similar to those in argon. Their precise positions are indicated by the vertical lines as obtained with a flash tube continuum light source (Samson, 1964d). Similar absorption lines have been reported by Madden and Codling (1964). The N_1 edge is the X-ray terminology for the ionization potential of the 4*s* electrons and is normally characterized by an abrupt increase in the absorption coefficient. However, in the case of the rare gases these abrupt changes either do not exist or are extremely small for the outer shells. As can be seen in Fig. 8, the absorption coefficients decrease

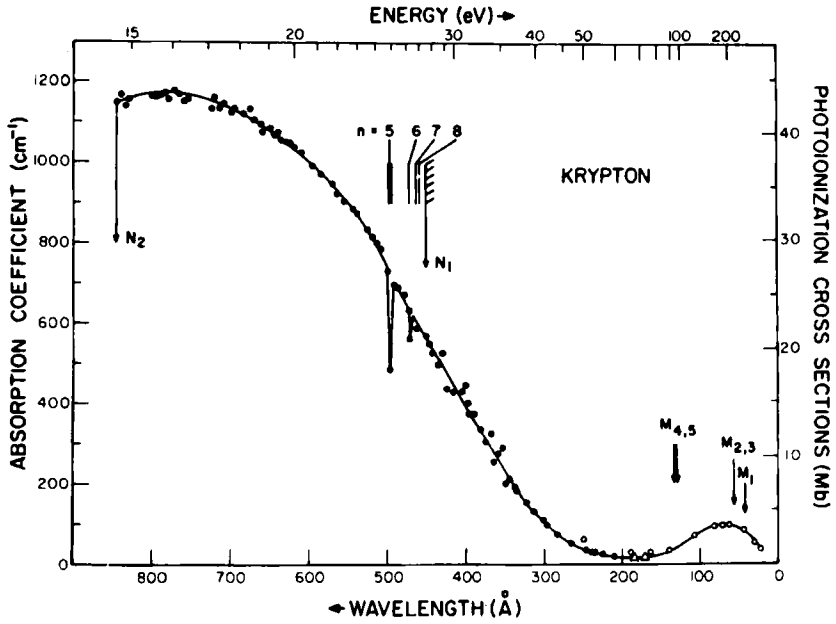

FIG. 8. Photoionization cross sections of krypton. Present data, ●; Lukirskii *et al.*, O; Ederer and Tomboulian, △.

smoothly before and after the N_1 edge. The recent Kr spectrum taken by Codling and Madden (1964) in the vicinity of 130 Å also shows a smooth absorption curve on either side of $M_{4,5}$ edge (i.e., the ionization limit of the 3*d* electrons).

The *k* value at the spectral head ($^2P_{1/2}$) is found to be 1150 cm^{-1} $\pm 5\%$ in excellent agreement with Pery-Thorne and Garton (1960) who quote

TABLE XIV

KRYPTON ABSORPTION COEFFICIENTS FROM 0.01 TO 250 Å

Shell	λ (Å)	Experimental, k (cm^{-1})	Empirical[b], k (cm^{-1})	Shell	λ (Å)	Experimental, k (cm^{-1})	Empirical[b], k (cm^{-1})
K	0.010	—	0.183×10^{-3}	*L*	0.866	—	—
	0.012	—	0.201×10^{-3}		7.401	—	—
	0.015	—	0.227×10^{-3}				
	0.020	—	0.263×10^{-3}	*M*	7.40	—	—
	0.025	—	0.298×10^{-3}		23.60	35.5[c]	—
	0.030	—	0.334×10^{-3}		31.40	53.7[c]	—
	0.040	—	0.414×10^{-3}		44.40	86.1[c]	—
	0.050	—	0.514×10^{-3}		44.60	118.0[a]	—
	0.060	—	0.649×10^{-3}		64.35	97.7[c]	—
	0.080	—	1.037×10^{-3}		72.20	93.3[c]	—
	0.098	2.1×10^{-3} [a]	—		81.98	89.1[c]	—
	0.100	—	1.64×10^{-3}		108.65	66.8[c]	—
	0.120	—	2.50×10^{-3}		132.14	—	—
	0.150	—	4.40×10^{-3}				
	0.200	10.8×10^{-3} [a]	9.56×10^{-3}	*N*	132.14	—	—
	0.260	21×10^{-3} [a]	—		139.50	31.6[c]	—
	0.417	77×10^{-3} [a]	—		165.60	26.9[c]	—
	0.497	129×10^{-3} [a]	—		190.30	30.2[c]	—
	0.631	238×10^{-3} [a]	—		250.50	66.1[c]	—
	0.710	338×10^{-3} [a]	—				
	0.800	408×10^{-3} [a]	—				
	0.866	—	—				

[a] Determined from the mass absorption coefficients compiled by Allen (1935).
[b] Victoreen (1949).
[c] Lukirskii *et al.* (1964).

a value of 1120 cm^{-1} $\pm 18\%$. Other investigators (G. R. Cook and Metzger, 1964; Huffman *et al.* 1963b; Rustgi *et al.* 1964) do not quote a value; however, from their curves they are in approximate agreement with the present results.

No data exist for the *L* shell of krypton. Recently Lukirskii *et al.* completed measurements on the *M* shell and at a few points to longer wavelengths. Where the data points overlap, Lukirskii's values tend to be larger. In their paper they quote that their krypton had an impurity of 1% xenon. Provided xenon has a cross section less than or equal to that of krypton no appreciable error is encountered; however, xenon has a cross section 20–40 times as large as krypton in the region 100–150 Å. This would make their results 10–20% too high.

Preliminary data by Ederer and Tomboulian (1964b) give a value of 16 cm^{-1} for the absorption coefficient at 170 Å and 185 Å.

Table XIV lists the available absorption coefficients from 0.01 Å to 250 Å,

TABLE XV

KRYPTON ABSORPTION COEFFICIENTS FROM THRESHOLD TO 209 Å[a]

λ (Å)	k (cm^{-1})	λ (Å)	k (cm^{-1})	λ (Å)	k (cm^{-1}	λ (Å)	k (cm^{-1})
209.3	20	397.2	400	539.6	877	721.2	1163
225.8	27	400.3	449	545.4	888	725.6	1132
234.8	30	405.7	435	555.1	904	755.1	1154
240.0	30	410.6	438	564.6	923	760.4	1151
247.2	38	416.6	428	570.6	948	766.1	1169
266.3	54	423.3	439	586.0	972	772.7	1180
283.6	76	425.5	435	596.6	993	779.4	1157
297.6	100	429.7	532	609.8	1028	783.1	1176
303.1	110	436.5	498	618.9	1041	789.1	1164
315.0	138	442.8	527	625.6	1049	795.6	1162
323.0	157	447.3	549	630.2	1053	800.8	1161
335.4	187	450.6	570	636.6	1057	827.4	1153
338.5	193	462.8	591	640.8	1077	834.8	1140
345.0	213	471.4	562	644.6	1070	840.1	1167
349.5	201	474.4	634	649.7	1086	844.6	1147
352.6	291	479.4	675	660.6	1078	850.4	878
358.0	278	487.2	695	663.6	1096	857.6	891
364.4	256	492.2	699	671.1	1104	870.3	812
368.7	325	496.3	483	675.6	1037	878.6	1276
376.0	305	500.8	727	685.0	1121	883.6	488
380.0	340	508.8	785	694.6	1136	885.6	Threshold
382.4	333	514.6	803	700.6	1122		
390.7	376	519.6	815	709.1	1146		
394.0	374	526.7	835	714.1	1136		

[a] Present data.

while the absorption coefficients from threshold to 209 Å are listed in Table XV. The scattering cross sections are given in Table XVI.

TABLE XVI

KRYPTON: TOTAL ABSORPTION (σ_t) AND SCATTERING (σ_s) CROSS SECTIONS[a]

Shell	λ (Å)	σ_t (cm²)	σ_s (cm²)
K	0.098	7.2×10^{-23}	2.03×10^{-23}
	0.200	38.7×10^{-23}	3.80×10^{-23}
	0.417	279.0×10^{-23}	7.54×10^{-23}
	0.631	808.0×10^{-23}	11.77×10^{-23}
	0.710	1097.0×10^{-23}	12.50×10^{-23}

[a] Woo and Sun (1937–1947).

Since no data exist for the *L* shell, the total value of f_c is unknown. Using the data in Tables XIV and XV the individual contributions to f_c are as follows:

$$\begin{aligned} {}^2P_{3/2} \textit{ to } N_1 \textit{ edge} &= 4.35 \\ N_1 \textit{ edge to } M \textit{ edge} &= 1.8 \\ M \textit{ edge to } L \textit{ edge} &= 17.7 \\ L \textit{ edge to } K \textit{ edge} &= ? \\ K \textit{ edge to } 0.01 \textit{ Å} &= 1.63 \\ \textit{Total} &= 25.48 + L \textit{ shell} \end{aligned}$$

The continuum and Beutler lines between the ${}^2P_{1/2,3/2}$ edges contribute 0.216 according to G. R. Cook and Metzger (1964), or 0.287 according to Huffman *et al.* (1963b). The mean of the two values, namely, $f = 0.252$, was used above.

If the *L* shell is assumed to contribute eight to the oscillator strengths, that is, an *f* value equal to the number of electrons within the shell, the total $f_c = 33.5$, leaving 2.5 for the contribution of all the discrete transitions to make a total oscillator strength of 36.

If the interaction of the outer $4s^2\ p^6$ electrons continues to decrease at photon energies greater than the *M* edge, an estimate of their contribution to the *f* value is approximately 0.35. Adding this value to the measured f_c between the ${}^2P_{3/2}$ threshold and the *M* edge gives a total contribution by the *s* and *p* electrons to f_c of 6.5 ± 0.4. If the eight $4s^2p^6$ electrons are assumed to contribute eight to the total *f* value, then the discrete transitions of the outer *s* and *p* electrons must contribute approximately 1.5 ± 0.4.

Geiger (1962) gives an experimental value of 0.345 for the joint contribution of the 1165- and 1236-Å resonance lines.

F. Xenon

Prior to 1962 no data existed on the photoionization cross sections of xenon at wavelengths longer than 1.5 Å. Further, no theoretical treatment of the xenon cross sections has yet been made.

The first measurements of the xenon cross sections were made by Cairns and Weissler (1962) at 760 Å and at 555 Å in a program designed to measure the cross section of Xe^+. Their results on Xe^+ indicated no absorption at 760 Å, while at 555 Å the cross section was approximately 16 Mb.

Cross section measurements from the ionization onset (1022.14 Å) to 600 Å have been made by Huffman *et al.* (1963a), Weissler (1962), Blackwell *et al.* (1964), and G. R. Cook and Metzger (1964). Excellent details of the autoionized lines between the $^2P_{1/2,3/2}$ edges are given in the paper of Huffman *et al.* (see Section H). Extended measurements have been made from the $^2P_{1/2}$ threshold to 280 Å by Samson (1964e) and Rustgi *et al.* (1964). Ederer (1964) contributed measurements from 200 to 80 Å, while Lukirskii *et al.* (1964) measured the cross sections from 165 to 23 Å. The present measurements have been extended to 209 Å. The only gap now existing is between 2.6 and 18.4 Å, namely, the entire M shell. Watanabe (1965) has measured the cross section at 2.59 Å as a result of his measurements on the L edge absorption jump at this wavelength.

Figure 9 shows the present experimental results along with those of Ederer (1964) and Lukirskii *et al.* (1964). The cross section at the $^2P_{1/2}$ threshold is 1685 cm^{-1} (63 Mb). The vertical lines indicate the position of the $5s$-np transition absorption lines as obtained using a flash tube continuum light source with a $2m$ normal incidence spectrograph (Samson, 1964d). The dashed lines also represent absorption lines, which are as yet unclassified. The $5s$-np absorption series are all of the "window" type; that is, they show a large decrease in absorption relative to the ionization continuum background. As in krypton no discontinuity at the O_1 edge was observed. The cross sections continue to decrease toward shorter wavelengths. The data join smoothly onto Ederer's data at the $N_{4,5}$ edge. His data begin to increase at this point reaching a maximum of 30 Mb at approximately 125 Å, then decrease to 2 Mb at 80 Å. This increase in cross section is caused by ejection of the $4d^{10}$ electrons. Cooper (1964) has shown that the $4d^{10}$ subshell should have two maxima in its photoionization cross section analogous to that of the $3p^6$ subshell in argon. These maxima have been observed experimentally as shown in Fig. 9. Figure 10 reproduces Cooper's results for the first maximum in the $4d^{10}$ subshell along with Ederer's experimental curve.

From the onset of excitation of the inner shell electrons at 600 Å many discrete absorption lines exist down to the $N_{4,5}$ edge, due probably to double electron excitations. Recent spectra by Codling and Madden (1964) and

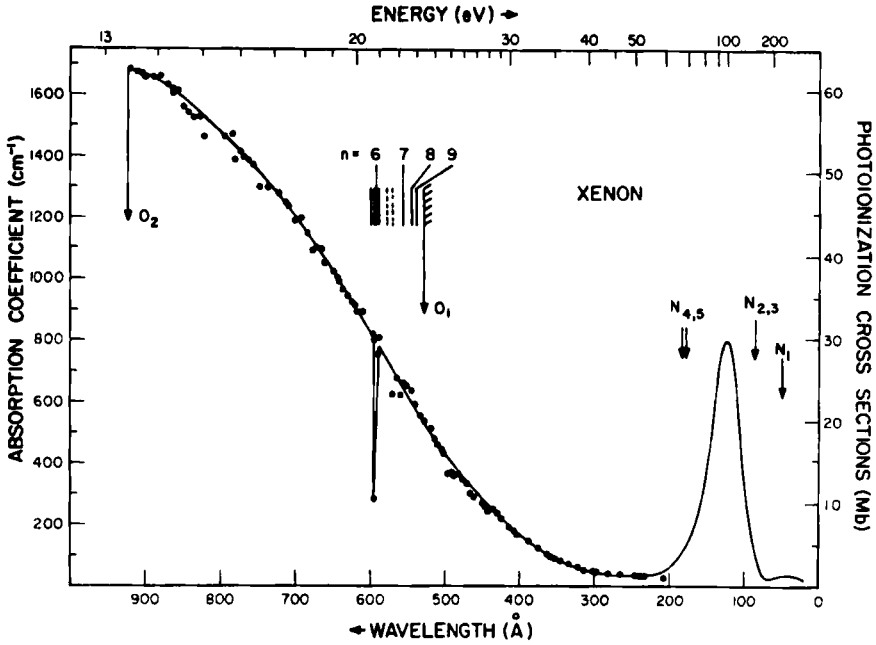

FIG. 9. Photoionization cross sections of xenon. The data of Ederer and Tomboulian increase from the $N_{4,5}$ edge to a maximum of 30 Mb at 130 Å.

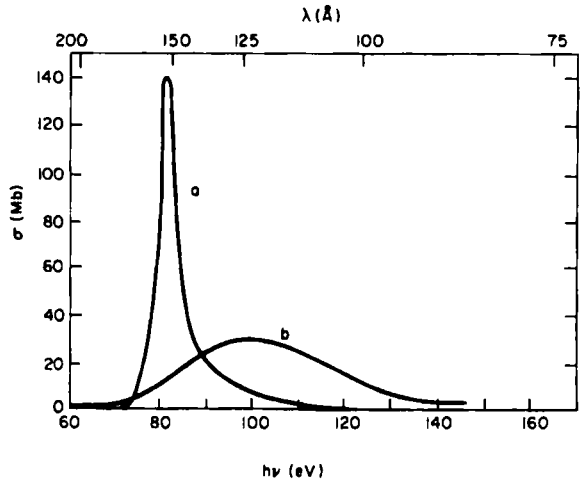

FIG. 10. Theoretical cross sections for ionization of the $5p^6$ electrons in xenon (Cooper, curve *a*) compared to the measurements of the total cross section (Ederer, curve *b*).

Astoin and Kastler (1964) in the vicinity of 200 Å clearly show the absorption series due to excitation of the 4*d* electrons. Two series are observed terminating at the N_4 and N_5 edges, respectively. Again, no abrupt change in absorption is seen on passing over those critical edges. The limits assigned to the two series at 178.33 Å and 183.55 Å by Codling and Madden provide the first experimental values of the critical absorption energies for the N_4 and N_5 edges of xenon, respectively. These values compare favorably with the calculated ones of 188 Å and 191 Å (Hill *et al.*, 1952). Lukirskii *et al.* quote values of 84.7, 180, and 184.5 Å for the N_3, N_4, and N_5 edges, respectively.

The assignment of the above absorption series as 4*d-np* type transitions can be verified on the basis of the discussions given in Section H. Briefly, this assigns a binding energy to electrons in the *np* shells. Adding these binding energies to the observed term values leads to consistent series limits within approximately ± 200 cm^{-1} of each other. On the other hand, if the binding energies of the *nf* electrons are added to the observed terms, the resulting series limits lie within ± 6000 cm^{-1}. Since the *f* orbits are less penetrating the spread in the series limits should be much less than for *p* orbits. That this is not the case verifies the identification of the transition as 4*d-np*. It is of interest to note that, given the series limit, the wavelengths of the 4*d-np* transitions can be readily calculated by the method described in Section H. Using the 183.55-Å series limit quoted by Codling and Madden this technique predicts absorption lines at 190.63, 186.86, and 185.49 Å for $n = 6$, 7, and 8, respectively. These are to be compared with the values observed by Codling and Madden at 190.41, 186.81, and 185.47 Å.

Tables XVII–XIX list all the known cross sections of xenon from 0.01 Å to the ionization threshold. Table XX includes information on the scattering cross sections.

The total continuum oscillator strength for xenon could be measured but for the lack of information regarding the *M* shell. However, if the eighteen electrons in the *M* shell contribute eighteen to f_c, then from the data in Tables XVII–XIX the total continuum oscillator strength is approximately 48. The individual contributions of the various shells are as follows:

$^2P_{3/2}$ *edge to* $^2P_{1/2}$ *edge*	= 0.56
$^2P_{1/2}$ *edge to* O_1 *edge*	= 3.67
O_1 *edge to* N *edge*	= 1.91
N *edge to* M *edge*	= 16.25
M *edge to* L *edge*	= ?
L *edge to* K *edge*	= 6.00
K *edge to* 0.01 *Å*	= 1.57
Total	= 29.96 + M *shell*

The value of the oscillator strength between the $^2P_{3/2}$ and $^2P_{1/2}$ edges is the

average of the experimental values quoted by G. R. Cook and Metzger (1964) and Huffman *et al.* (1963a).

TABLE XVII

XENON ABSORPTION COEFFICIENTS FROM 0.01 TO 165.6 Å

Shell	λ (Å)	Experimental, k (cm^{-1})	Theoretical,[a] k (cm^{-1})	Empirical,[b] k (cm^{-1})
K	0.010	—	—	0.287×10^{-3}
	0.012	—	—	0.318×10^{-3}
	0.015	—	—	0.366×10^{-3}
	0.020	—	—	0.444×10^{-3}
	0.025	—	—	0.536×10^{-3}
	0.030	—	—	0.646×10^{-3}
	0.040	—	—	0.946×10^{-3}
	0.050	—	—	1.39×10^{-3}
	0.060	—	—	2.02×10^{-3}
	0.080	—	—	3.94×10^{-3}
	0.098	8.2×10^{-3} [c]	—	—
	0.100	—	—	6.96×10^{-3}
	0.120	—	—	11.30×10^{-3}
	0.150	—	—	20.65×10^{-3}
	0.175	31.3×10^{-3} [c]	—	—
	0.200	—	—	44.90×10^{-3}
	0.209	44.7×10^{-3} [d]	—	—
	0.247	69.0×10^{-3} [d]	74.4×10^{-3}	—
	0.250	—	—	81.40×10^{-3}
	0.282	103.0×10^{-3} [d]	—	—
	0.300	—	—	129.50×10^{-3}
	0.317	141.0×10^{-3} [d]	142.0×10^{-3}	—
	0.359	—	193.0×10^{-3}	—
L	0.359	—	30.7×10^{-3}	—
	0.423	52.2×10^{-3} [d]	48.0×10^{-3}	—
	0.528	97×10^{-3} [d]	—	—
	0.634	159×10^{-3} [d]	142.0×10^{-3}	—
	0.708	204×10^{-3} [d]	—	—
	0.794	283×10^{-3} [d]	262.0×10^{-3}	—
	0.891	419×10^{-3}	—	—
	1.000	542×10^{-3} [d]	495.0×10^{-3}	—
	1.096	682×10^{-3} [d]	—	—
	1.473	1620×10^{-3} [d]	1400.0×10^{-3}	—
	2.274	3900×10^{-3} [e]	—	—
	2.431	4100×10^{-3} [e]	—	—
	2.593	3000×10^{-3} [e]	—	—
M	2.59	1300×10^{-3} [e]	—	—
	18.40	—	—	—

TABLE XVII (*continued*)

Shell	λ (Å)	Experimental, k (cm^{-1})	Theoretical,[a] k (cm^{-1})	Empirical,[b] k (cm^{-1})
N	18.40	—	—	—
	23.60	24.0[f]	—	—
	31.40	30.2[f]	—	—
	44.40	37.2[f]	—	—
	44.60	39.5[f]	—	—
	58.50	30.2[f]	—	—
	64.35	23.4[f]	—	—
	72.20	26.9[f]	—	—
	81.98	50.1[f]	—	—
	108.65	724.0[f]	—	—
	139.50	724.0[f]	—	—
	165.60	263.0[f]	—	—
	183.55	—	—	—
O	183.55	—	—	—

[a] Woo and Sun (1937-1947).
[b] Victoreen (1949).
[c] Determined from the mass absorption coefficients compiled by Allen (1935).
[d] White (1934).
[e] Watanabe (1965).
[f] Lukirskii *et al.* (1964)

TABLE XVIII

XENON ABSORPTION COEFFICIENTS FROM 80 TO 202 Å[a]

λ (Å)	k (cm^{-1})	λ (Å)	k (cm^{-1})	λ (Å)	k (cm^{-1})	λ (Å)	k (cm^{-1})
80.0	61	125.0	810	164.4	216	192.9	61
83.6	68	138.0	676	166.3	203	194.9	60
85.4	89	139.2	622	168.3	200	195.9	60
90.3	175	140.3	527	171.1	152	200.8	60
91.4	182	145.0	483	172.3	141	202.3	58
96.6	252	145.3	416	173.5	129	203.9	59
97.3	253	147.5	446	178.0	127	207.9	53
99.5	269	149.8	412	181.1	120	209.0	58
101.0	403	151.5	410	182.0	114	213.0	67
105.0	460	154.0	294	182.6	114	214.2	55
106.7	460	156.2	329	184.0	95	215.1	52
110.0	568	158.9	294	185.8	93	220.0	66
116.5	730	162.4	273				

[a] Ederer and Tomboulian (1964b) and Ederer (1964).

TABLE XIX

XENON ABSORPTION COEFFICIENTS FROM THRESHOLD TO 209 Å[a]

λ (Å)	k (cm^{-1})	λ (Å)	k (cm^{-1})	λ (Å)	k (cm^{-1})	λ (Å)	k (cm^{-1})
209.3	30	473.1	336	646.1	1006	870.1	1633
234.8	34	477.4	351	650.8	1025	880.3	1664
240.0	36	482.0	365	661.8	1055	888.0	1661
247.7	35	488.9	359	665.9	1099	902.5	1656
266.3	39	493.8	394	672.6	1109	906.3	1671
283.6	44	497.8	367	677.2	1090	911.6	1674
297.6	48	502.7	434	686.3	1150	920.6	1684
300.2	50	506.8	443	696.2	1201	924.3	1443
303.1	51	510.3	463	701.7	1189	924.9	1392
315.0	59	515.4	486	710.4	1238	928.8	1129
323.0	64	521.0	514	715.6	1250	935.2	1622
335.4	73	528.1	537	722.1	1279	938.5	1695
345.0	84	534.2	558	726.3	1277	941.6	1326
352.0	91	540.7	594	738.5	1296	943.5	1929
358.5	99	546.3	640	746.8	1298	946.9	883
362.9	106	552.9	661	756.4	1371	951.9	2466
374.7	124	557.1	667	762.2	1385	955.9	629
387.5	148	560.4	620	769.1	1395	959.6	1318
405.7	169	566.3	684	776.3	1415	964.4	2416
410.6	185	572.4	627	781.6	1387	969.5	1966
416.6	194	588.0	818	784.9	1474	975.0	650
423.4	214	590.4	759	796.4	1462	979.5	1121
425.8	219	595.9	283	802.3	1482	983.1	1466
429.9	236	596.2	800	805.1	1488	988.1	2240
436.6	253	597.8	819	823.0	1463	991.6	2495
442.8	246	611.5	890	828.5	1530	996.1	3370
447.5	260	620.5	921	836.0	1525	1003.5	413
451.2	270	626.8	932	845.7	1540	1008.5	420
461.3	294	631.7	945	851.5	1561	1015.6	782
463.6	299	638.6	971	858.7	1614	1018.5	937
466.6	302	642.8	994	865.2	1607	1022.14	Threshold

[a] Present data.

An analysis similar to that used for krypton gives approximately 1.5 for the total oscillator strength for the discrete transitions of the $5s^2p^6$ electrons. The experimental results of Anderson (1965) give values of 0.256 ± 0.008 and 0.238 ± 0.015 for the 1470-Å and 1296-Å resonance lines, respectively. Geiger gives a value of 0.263 for the 1470-Å line.

G. CRITICAL ABSORPTION ENERGIES

The critical absorption energy of an atom is the energy required to remove an electron from a given shell within the atom to infinity with zero kinetic

energy. That is, it is an ionization potential of the atom. For the outer electrons these ionization potentials can be determined very accurately by spectroscopic means. However, for inner shell electrons and especially K

TABLE XX

XENON: TOTAL ABSORPTION (σ_t) AND SCATTERING (σ_s) CROSS SECTIONS[a]

Shell	λ (Å)	σ_t (cm^2) ($\times 10^{-23}$)	σ_s (cm^2) ($\times 10^{-23}$)
K	0.089	28.8	3.57
	0.175	116.4	6.50
	0.247	276.0	9.62
	0.317	528.0	13.00
	0.358	720.0	15.10
L	0.358	113.8	15.10
	0.423	179.0	18.60
	0.634	527.0	30.10
	0.794	976.0	39.30
	1.000	1844.0	47.50
	1.473	5210.0	72.80

[a] Woo and Sun (1937–1947)

shell electrons the resonance absorption lines preceding the ionization limit may overlap one another and with the main absorption edge. Thus, it may or may not be possible to observe the true absorption edge and, in fact, many of the reported X-ray critical absorption energies actually represent minimum excitation energies.

If we know the binding energy of the electron in the first excited state of the atom we can determine the true absorption edge by subtracting this binding energy from the observed critical absorption energy. An approximate method for finding the binding energies for s electrons in the rare gases is given in the next section.

Table XXI presents the known critical absorption energies for the rare gases. There is still a lack of experimental data for some absorption edges, thus, the semiempirical values given by Hill *et al.* (1952) are also listed. These values are actually interpolated values obtained after revising the critical X-ray energies tabulated by Siegbahn (1931). The values quoted by Hill have been converted back into angstrom units using the same conversion factor of 1 eV = 12,396.44 $\times$ 10^{-8}cm^{-1}. X-ray absorption energies are usually measured in X-ray units (xu) which are based on the lattice spacing

TABLE XXI

CRITICAL ABSORPTION ENERGIES OF THE RARE GASES EXPRESSED IN ANGSTROM UNITS OF WAVELENGTH

Edge	He		Ne		Ar		Kr		Xe	
	Exp.	Theo.	Exp.	Calc.[d]	Exp.	Calc.[d]	Exp.	Calc.[d]	Exp.	Calc.[d]
K	504.26[a]	504.26[b]	14.298[c]	14.20	3.87147[c]	3.87	0.86555[c]	0.8657	0.3585[c]	0.3588
L_1			255.77[e]	—	43.2[g]	43.0	6.5107[c]	6.46	2.2737[c]	2.27
L_2			572.37[e]	—	50.1880[c]	50.0	7.1822[c]	7.14	2.4307[c]	2.43
L_3			574.93[e]	—	50.5977[c]	51.0	7.4009[c]	7.42	2.5929[c]	2.59
M_1					424.03[e]	—	—	43.0	—	10.9
M_2					777.96[e]	—	56.3475[c]	58.0	13.1737[c]	12.5
M_3					786.72[e]	—	58.7509[c]	59.0	13.1737[c]	13.3
M_4							130.45[f]	130.0	—	18.1
M_5							132.14[f]	130.0	—	18.4
N_1							450.62[e]	—	—	50
N_2							845.42[e]	—	—	80
N_3							885.62[e]	—	84.7[g]	83
N_4									178.33[f]	188
N_5									183.55[f]	191
O_1									529.92[e]	—
O_2									922.75[e]	—
O_3									1022.14[e]	—

[a] Herzberg (1958). The actual value quoted is I.P.(He) = 198,310.82 ± 0.15 cm^{-1}.
[b] Chandrasekhar and Herzberg (1955). The actual value quoted is 198,310.4 ± 2 cm^{-1}.
[c] Cauchois (1955). For the $M_{4,5}$ edge of Kr she quotes 142.488 Å.
[d] Hill *et al.* (1952).
[e] Moore (1949, 1952, 1958).
[f] Codling and Madden (1964).
[g] Lukirskii *et al.* (1964).

of NaCl. At present these x units are 0.202% smaller than the angstrom unit of length (10^{-8} cm). The critical absorption energies for the outer shell electrons were obtained from optical data.

H. Autoionized Energy Levels

The first absorption spectra of the rare gases in the vicinity of their ionization continua were obtained by Beutler (1935). He observed a series of diffuse absorption lines between the $^2P_{3/2}$ and $^2P_{1/2}$ edges in Ar, Kr, and Xe. These absorption lines appeared at higher energies than the first ionization potentials of the atoms. The interaction between these discrete levels and the underlying ionization continuum caused the levels to broaden considerably. In general, a radiationless transition takes place from the discrete levels into the continuum accompanied with the ejection of an electron. When this occurs the states are known as autoionized states. Measurements of the ionization yields within these diffuse states have been made by two methods. One by the direct use of a thermopile to measure the absolute intensity of the ionizing radiation and the other by measuring the yield relative to that of another rare gas. In each case the yield was found to be 100%. Figures 11, 12, and 13 illustrate

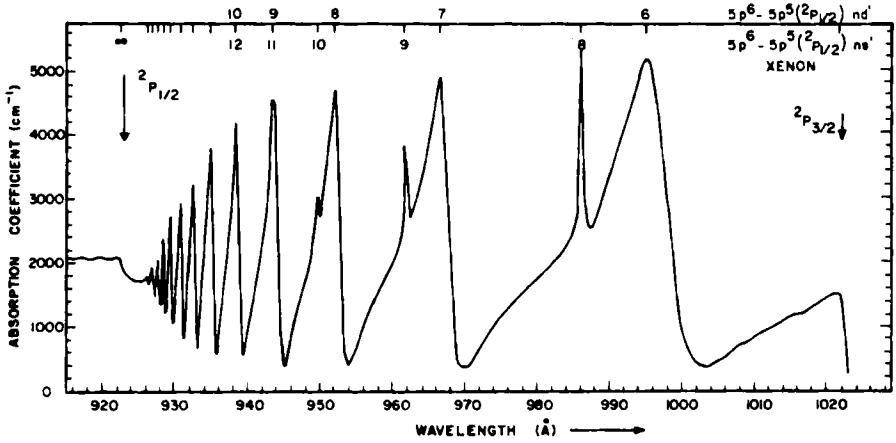

FIG. 11. Beutler autoionized lines of xenon as measured by Huffman *et al.* (1963a).

these Beutler lines in Xe, Kr, and Ar, respectively, as obtained by Huffman *et al.* (1963*a*, *b*) using photoelectric absorption techniques.

Beutler looked for absorption lines associated with the removal of inner *s* electrons without success. Since he used the molecular helium continuum, which provided useful radiation only down to 600 Å, he concluded that if absorption lines exist they must appear at wavelengths below 600 Å. It was

not until 1963, however, when utilizing the continuous radiation from a 180-MeV synchrotron that Madden and Codling (1963) first observed the absorption spectra of the rare gases below 600 Å. Concurrent work on the total absorption cross sections of the rare gases using a densely populated line emission light source and a continuum provided by a flash tube also revealed

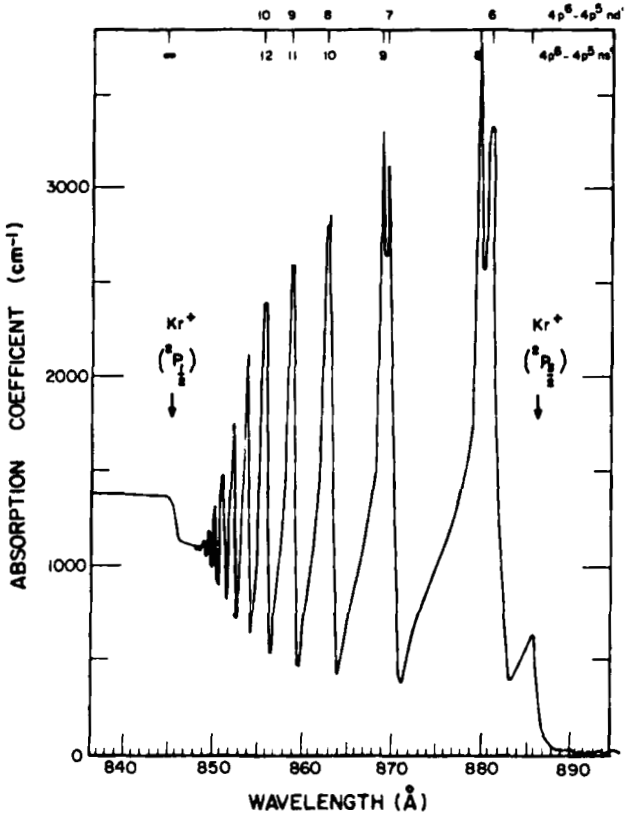

FIG. 12. Beutler autoionized lines of krypton as measured by Huffman *et al.* (1963b).

absorption structure between 400 and 600 Å (Samson, 1963, 1964d). These can be seen in Figs. 14(a), (b), and (c). White indicates emission, while black indicates absorption. The resonance "absorptions" appear as white emission lines. Superimposed on the continuous spectrum are atomic emission lines generated within the flash tube. It was shown that the position of the resonance absorption lines could be predicted on the basis of the similarity between the electron configuration of the rare gases and the alkali metals.

The predicted absorption energies were determined as follows: Consider

the 5*s*-*np* transitions in Xe and the 6*s*-*np* transitions in Cs. In both cases the electrons excited into the vacant *p* shells see an atomic core of charge $Z = 1$ surrounded by a completed subshell of six *p* electrons. It is assumed that the excited electrons in the *np* shells of Cs are bound to their core with the same energies as required for electrons in the *np* shells of Xe. The binding energies

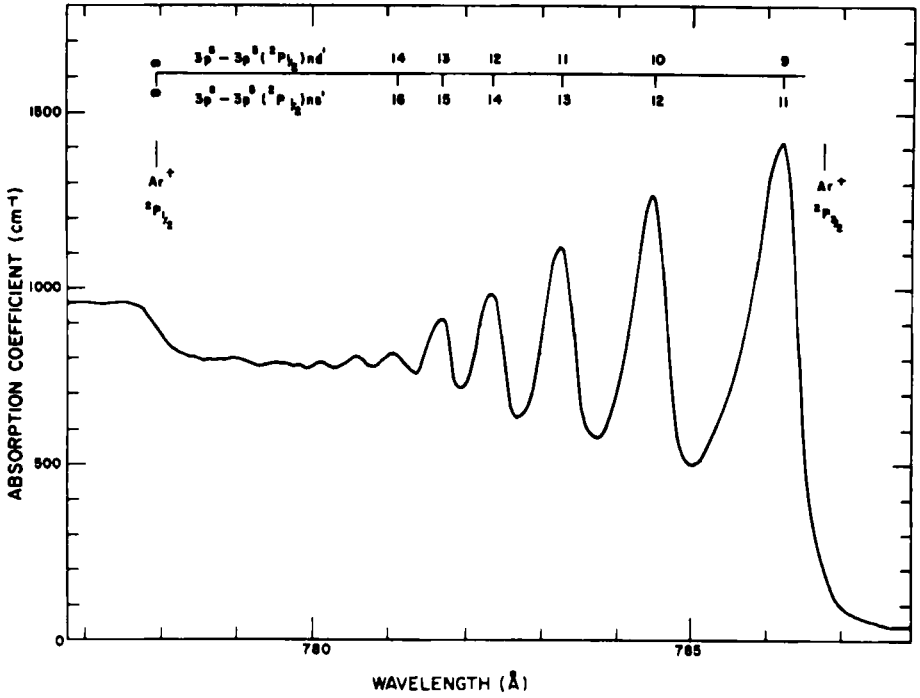

FIG. 13. Beutler autoionized lines of argon as measured by Huffman *et al.* (1963a).

for the *np* electrons in Cs are readily found from known spectroscopic term values. Table XXII lists the binding energies for the *np* shell sin Cs, Na, K, and Rb. Equating these energies to the *np* shell in the rare gases and subtracting them from the ionization potentials of the *s* electrons, the position of the *ms*-*np* absorption series can be found. Table XXIII compares the observed and predicted absorption spectra. The first observed absorption line in Kr and Xe appears to be split into four levels which is compatible with *LS* or *jj* coupling, although not all of the transitions are allowed by the selection rules. In the case of Kr the absorption spectrum obtained by Madden and Codling (1964) clearly shows only three levels, the line at 501.11 Å being absent. In the present spectrum the 501.11-Å line is extremely weak and its appearance was quite sensitive to the Kr pressure in the spectrograph. The first two

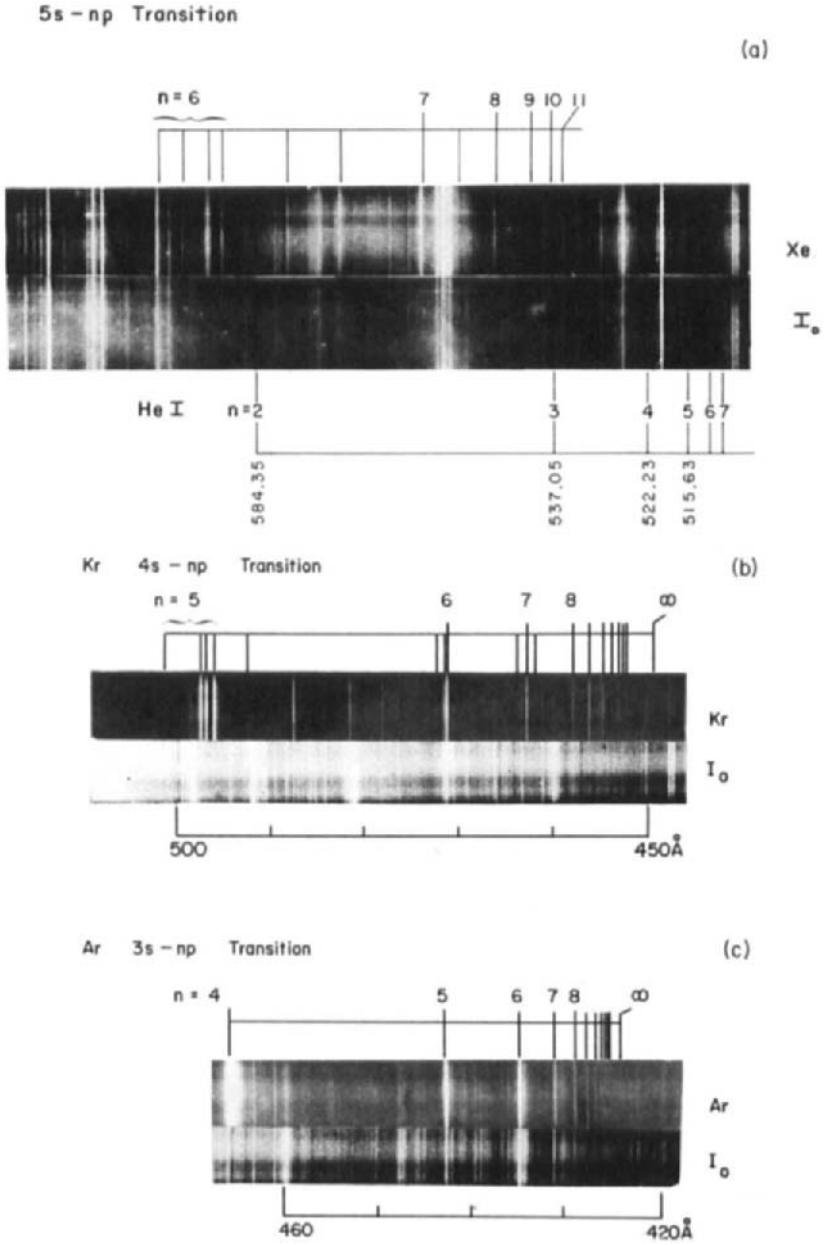

FIG. 14. Spectra showing *ms–np* type transitions in (a) xenon, (*b*) krypton, and (c) argon. The white lines common to both exposures represent discrete emission lines from the flash tube, while the marked lines represent discrete windows in the absorption continuum.

predicted lines in Ar, Kr, and Xe were obtained by using $J = 1/2$ and $3/2$ when determining the binding energies, all other predicted values were found for $J = 1/2$. The agreement between the predicted and observed values is very good with exception of the $8p$ level in krypton. This anomolous term deviates by about 0.8 Å from the expected value, whereas the measurements are accurate to within ± 0.05 Å.

TABLE XXII

BINDING ENERGIES FOR THE VALENCE ELECTRON IN EXCITED p SHELLS OF THE ALKALI METALS[a]

Designation	Binding energies (cm^{-1})			
	Sodium	Potassium	Rubidium	Cesium
$3p$	24,493.47	—	—	—
$4p$	11,182.77	22,024.61	—	—
$5p$	6,409.38	10,308.34	21,112.06	—
$6p$	4,153.14	6,010.49	9,975.83	20,228.47
$7p$	2,909.25	3,939.80	5,855.97	9,641.06
$8p$	2,151.11	2,782.36	3,856.06	5,697.57
$9p$	1,655.12	2,069.44	2,732.08	3,769.42
$10p$	1,312.42	1,599.44	2,037.14	2,679.62

[a] Obtained from optical term values (Moore, 1949, 1952, 1958).

Several unclassified resonances were also observed. In Kr a very faint line, similar to the 501.11-Å line, was observed at 492.47 Å, while in Xe rather strong resonances were observed at 579.25, 570.90, and 552.07 Å. All of these resonances were of the "window" type. In Ar a broad conventional absorption line was observed at 402 Å, while a very narrow absorption line was found at 392 Å. The spectra obtained by Madden and Codling contain many other unclassified discrete lines, some probably due to double electron excitations.

The above method for predicting the absorption series of a rare gas can be applied to the more tightly bound electrons. In fact, it was applied to argon as early as 1926 by Coster and Van der Tuuk (1926) to explain the fine structure in the vicinity of the K absorption edge. Parrat (1939) obtained a more highly resolved K absorption spectrum in argon which clearly resolved the first two members of the $1s$-np series ($n \geq 4$). Using the binding energies for the np shells of potassium and the observed wavelengths of the argon absorption lines, he placed the main absorption edge (i.e., the K ionization potential) at a wavelength position some 4 xu less than its usually accepted measured value.

TABLE XXIII

OBSERVED AND PREDICTED ABSORPTION SPECTRA DUE TO EXCITATIONS OF THE TYPE *ms–np* IN THE RARE GASES (WAVELENGTHS ARE EXPRESSED IN ANGSTROMS)

	Ne *2s–np*		Ar *3s–np*		Kr *4s–np*		Xe *5s–np*	
n	Pred.[a]	Obs.[b]	Pred.[a]	Obs.[c]	Pred.[a]	Obs.[c]	Pred.[a]	Obs.[d]
3	272.86	272.21	—	—	—	—	—	—
4	263.30	263.11	467.71	465.62	—	—	—	—
			467.58	—	—	—	—	—
						501.14		
5	260.03	259.96	443.41	442.79	498.00	497.44	—	—
					497.41	496.85		
						496.00		
								599.95
6	258.51	258.48	435.12	434.86	471.82	471.55	593.54	595.92
							591.60	591.81
								589.62
7	257.68	257.68	431.22	431.07	462.83	462.69	558.45	557.92
8	257.18	257.10	429.09	428.99	458.56	457.85	546.42	546.16
9	256.85	—	427.78	427.70	456.24	456.10	540.72	540.71
10	256.63	—	426.93	426.85	454.79	454.71	537.55	537.40
11	256.47	—	426.33	426.37	453.84	453.71	535.60	535.62
12	—	—	425.90	425.85	453.18	453.14	534.32	—
13	—	—	425.59	425.53	452.71	452.67	—	—
14	—	—	425.34	425.30	452.35	452.32	—	—
15	—	—	425.15	425.12	452.08	452.01	—	—
16	—	—	425.00	424.95	451.87	451.85	—	—
17	—	—	424.88	424.85	—	—	—	—
∞	255.77[a]		424.03[a]		450.62[a]		529.92[a]	

[a] Energy levels used in the calculations were obtained from Moore (1949, 1952, 1958).
[b] Madden and Codling (1963–1965b).
[d] Samson (1964[d]).
[c] Present data.

The *K* absorption spectrum for Kr has been measured by Shaw (1940). No discrete structure due to *1s-np* type transitions was observed. It is possible that the discrete structure cannot be resolved due to their natural width overlapping with each other and with the *K* edge.

I. SUMMARY

The photoionization cross sections of the rare gases have been measured from their ionization thresholds to 200 Å. Published and unpublished data

have been compiled and tabulated. In the case of He, Ne, and Ar the tabulated data provide absorption coefficients continuously from threshold to 0.01 Å. For Kr and Xe cross section measurements are complete except for the *L* shell in Kr and the *M* shell in Xe. Figure 15 summarizes the photoionization cross sections of the rare gases as a function of wavelength. The vertical lines indicate the positions of the "window" type discrete absorption lines.

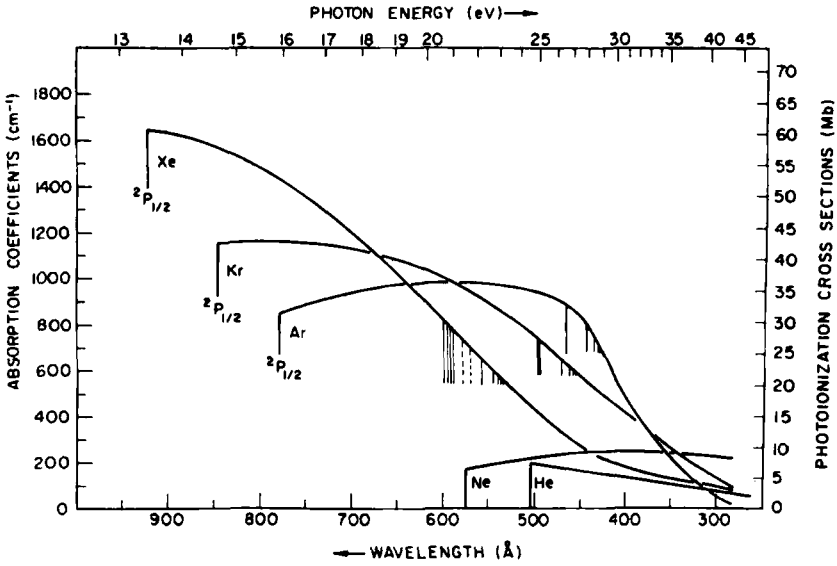

FIG. 15. Photoionization continuum cross sections of the rare gases as a function of wavelength. The vertical lines indicate the positions of the discrete "window" type absorption lines in Ar, Kr, and Xe due to (*ms–np*) type transitions.

On the whole, very little theoretical work has been performed on the photoionization cross sections of the rare gases. Helium has been studied thoroughly and the theoretical results are in excellent agreement with experiment. The theoretical results of neon are also in good agreement with experiment. In the case of argon and krypton only order of magnitude agreement is obtained, while no theoretical treatment of xenon has yet been attempted. Figure 16 shows the absorption coefficients of the rare gases plotted as a function of energy above the $^2P_{\frac{1}{2}}$ threshold. This is perhaps a more convenient plot for comparison with theoretical results. It is of interest to point out that the curves for Ar, Kr, and Xe all intersect at one point approximately 6 eV above the $^2P_{\frac{1}{2}}$ threshold.

The position of previously unknown discrete absorption structure overlying the ionization continuum has been sought and, in many cases, found. Over

and above their importance to atomic structure it is desirable to know the position of the discrete lines, since these are regions to be avoided if possible when using the rare gases in ion chambers for absolute intensity measurements of vacuum ultraviolet radiation.

The oscillator strengths for excitations into the photoionization continuum have been discussed. It has been shown, in the case of helium, that knowledge of the total continuum oscillator strength in conjunction with the Thomas–

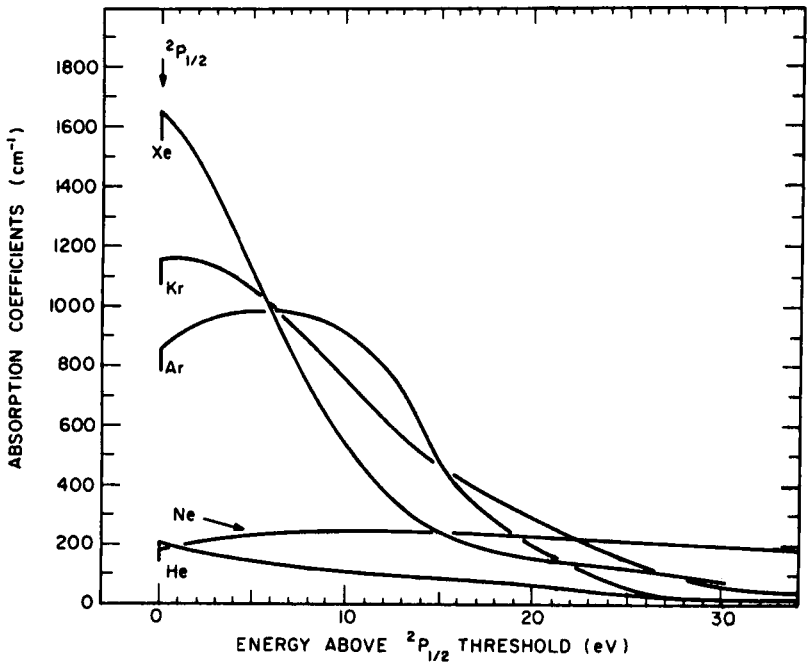

FIG. 16. Photoionization absorption coefficients vs energy above the $^2P_{1/2}$ threshold.

Kuhn sum rule provides immediately the total discrete f values. For this approach, however, it is necessary to know the values of the absorption coefficients to a high degree of accuracy. For helium an uncertainty of $\pm 5\%$ in the value of the absorption coefficients will give an uncertainty of $\pm 17\%$ for the total discrete oscillator strength.

A summary of the continuum f values is given in Table XXIV. These values refer to the total contribution by the continuum for energies lying between the absorption edges. For example, the contribution to the f value between the onset for L-shell ionization and K-shell ionization is listed under L. Although the absorption will be due primarily to L-shell ionization small contributions will occur from the M, N shells, etc., while contributions for

TABLE XXIV

SUMMARY OF THE CONTINUUM OSCILLATOR STRENGTHS FOR THE RARE GASES

Gas	Continuum f values					Σf_c	Theoretical total, $\Sigma f_c + \Sigma f_{\text{lines}} = Z$
	K	L	M	N	O		
He	1.54	—	—	—	—	1.54	2
Ne	1.81	7.60	—	—	—	9.41	10
Ar	1.77	7.51	6.87	—	—	16.15	18
Kr	1.63	—	17.70	6.40	—	25.73 + L shell	36
Xe	1.57	6.00	—	16.25	6.14	29.96 + M shell	54

energies greater than the K edge will not be included. For the K shell the f values were evaluated down to 0.01 Å. The contributions to the outermost shells include the f values of the Beutler lines.

III. Atomic Oxygen, Nitrogen, and Hydrogen

A. Experimental Procedure

1. Atom Production

The partial dissociation of molecules can be accomplished by passing the molecular gas through a discharge. Microwave or radio frequency discharges are the most commonly used methods for atom production. The degree of dissociation depends on many factors, however, it is generally only a few percent in oxygen and nitrogen, increasing perhaps to 30 or 40% in hydrogen.

Dissociation is enhanced by the presence of small amounts of certain impurities. For oxygen a trace of N_2, H_2, or H_2O can increase dissociation from 5% to about 10%, or with a 1% impurity of sulphur hexafluoride the dissociation increases to ~25%. The use of purified O_2 with liquid nitrogen traps upstream of the discharge will produce very little dissociation, perhaps 1–2%. For each of the molecules the degree of dissociation increases when the gas is mixed with either argon or helium. A mixture of four parts of helium to one part oxygen has produced 15 to 20% dissociation. Although the actual atom concentration will go down, the per cent dissociation will increase as the ratio of helium to molecular gas increases. Dissociation also increases, although not linearly, with the power dissipated within the discharge. Figure 17 shows a schematic diagram of the apparatus used by Cairns and Samson (1965) for the production and cross section measurements of atomic oxygen.

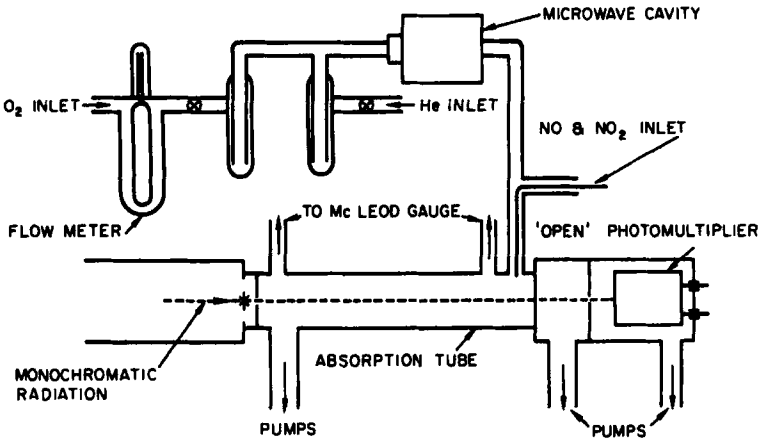

FIG. 17. Apparatus for the production and cross section measurements of atomic oxygen.

2. Atom Concentration

A general instrument for the measurement of atom concentrations is the Wrede–Harteck gauge (Wrede, 1928; Harteck, 1928). This gauge consists of a small volume separated from the discharged gas by a small hole ($\sim 50\ \mu$). The atoms will diffuse through the hole faster than the molecules, however, once the atoms enter the small volume they rapidly recombine due to the presence of an efficient catalyst, such as silver foil. Thus, no atoms diffuse back into the main volume and a pressure differential is setup. This pressure difference can be measured readily by a differential micromanometer (D. B. Cook and Danby, 1953; Beynon and Cairns, 1964). If p is the pressure of the discharged gas and Δp the pressure differential across the hole, then the fraction α of atomic species is given by

$$\alpha = 3.41\ \Delta p/p. \tag{5}$$

Another method for measuring the concentration of atomic oxygen is the NO_2 titration method. The addition of NO_2 to the discharged gas (see Fig. 17) produces the very fast reaction

$$O + NO_2 \rightarrow NO + O_2, \tag{6}$$

the NO then reacts to produce a chemiluminescent white glow by the slower reaction

$$O + NO \rightarrow NO_2 + h\nu. \tag{7}$$

A bright glow is observed as long as O atoms are present in excess, because reaction (6) rapidly produces an equivalent amount of NO. When the flow of NO_2 is just equal to that of the O atoms, the glow is sharply extinguished.

Thus, knowing the NO_2 flow rate, the O atom concentration can be determined.

Harteck *et al.* (1958) and Kistiakowsky and Volpi (1957) have discussed the NO titration technique for the measurement of atomic nitrogen concentrations. The principle of the method is as follows: On addition of NO to the discharged N_2 the very rapid reaction

$$NO + N \rightarrow N_2 + O \tag{8}$$

occurs. When the NO is in excess and all the N atoms are consumed, the secondary reaction (7) takes place giving the characteristic white afterglow. If, however, insufficient NO is present the N atoms react with the atomic oxygen to form NO in excited states. The NO* produces a characteristic blue color. Thus, at the point when the white glow fades and the blue color appears the N atom concentration is just equal to that of the nitric oxide.

References to the considerable amount of work done on atom production and concentration measurements can be found in articles by Kaufman (1961) and by Morse and Kaufman (1965).

The use of tungsten furnaces can produce almost complete dissociation of H_2 within a practical range of temperatures (Duffendack, 1922; Compton, 1922). These furnaces have been used in atomic beam studies and a description of their construction is given by Lamb and Retherford (1950), in addition to the authors cited above.

The fractional dissociation, X, as quoted by Lamb and Retherford, is given by

$$X^2/(1 - X) = K(T)/P, \tag{9}$$

where P is the total pressure (in atmospheres) of the atomic and molecular hydrogen and X is the ratio of the partial pressure of atomic hydrogen to P. The equilibrium constant $K(T)$ is given in atmospheres as a function of the absolute temperature by the equation

$$\log_{10}K = -21200/T + 1.765 \log_{10}T - 9.85 \times 10^{-5}T - 0.265, \tag{10}$$

provided thermal equilibrium exists. Figure 18 shows X in per cent as a function of temperature for pressures of 7.6, 76, and 760 μ. At the lower pressures the degree of dissociation is much greater for a given temperature. The tungsten furnaces are capable of reaching 2800°K, at which temperature total dissociation should occur for pressures less than 100 μ.

The major problem in measuring the absorption cross sections of atoms which are not normally in the free state is in the production of sufficient numbers of atoms free from excited atomic and molecular states. The general equation describing the absorption of radiation by a mixture of gases is given by

$$I = I_0 \exp -(n_1\sigma_1 + n_2\sigma_2 + \cdots)L, \tag{11}$$

where n_1, n_2, ... refer to the number densities of the various species whose cross sections are σ_1, σ_2, ... etc. It is desirable, of course, to keep the number of species to a minimum and to know the actual number densities of those present. This is certainly not always possible, thus, experiments must be

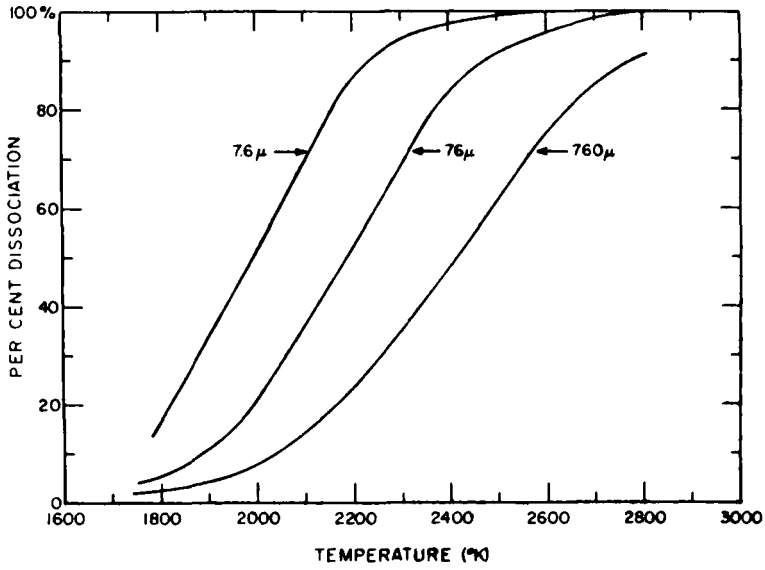

FIG. 18. The degree of dissociation of H_2 expressed as the ratio of the partial pressures of H to (H + H_2).

designed to provide a sufficient number of independent equations relating the unknowns to measurable quantities. This is illustrated for the case of atomic oxygen (Cairns and Samson, 1965). Passing molecular oxygen through a microwave discharge produces atomic oxygen in the ground ^3P state, molecular oxygen in the ground $^3\Sigma_g^-$ state, and excited O_2 in the $^1\Delta_g$ state. These are the three major constituents of the discharged gas. The oxygen atoms can be preferentially removed if the discharged gas is made to pass over a catalytic probe of mercuric oxide. Thus, the measurement of the attenuation of the incident radiation is programed as follows:

(*a*) No discharge, $O_2(^3\Sigma_g^-)$
(*b*) Discharge with mercuric oxide probe, $O_2(^3\Sigma_g^-)$, $O_2^*(^1\Delta_g)$
(*c*) Discharge, $O_2(^3\Sigma_g^-)$, $O_2^*(^1\Delta_g)$, $O(^3P)$.

This procedure results in a set of equations, such as Eq. (11), from which the atomic oxygen cross section can be calculated.

B. Oxygen (I.P. 910.443 Å)

The first theoretical estimate of the continuous absorption cross sections for atomic oxygen was made by Bates *et al.* (1939) using the relation between emission and absorption cross sections. A more precise calculation at the spectral head was carried out by Bates and Seaton (1949). They obtained a value of 2.6 Mb. The approximate calculations of Dalgarno and Parkinson (1960) have been superseded by the more accurate calculations of Dalgarno *et al.* (1964). They have computed, using both the dipole length and velocity approximations, the cross sections for the individual transitions

$$O(1s^2\ 2s^2\ 2p^4)^3P + h\nu \rightarrow O^+(1s^2\ 2s^2\ 2p^3)^4S^0, {}^2D^0, {}^2P^0 + e^-$$

and

$$O(1s^2\ 2s^2\ 2p^4)^3P + h\nu \rightarrow O^+(1s^2\ 2s\ 2p^4)^4P, {}^2P, + e^-$$

over the spectral range from threshold (910.443 Å) to the K edge (23.3 Å). Figure 19 shows their theoretical values plotted as a function of wavelength and compared with the experimental values of Cairns and Samson (1965). The theoretical values were estimated by Dalgarno *et al.* to be accurate within $\pm 25\%$, while the error in the measured values was estimated to be $\pm 30\%$. Most of the measured values agree with theory within the respective error limits, however, there appears to be a real discrepancy at a few points. The discrepancies can be explained as being due to autoionized structure superimposed on the ionization continuum. The theoretical calculations did not take into account the perturbing effects of discrete energy levels at wavelengths shorter than the ionization threshold. It is difficult to predict the effect of these perturbations; however, in general if a radiationless transition takes place between the discrete levels and the adjacent continuum, considerable broadening of the absorption lines occurs. Some excellent examples are shown in Section V in addition to those observed in the rare gases.

Numerous discrete absorption series terminating in the ${}^2D^0$ and ${}^2P^0$ states of the ion are permitted by the selection rules (Herzberg, 1944). Many of these series conform to the selection rules governing autoionization; namely, the continuum and discrete states must have the same J, L, S, and parity. Transitions which can autoionize into the ${}^4S^0$ continuum are

$$2p^4\ {}^3P \rightarrow 2p^3({}^2D^0)ns\ {}^3D^0$$

$$\rightarrow 2p^3({}^2D^0)nd\ {}^3S^0, {}^3D^0,$$

while autoionization transitions into the ${}^2D^0$ continuum are

$$2p^4\ {}^3P \rightarrow 2p^3({}^2P^0)nd\ {}^3D^0, {}^3P^0.$$

None of these autoionization transitions has yet been observed; however,

it is to be expected that the photoionization cross section of atomic oxygen will be modified by such transitions into the ^4S and ^2D continua. In the experimental work of Cairns and Samson a line emission light source was used and data were obtained only at the most intense lines. Thus, although discrete structure is indicated by their results the position of maximum absorption and line profiles cannot be inferred.

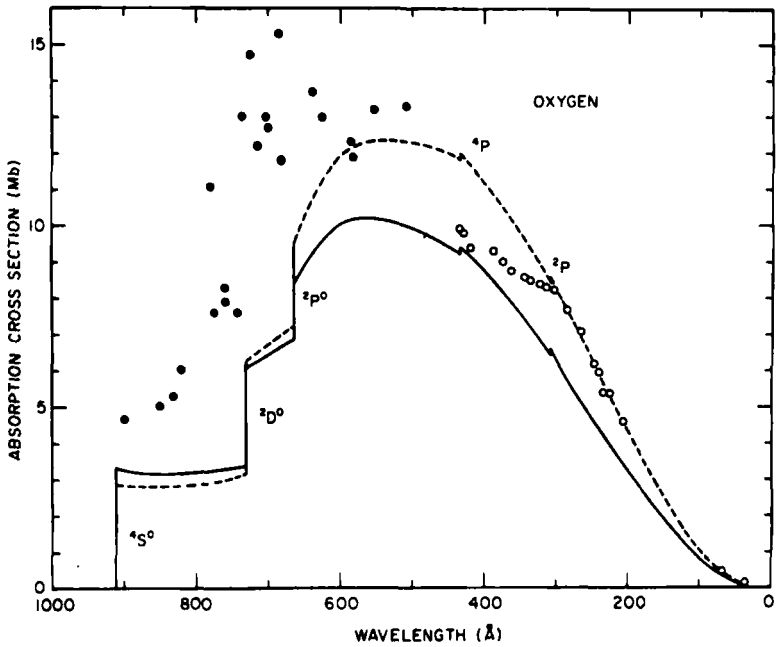

FIG. 19. Atomic oxygen absorption cross section. Solid line represents the dipole velocity approximation and the broken line the dipole length approximation (after Dalgarno *et al.*, 1964). Direct measurements of $\sigma(O)$ are represented by the solid points while the open points represent values of $\frac{1}{2}\sigma(O_2)$.

No other experimental data exist on the direct measurements of the atomic cross sections. At very high photon energies, however, the atomic cross sections might be expected to be approximately one-half of the molecular cross sections. In the X-ray region molecular cross section data have been compiled by Allen (1935). Between 200 and 435 Å, molecular cross sections have been measured by Weissler and Lee (1952) and by Samson and Cairns (1965). Although numerous measurements have been reported at wavelengths longer than 435 Å, these cannot be considered as being related to the atomic cross section since the photons interact with the outer electrons which are directly involved in the chemical bond. Wavelengths shorter than 435 Å are

sufficiently energetic to eject an inner 2*s* electron from the atom provided the binding energy of the electron is not modified when the atoms are bound together.

The values of $\frac{1}{2}\sigma(O_2)$ are shown in Fig. 19. Excellent agreement with the dipole length approximation is obtained from 44 to 310 Å. The sudden discontinuity at 310 Å, coinciding with the ^2P edge of the ion, suggests that in fact the molecular cross sections are related to the atomic cross sections at these and shorter wavelengths.

TABLE XXV

THEORETICAL PHOTOIONIZATION CROSS SECTIONS OF ATOMIC OXYGEN[a]

	σ (Mb)			σ (Mb)	
λ (Å)	*DL*	*DV*	λ (Å)	*DL*	*DV*
910.443	2.7	3.4	500	12.3	9.9
900.0	3.0	3.3	475	12.1	9.7
850.0	2.7	3.1	450	11.9	9.5
800.0	2.9	3.2	435	11.7	9.2
750.0	3.1	3.4			
731.7	3.2	3.4	435	11.8	9.3
			400	11.2	8.7
731.7	6.4	6.1	350	9.8	7.6
700.0	7.0	6.5	310	8.5	6.4
665.3	7.6	6.9			
			310	8.6	6.6
665.3	9.6	8.4	300	8.2	6.3
650	10.3	9.0	250	6.3	4.6
625	11.3	9.6	200	4.3	3.2
600	11.9	10.0	150	2.4	1.7
575	12.2	10.1	100	0.9	0.7
550	12.3	10.1	75	0.4	0.3
525	12.3	10.0	50	0.1	0.1

[a] Dalgarno *et al.* (1964).

The theoretical cross sections of Dalgarno *et al.* are tabulated in Table XXV. The experimental atomic cross sections are given in Table XXVI. Since these measurements were made with an instrumental resolution of 1.8 Å, several source emission lines were included at many points. The unresolved lines are bracketed. Table XXVII lists $\frac{1}{2}\sigma(O_2)$ for wavelengths between 200 and 435 Å, while Table XXVIII lists the cross sections from 0.01 to 68 Å. Finally, Table XXIX tabulates the theoretical scattering and absorption

TABLE XXVI

ABSORPTION CROSS SECTION OF ATOMIC OXYGEN[a]

λ (Å)	σ (Mb)	λ (Å)	σ (Mb)
508.434 Ar III 508.595 Ar III	13.3	725.542 Ar II	16.7
551.371 Ar VI	13.2	735.89 Ne I	14.3
584.331 He I	11.9	743.70 Ne I	7.6
585.754 Ar VII	12.3	758.677 O V 759.440 O V 760.229 O V 760.445 O V 761.130 O V 762.001 O V	8.3
624.617 O IV 625.130 O IV 625.852 O IV	13.0		
636.818 Ar III 637.282 Ar III	13.7	760.439 Ar IV	7.9
683.278 Ar IV	11.8	774.522 O V	7.6
684.996 N III 685.513 N III	17.3	779.821 O IV 779.905 O IV	11.1
685.816 N III		822.159 Ar V	6.0
686.335 N III 699.408 Ar IV 700.277 Ar IV	12.7	832.754 O II 832.927 O III 833.326 O II	5.3
702.332 O III 702.822 O III 702.899 O III	13.0	833.742 O III 834.462 O II	
703.850 O III 715.599 Ar V 715.645 Ar V	12.2	850.602	5.0
		901.168 Ar IV 901.804 Ar IV	4.7
		910.443 Threshold	—

[a] Cairns and Samson (1965).

TABLE XXVII

ABSORPTION CROSS SECTIONS OF OXYGEN ASSUMING $\sigma(O) = \frac{1}{2}\sigma(O_2)$[a]

λ (Å)	$\frac{1}{2}\sigma(O_2)$ (Mb)	λ (Å)	$\frac{1}{2}\sigma(O_2)$ (Mb)
209.3	4.5	323.6	8.4
225.2	5.3	335.1	8.4
234.2	5.3	345.1	8.5
239.6	6.0	362.9	8.8
247.2	6.2	374.4	9.0
266.3	7.0	387.4	9.3
283.5	7.6	428.2	9.7
303.1	8.7	434.3	9.8
314.9	8.2		

[a] Samson and Cairns (1965).

TABLE XXVIII

OXYGEN ABSORPTION CROSS SECTIONS FROM 0.01 TO 68Å

Shell	λ (Å)	Experimental,[a] $\sigma(0) = \frac{1}{2}\sigma(O_2)$ (Mb)	Semiempirical, σ(O) (Mb)	Shell	λ (Å)	Experimental,[a] $\sigma(O) = \frac{1}{2}\sigma(O_2)$ (Mb)	Semiempirical, σ(O) (Mb)
K	0.01	—	1.52×10^{-6} [b]	*K (cont.)*	1.389	2.15×10^{-4}	—
	0.02	—	2.11×10^{-6} [b]		1.540	2.97×10^{-4}	—
	0.03	—	2.50×10^{-6} [b]		1.934	5.84×10^{-4}	—
	0.04	—	2.80×10^{-6} [b]		2.50	1.21×10^{-3}	—
	0.05	—	3.02×10^{-6} [b]		3.57	3.99×10^{-3}	—
	0.06	—	3.24×10^{-6} [b]		4.36	6.86×10^{-3}	—
	0.064	3.45×10^{-6}	—		5.17	1.10×10^{-2}	—
	0.072	3.64×10^{-6}	—		6.97	2.59×10^{-2}	—
	0.080	—	3.56×10^{-6} [b]		8.32	4.22×10^{-2}	4.10×10^{-2} [c]
	0.098	3.83×10^{-6}	—		9.87	7.12×10^{-2}	—
	0.100	—	3.83×10^{-6} [b]		13.37	1.45×10^{-1}	1.44×10^{-1} [c]
	0.13J	4.16×10^{-6}	—		17.67	2.65×10^{-1}	2.86×10^{-1} [c]
	0.175	4.50×10^{-6}	—		21.7	—	4.40×10^{-1} [c]
	0.200	4.87×10^{-6}	5.02×10^{-6} [b]		23.3	—	—
	0.260	5.58×10^{-6}	—				
	0.417	9.89×10^{-6}	—	*L*	23.3	—	—
	0.497	1.38×10^{-5}	—		23.7	—	2.6×10^{-2} [c]
	0.631	2.39×10^{-5}	—		27.4	—	3.9×10^{-2} [c]
	0.710	3.23×10^{-5}	—		31.6	—	4.3×10^{-2} [c]
	0.880	5.84×10^{-5}	—		36.3	—	8.4×10^{-2} [c]
	1.000	8.36×10^{-5}	8.75×10^{-5} [b]		44.6	1.54×10^{-1}	—
	1.235	1.52×10^{-4}	—		68.0	4.30×10^{-1}	—

[a] Determined from the mass absorption coefficients compiled by Allen (1935).
[b] Victoreen (1949).
[c] Henke (1957).

cross sections of Woo and Sun (1937–1947) for wavelengths between 0.064 and 8.32 Å.

TABLE XXIX

OXYGEN: TOTAL ABSORPTION (σ_t) AND SCATTERING (σ_s) CROSS SECTIONS[a]

Shell	λ (Å)	σ_t (Mb)	σ_s (Mb)
K	0.064	3.1×10^{-6}	3.1×10^{-6}
	0.098	3.7×10^{-6}	3.6×10^{-6}
	0.130	4.1×10^{-6}	4.0×10^{-6}
	0.260	5.8×10^{-6}	4.9×10^{-6}
	0.417	1.00×10^{-5}	5.7×10^{-6}
	0.631	2.27×10^{-5}	6.9×10^{-6}
	0.710	3.04×10^{-5}	7.4×10^{-6}
	1.000	7.70×10^{-5}	9.2×10^{-6}
	1.235	1.42×10^{-4}	1.09×10^{-5}
	1.540	2.74×10^{-4}	1.31×10^{-5}
	1.934	5.43×10^{-4}	1.60×10^{-5}
	2.500	1.18×10^{-3}	1.99×10^{-5}
	3.570	3.42×10^{-3}	2.77×10^{-5}
	5.170	9.97×10^{-3}	3.98×10^{-5}
	6.970	2.414×10^{-2}	5.08×10^{-5}
	8.320	4.069×10^{-2}	5.71×10^{-5}

[a] Woo and Sun (1937–1947).

C. NITROGEN (I.P. 852.188 Å)

Ehler and Weissler (1955) have measured the relative cross sections of discharged nitrogen. Using a Philips Ionization Gauge type discharge they measured the attenuation of the incident radiation a few milliseconds after the discharge was shut off. However, since the concentrations of the various species were unknown, they were only able to guess at the probable atomic nitrogen cross section. Assuming the N-atom concentration to be 25% and that no species other than N_2 were present, they estimated that $\sigma(N) \sim$ 12.8 Mb at 650 Å. This is about a factor of four greater than the theoretical results of Dalgarno and Parkinson (1960).

Bates and Seaton (1949) calculated the cross section at the spectral head using both the dipole length and velocity approximations obtaining 10.2 and 7.7 Mb, respectively. Using a more approximate treatment based on the dipole length formulation they computed the variation in cross section with wavelength, neglecting the absorption due to the inner shell electrons.

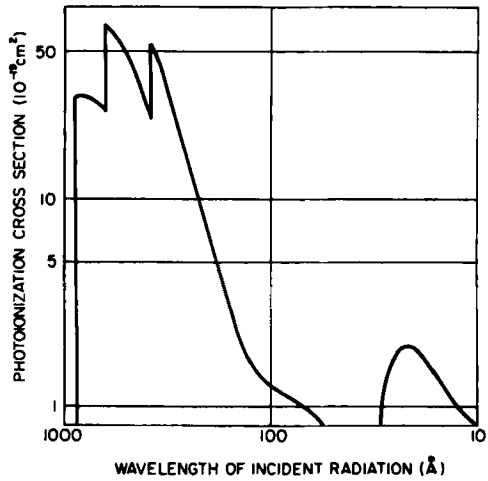

FIG. 20. Theoretical photoionization cross section of atomic nitrogen (after Dalgarno and Parkinson, 1960).

Dalgarno and Parkinson modified the approximate treatment described by Bates (1946a) to include the dipole velocity formulation, and used this treatment to extend the calculations to shorter wavelengths. Their calculations also took into account absorption by the 2*s* electrons. The theoretical cross sections are reproduced in Fig. 20. In general, the dipole length approximation is preferred at the spectral head, while the velocity approximation is considered more reliable at shorter wavelengths.

TABLE XXX

ABSORPTION CROSS SECTIONS OF NITROGEN ASSUMING $\sigma(N) = \frac{1}{2}\sigma(N_2)$[a]

λ (Å)	$\frac{1}{2}\sigma(N_2)$ (Mb)	λ (Å)	$\frac{1}{2}\sigma(N_2)$ (Mb)
209.3	3.2	358.5	7.9
247.2	4.9	362.9	8.1
266.3	5.3	374.4	8.7
283.5	5.5	387.4	9.3
297.6	5.8	428.2	11.0
303.1	5.8	434.3	11.2
314.9	6.2	452.2	11.3
323.6	6.6	463.7	11.3
335.1	7.0	508.2	11.4
345.1	7.4	512.1	11.6

[a] Samson and Cairns (1965).

TABLE XXXI

NITROGEN ABSORPTION CROSS SECTIONS FROM 0.01 TO 68 Å

Shell	λ (Å)	Experimental,[a] $\sigma(N) = \frac{1}{2}\sigma(N_2)$ (Mb)	Semiempirical, $\sigma(N)$ (Mb)	Shell	λ (Å)	Experimental,[a] $\sigma(N) = \frac{1}{2}\sigma(N_2)$ (Mb)	Semiempirical, $\sigma(N)$ (Mb)
K	0.01	—	1.32×10^{-6} [b]	*K (cont.)*	3.57	2.23×10^{-3}	—
	0.02	—	1.84×10^{-6} [b]		4.36	3.86×10^{-3}	—
	0.03	—	2.18×10^{-6} [b]		5.17	6.34×10^{-3}	—
	0.04	—	2.45×10^{-6} [b]		6.97	1.50×10^{-2}	—
	0.05	—	2.64×10^{-6} [b]		8.32	2.58×10^{-2}	2.44×10^{-2} [c]
	0.06	—	2.83×10^{-6} [b]		9.87	4.17×10^{-2}	—
	0.08	—	3.10×10^{-6} [b]		13.37	8.91×10^{-2}	8.80×10^{-2} [c]
	0.098	3.32×10^{-6}	—		17.67	1.62×10^{-1}	1.84×10^{-1} [c]
	0.100	—	3.32×10^{-6} [b]		21.7	—	3.05×10^{-1} [c]
	0.200	—	4.20×10^{-6} [b]		23.7	—	3.80×10^{-1} [c]
	0.710	2.02×10^{-5}	—		27.4	—	5.23×10^{-1} [c]
	0.880	3.46×10^{-5}	—		31.1	—	—
	1.000	4.90×10^{-5}	5.12×10^{-5} [b]				
	1.235	9.18×10^{-5}	—	*L*	31.1	—	—
	1.389	1.28×10^{-4}	—		31.6	—	3.35×10^{-2} [c]
	1.540	1.72×10^{-4}	—		36.3	—	4.85×10^{-2} [c]
	1.934	3.25×10^{-4}	—		44.6	8.88×10^{-2}	8.45×10^{-2} [c]
	2.50	6.74×10^{-4}	7.2×10^{-4} [b]		68.0	2.53×10^{-1}	—

[a] Determined from the mass absorption coefficients compiled by Allen (1935).
[b] Victoreen (1949).
[c] Henke (1957).

The experimental values of $\frac{1}{2}\sigma(N_2)$ from 200 to 500 Å are tabulated in Table XXX. There are no theoretical grounds to expect that these cross sections should be approximately equal to $\sigma(N)$ other than that they are energetic enough to penetrate into the L_1 subshell of the atom. However, owing to the lack of experimental data, these values may give an approximate idea of the magnitude to be expected. Table XXXI lists $\frac{1}{2}\sigma(N_2)$ from 0.01 to 68 Å.

D. Hydrogen (I.P. 911.754 Å)

The theoretical formula for the photoionization cross section of atomic hydrogen is expected to be precise. Exact calculations on hydrogen-like systems have been made by Sugiura (1927), Gaunt (1930), and Menzel and Pekeris (1935). The cross section is given by

$$\sigma = g(32\pi^2 e^6 R)/(3^{3/2} h^3 \nu^3 n^5); \tag{12}$$

that is,

$$\sigma \quad (\text{Mb}) = 1.044 \times 10^{-8} g\lambda^3 \quad (\text{Å}), \tag{13}$$

where R is the Rydberg constant, n is the principal quantum number, and g is the Gaunt factor which is a function of the frequency ν. If we set $g = 1$ in Eq. (12), $\sigma(H)$ reduces to that given by Kramers (1923). The Gaunt factors vary from 0.8 at threshold to a maximum of 1.0 at approximately 200 Å, then fall rapidly to extremely low values in the X-ray region. Using the Gaunt factors tabulated by Karzas and Latter (1961) and Eq. (13), the theoretical photoionization cross sections for atomic hydrogen have been obtained and are shown in Fig. 21 as a function of wavelength. The values are tabulated in Table XXXII.

TABLE XXXII

Theoretical Cross Section of Atomic Hydrogen

λ(Å)	σ(Mb)	λ(Å)	σ(Mb)	λ(Å)	σ(Mb)	λ(Å)	σ(Mb)
1	2.09×10^{-8}	40	5.39×10^{-4}	300	2.78×10^{-1}	700	3.10
2	2.28×10^{-8}	50	1.10×10^{-3}	350	4.36×10^{-1}	750	3.74
4	2.51×10^{-8}	75	4.02×10^{-3}	400	6.43×10^{-1}	800	4.46
6	9.87×10^{-7}	100	9.92×10^{-3}	450	9.01×10^{-1}	850	5.26
8	2.62×10^{-6}	150	3.47×10^{-2}	500	1.22×10^{-1}	900	6.12
10	5.55×10^{-6}	200	8.33×10^{-2}	550	1.59×10^{-1}	911.753	6.31
20	5.56×10^{-5}	250	1.62×10^{-1}	600	2.02×10^{-1}	Threshold	
30	2.10×10^{-4}			650	2.53×10^{-1}		

The only experimental verification of Eq. (12) is the measurement at 850.6 Å by Beynon and Cairns (1965). Using a 200-W rf discharge at 11 Mc/sec they dissociated approximately 40% of the molecular hydrogen. A Wrede–Harteck gauge was used to determine the atom concentration. The experimental value of 5.15 Mb is in very good agreement with the theoretical value of 5.26 Mb.

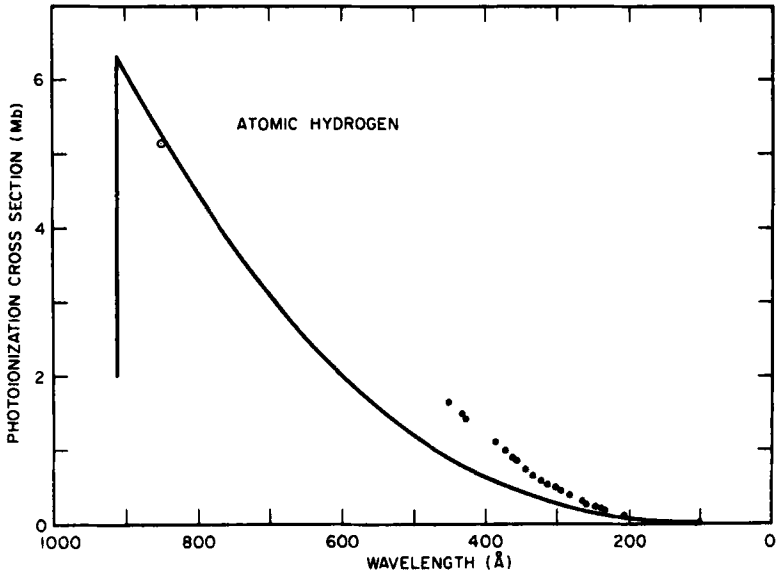

FIG. 21. Theoretical photoionization cross section of atomic hydrogen (solid line). Experimental points: ○, Beynon and Cairns (1965); ● [$\frac{1}{2}\sigma(H_2)$], Samson and Cairns (1965).

The cross sections for molecular hydrogen have been measured between 200 and 450 Å. These values, divided by two, are also shown in Fig. 21. On the average they are about a factor of two greater than the theoretical values. This disagreement is not too surprising since there are no inner shell electrons in hydrogen and the two electrons are involved in the molecular bond. $\frac{1}{2}\sigma(H_2)$ is still about a factor of two greater than $\sigma(H)$ at 44 Å. However, to shorter wavelengths the ratio rapidly increases until at 1 Å it is about 37:1. It is possible that this change in ratio is caused by the increased scattering cross section, which is not taken into account by Eq. (12). Thus, although theory predicts the cross section for ionization of atomic hydrogen, the total attenuation of radiation at these short wavelengths is probably influenced more by the scattering cross section.

The values of $\frac{1}{2}\sigma(H_2)$ between 200 and 450 Å are given in Table XXXIII, while those between 0.01 and 68 Å are given in Table XXXIV.

TABLE XXXIII

ABSORPTION CROSS SECTION; OF HYDROGEN ASSUMING $\sigma(H) = \frac{1}{2}\sigma(H_2)$[a]

λ (Å)	$\frac{1}{2}\sigma(H_2)$ (Mb)	λ (Å)	$\frac{1}{2}\sigma(H_2)$ (Mb)
209.3	0.13	323.6	0.61
234.2	0.20	335.1	0.68
239.6	0.22	345.1	0.76
247.2	0.25	358.5	0.88
260.5	0.29	362.9	0.92
266.3	0.32	374.4	1.02
283.5	0.40	387.4	1.13
297.6	0.48	428.2	1.44
303.1	0.51	434.3	1.51
314.9	0.56	452.2	1.68

[a] Samson and Cairns (1965).

TABLE XXXIV

HYDROGEN ABSORPTION CROSS SECTIONS FROM 0.01 TO 68 Å

λ(Å)	Experimental,[a] $\sigma(H) = \frac{1}{2}\sigma(H_2)$ (Mb)	Semiempirical, σ(H) (Mb)	λ(Å)	Experimental[a] $\sigma(H) = \frac{1}{2}\sigma(H_2)$ (Mb)	Semiempirical σ(H) (Mb)
0.01	—	1.90×10^{-7} [b]	1.000	7.36×10^{-7}	6.57×10^{-7} [b]
0.02	—	2.64×10^{-7} [b]	1.235	7.53×10^{-7}	—
0.03	—	3.12×10^{-7} [b]	1.389	7.86×10^{-7}	—
0.04	—	3.48×10^{-7} [b]	1.540	8.03×10^{-7}	—
0.05	—	3.76×10^{-7} [b]	1.934	8.36×10^{-7}	—
0.06	—	4.03×10^{-7} [b]	2.500	9.20×10^{-7}	—
0.064	4.10×10^{-7}	—	3.570	1.67×10^{-6}	—
0.072	4.18×10^{-7}	—	4.360	2.51×10^{-6}	—
0.080	—	4.30×10^{-7} [b]	5.17	3.68×10^{-6}	—
0.098	4.68×10^{-7}	—	6.97	8.03×10^{-6}	—
0.100	—	4.67×10^{-7} [b]	8.32	1.32×10^{-5}	1.25×10^{-5} [c]
0.130	5.35×10^{-7}	—	9.87	2.17×10^{-5}	—
0.175	6.02×10^{-7}	—	13.37	5.19×10^{-5}	5.02×10^{-5} [c]
0.200	6.27×10^{-7}	5.46×10^{-7} [b]	17.67	1.19×10^{-4}	1.17×10^{-4} [c]
0.209	6.69×10^{-7}	—	21.7	—	2.17×10^{-4} [c]
0.260	6.27×10^{-7}	—	23.7	—	2.84×10^{-4} [c]
0.417	6.52×10^{-7}	—	27.4	—	4.35×10^{-4} [c]
0.497	7.28×10^{-7}	—	31.6	—	6.70×10^{-4} [c]
0.631	7.28×10^{-7}	—	36.3	—	1.04×10^{-3} [c]
0.710	7.28×10^{-7}	—	44.6	1.67×10^{-3}	1.84×10^{-3} [c]
0.880	7.36×10^{-7}	—	68.0	5.02×10^{-3}	—

[a] Determined from the mass absorption coefficients compiled by Allen (1935).
[b] Victoreen (1949).
[c] Henke (1957).

IV. The Alkali Metals

A. Experimental Procedure

The first photoionization study of the alkali metals was the work of Foote and Mohler (1925) on cesium vapor. Their technique utilized the space-charge effect of positive ions on the thermoionic emission from a hairpin cathode. When used as a diode with only one or two volts across it the current was limited by the space-charge; however, if an ion was produced in the vicinity of the filament it could liberate as many as 10^4 electrons. This large amplification factor enabled the photoionization current to be measured. Figure 22 illustrates the type of space-charge tube used.

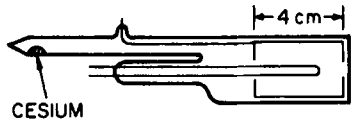

Fig. 22. Space-charge tube for positive ion detection (after Mohler and Boeckner, 1929).

This method is capable of measuring relative photoionization cross sections, provided certain assumptions are valid. The cross section is given, approximately, by

$$\sigma = \left(\frac{1}{genL}\right)\frac{i}{I_0}, \tag{14}$$

where i is the increase in current from the diode and I_0 is the incident light intensity. The constants g, e, n, and L are, respectively, the gain of the diode, the electronic charge, the atom concentration, and the pathlength traversed by the light beam in the vapor. Equation (14) will be valid when $\sigma nL \ll 1$ and provided the gain g is independent of wavelength and intensity. With the low vapor pressures and the small pathlength used, the assumption that σnL is less than unity is generally true. Later work, however, indicated that g probably was wavelength dependent. This seems somewhat surprising. One would expect g to remain wavelength independent until the ejected photoelectrons were sufficiently energetic to excite the atoms; whereupon a collision with an unexcited atom could lead to the production of a molecular ion (Mohler and Boeckner, 1930), thereby increasing the gain. More likely, the gain will be a function of the number of ions produced and hence of the incident intensity.

The relative photoionization cross sections were placed on an absolute scale by using a standard ion chamber whereby the constants could be measured accurately. In this case $g = 1$ and measurements could only be made at a few very intense spectral lines. Figure 23 shows the type of standard ion chamber used by Mohler and Boeckner (1929).

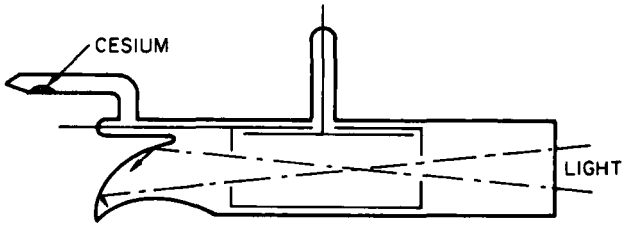

FIG. 23. Standard ion chamber of Mohler and Boeckner (1929).

Instead of using the space-charge method, Ditchburn and associates (1943) made direct measurements on the attenuation of radiation passing through a furnace containing the alkali metal vapors.

To produce atomic vapors at pressures suitable for absorption measurements the alkali metals must be heated to temperatures in the range 200° to 800°C. A small percentage of the vapor will be in the molecular state and must be taken into consideration for accurate results. The vapor pressures of the atoms and molecules as a function of temperature have been reported by several authors (JANAF, 1962; Honig, 1957, 1962; Hultgren *et al.*, 1963; Nesmeyanov, 1963). As an example of these vapor pressures, Table XXXV lists the values quoted by Nesmeyanov. The different values quoted by the four authors above can vary by $\pm 10\%$ from the average.

The absorption of radiation is defined as before by the Lambert–Beer law; however, when a second species is present the form of Eq. (1) becomes

$$\ln(I_0/I) = (\sigma_a n_a + \sigma_m n_m)L, \tag{15}$$

where σ_a and σ_m are the absorption cross sections for the atom and molecule, respectively. The number densities of the atoms and molecules are given by n_a and n_m, respectively, while L is the pathlength of the radiation within the vapor.

Ditchburn *et al.* (1943) separated the effects of the atoms and molecules by using the law of mass action, namely,

$$n_m = K n_a^2.$$

They assumed that the proportionality constant K was independent of the

TABLE XXXV

ATOMIC AND MOLECULAR VAPOR PRESSURES OF THE ALKALI METALS[a,b]

	mm Hg									
°K	Li	Li_2	Na	Na_2	K	K_2	Rb	Rb_2	Cs	Cs_2
400	—	—	—	—	—	—	—	—	2.92(−3)	1.29(−6)
425	—	—	—	—	—	—	4.10(−3)	3.37(−6)	1.08(−2)	8.23(−6)
450	—	—	—	—	—	—	1.39(−2)	1.83(−5)	2.41(−2)	4.20(−5)
475	—	—	—	—	6.84(−3)	6.03(−6)	3.91(−2)	8.11(−5)	1.07(−1)	1.79(−4)
500	—	—	—	—	2.06(−3)	2.71(−5)	1.10(−1)	3.06(−4)	2.40(−1)	6.50(−4)
550	—	—	6.23(−3)	4.41(−5)	1.32(−1)	3.58(−4)	5.88(−1)	3.04(−3)	1.29	5.94(−3)
600	—	—	3.39(−2)	4.75(−4)	6.19(−1)	3.01(−3)	2.37	2.09(−2)	4.32	3.69(−2)
650	—	—	1.95(−1)	3.51(−3)	2.27	1.79(−2)	7.62	1.06(−1)	13.0	1.71(−1)
700	—	—	7.50(−1)	1.93(−2)	6.88	8.10(−2)	20.6	3.96(−1)	33.1	6.25(−1)
750	1.55(−3)	8.55(−6)	2.40	8.35(−2)	17.9	2.97(−1)	50.1	1.13	74.1	1.89
800	7.39(−3)	6.06(−5)	6.61	2.96(−1)	41.0	9.57(−1)	102.0	2.66	149.0	4.86
850	2.89(−2)	3.37(−4)	16.0	8.92(−1)	85.0	2.46(−1)	182.0	6.17	271.0	11.0
900	9.53(−2)	1.52(−3)	35.0	2.36	162.0	5.91	349.0	11.9	443.0	23.0
950	1.87(−1)	6.04(−3)	70.4	5.62	289.0	12.9	550.0	40.7	689.0	52.0
1000	7.17(−1)	2.04(−2)	133	12.3	481.0	25.2	—	—	—	—
1100	3.86	1.62(−1)	389	46.2	—	—	—	—	—	—

[a] The symbol (−3) means 10^{-3}.

[b] Nesmeyanov (1963).

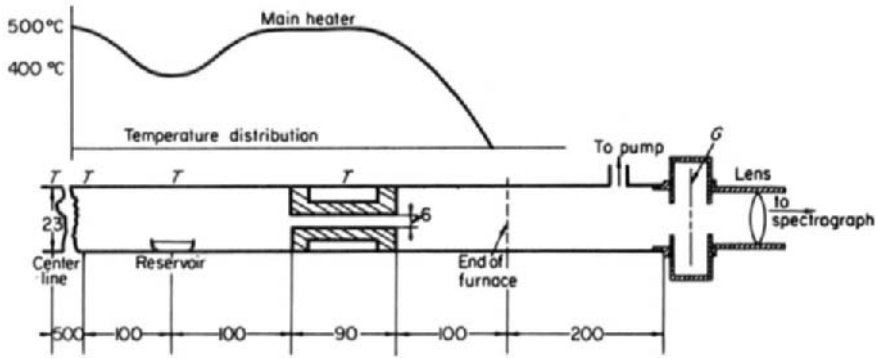

FIG. 24. Metallic vapor absorption tube and temperature distribution curve. Dimensions are in millimeters (after Ditchburn *et al.*, 1953).

temperature over the range used in their experiments. Thus, Eq. (15) becomes

$$\frac{\ln(I_0/I)}{n_a L} = \sigma_a + n_a K \sigma_m, \tag{16}$$

which is the equation of a straight line, the intercept giving σ_a. However, as Hudson (1964) points out, neither the JANAF nor the Nesmeyanov Tables support the assumption that K is independent of temperature; in fact, for sodium over the temperature range 400°–500°C, K varies by a factor of four. Moreover, σ_m is probably a function of temperature since the population of the vibrational and rotational states of the neutral molecule is a function of temperature.

The difficulties in measuring the cross sections of metallic vapors are compounded by the nonuniformity of the vapor density over the pathlength L. When this is the case, nL in Eq. (15) must be replaced by $\int_0^L n\, dl$. A method of producing a column of vapor for which this quantity can be readily calculated has been described by Ditchburn *et al.* (1943), and along with their furnace and absorption tube it has been the basis of all future work on metallic vapors. Figure 24 shows the absorption tube and temperature distribution used in the work of Ditchburn *et al.* (1953). It was found that by filling the absorption tube with an inert gas, usually helium, at a pressure a few millimeters Hg above the vapor pressure of the alkali metal the diffusion of the vapor was considerably slowed. With the addition of the 6-mm diameter plugs at each end of the absorption tube it was found that the main fall in the vapor pressure occurred in this region.

To observe the incident and transmitted radiation most experimenters in the past have used photographic plates as the detector and have placed the absorption cell between the light source and the entrance slit of the spectrograph. Hudson (1964) and Ross and Marr (1965) in their recent work have

replaced the photographic plates by photomultipliers and have positioned the absorption cell directly behind the exit slit. Hudson has utilized split beam photometry in his apparatus, thereby reducing errors due to light source fluctuations (see Fig. 25). Although higher resolution can be obtained using a spectrograph with photographic plates, the convenience and higher

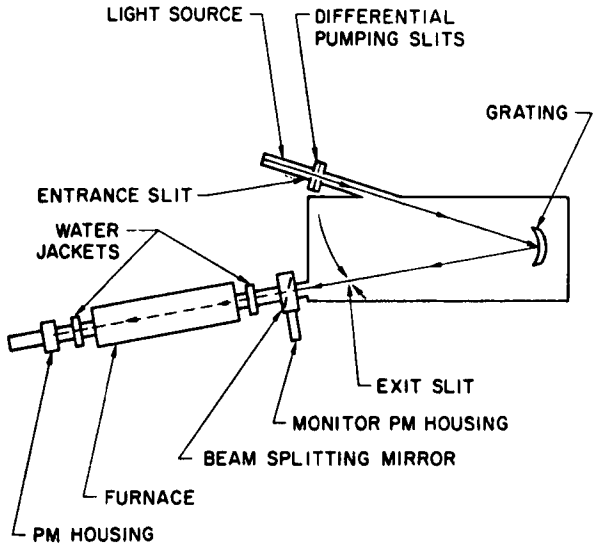

FIG. 25. Apparatus for split beam absorption measurements (after Hudson, 1964).

accuracy of the photoelectric method is more desirable when resolution is not vital. Present techniques can provide a resolution of 0.2 to 0.5 Å using photoelectric detectors. The infrared radiation emitted by the furnace can be discriminated against by using solar blind photomultipliers. These multipliers, however, are limited in their short wavelength response to radiation above the LiF window cutoff, namely, 1050 Å. To detect shorter wavelengths a conventional multiplier is used whose window is coated with sodium salicylate. A blue bandpass filter is necessary between the salicylate and the multiplier. Kodak Wratten filters Nos. 47 and 47B have been found suitable. The fluorescence band of sodium salicylate is rather broad with a maximum at 4100 Å.

The absorption cross sections for the alkali metals are discussed below.

B. LITHIUM (I.P. 2299.5 Å)

Early theoretical calculations were made by Hargreaves (1929) and Trumpy (1931) predicting cross sections at the spectral head of 3.3 and 3.7 Mb,

respectively. Trumpy's calculations gave a maximum cross section at the spectral head decreasing continuously to shorter wavelengths, while Hargreaves predicted a maximum at 1950 Å.

Experimental data were not available until 1953 when Tunstead (1953) presented the first measurements on lithium from threshold to 1800 Å. These results were in general agreement with the spectral shape predicted by Trumpy. However, a series of theoretical calculations by Stewart (1954), Burgess and Seaton (1960), and Tait (1964) all predicted an increase in the cross section from threshold to shorter wavelengths. These predications appear to be borne out by the recent experimental work of Marr (1963) and Hudson and Carter (1965a). Marr reinvestigated Tunstead's results in the light of more accurate vapor pressure data and found that they also showed a slight increase towards short wavelengths.

Figure 26 shows the experimental results of Hudson and Carter compared to other experimental and theoretical results. The apparent agreement between the two sets of experimental data is somewhat misleading since the vapor pressure data used by Hudson is about 15% lower than that used by Marr; thus, Marr's experimental results favor the theoretical approach used by Tait while Hudson's results favor that of Burgess and Seaton.

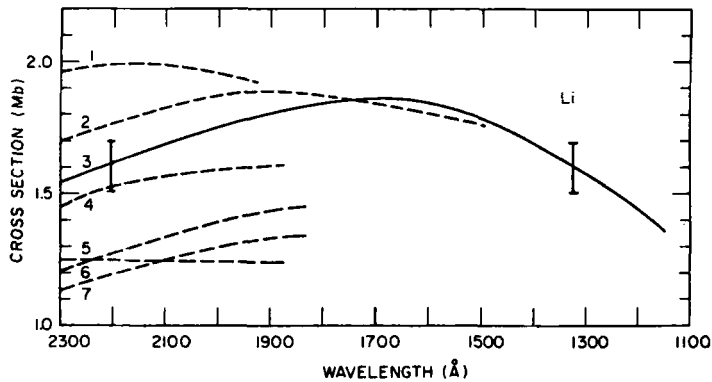

FIG. 26. Atomic lithium absorption cross section. (1) Tait (dipole length); (2) Marr (experimental); (3) Hudson and Carter (experimental); (4) Burgess and Seaton (dipole length); (5) Tait (dipole velocity); (6) Stewart (dipole length); (7) Stewart (dipole velocity). (After Hudson and Carter, 1965a)

C. SODIUM (I.P. 2412.6 Å)

With the exception of lithium all the alkali metals, characterized by a single electron outside of the closed shells, have a small value for the cross section at their spectral head, typically of the order of 0.1 Mb or less. The cross sections

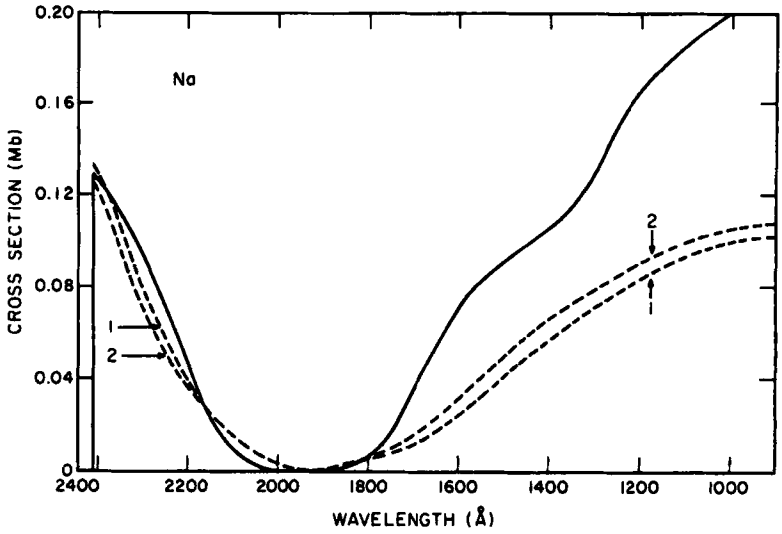

FIG. 27. Atomic sodium absorption cross section. Solid line represents the experimental data of Hudson; broken lines represent the theoretical results of Boyd: (1) dipole length, (2) dipole velocity.

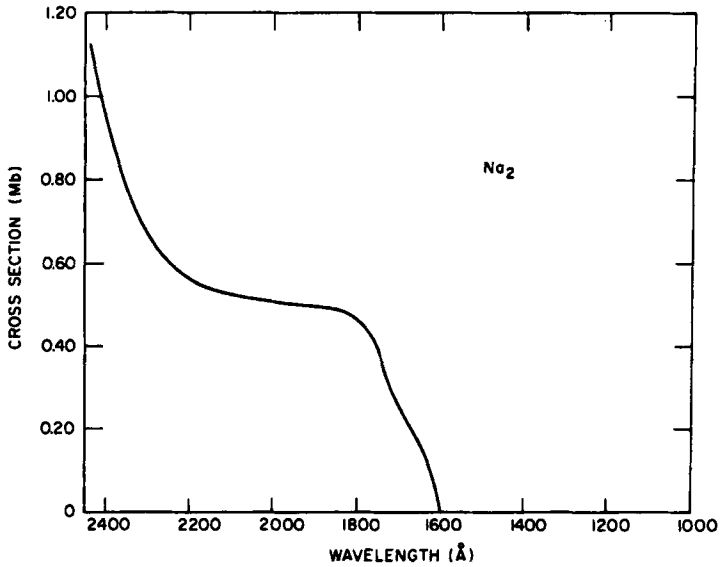

FIG. 28. Molecular sodium absorption cross section (after Hudson, 1964).

then decrease to a minimum about 1 eV beyond the ionization threshold and then start to increase. As yet no experimental data are available below 1000 Å.

Early investigations of the continuous absorption of light by sodium vapor were made by Harrison (1924) who obtained a curve similar to that described above; however, the results were only relative owing to difficulties in measuring $\int_0^L p\, dl$. Bott (1939) succeeded in measuring absolute cross sections but did not separate the molecular and atomic absorption. The first detailed measurement of the sodium cross section is due to Ditchburn *et al.* (1953). They obtained a minimum near 1900 Å. Hudson (1964), however, has found this minimum to be zero at 1900 Å and accounts for the difference as being due to the different methods used for separating the atomic and molecular absorptions. Hudson used Eq. (15) and the concentration values quoted by the JANAF Tables to obtain both the atomic and molecular absorption cross sections. Figures 27 and 28 show his results for the atomic and molecular absorption, respectively.

The theoretical results by Boyd (1964) are compared to the experimental results in Fig. 27. Excellent agreement is obtained from threshold to the zero minimum at 1900 Å. To shorter wavelengths theory predicts an increase in the cross section; however, at 1000 Å the theoretical value is about a factor of two smaller than the experimental results.

The dipole length approximation predicts a cross section of 0.136 Mb at the spectral head while the dipole velocity approximation predicts a value of

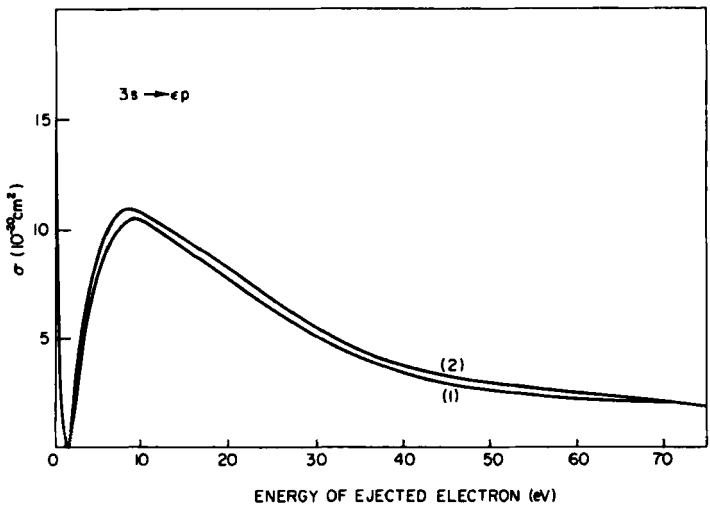

FIG. 29. Theoretical photoionization cross section of sodium for ejection of the 3*s* electron. (1) Dipole length; (2) dipole velocity. Threshold 2412.6 Å (after Boyd, 1964).

0.126 Mb. The experimental values are 0.130 ± 0.018 Mb (Hudson, 1964) and 0.116 ± 0.012 Mb (Ditchburn *et al.*, 1953).

Other theoretical calculations have been made using approximate wavefunctions (Seaton, 1951b; Cooper, 1962; Burgess and Seaton, 1960). For the alkali metals, particularly, it seems desirable to use as accurate wavefunctions as possible since the results are very sensitive to the wavefunctions owing to the high degree of cancellation which occurs between the positive and negative contributions to the integrand involved in the calculations.

The individual cross sections for ejection of the 3*s*, 2*p*, and 2*s* electrons from threshold to about 160 Å are given in Figs. 29, 30, and 31, respectively

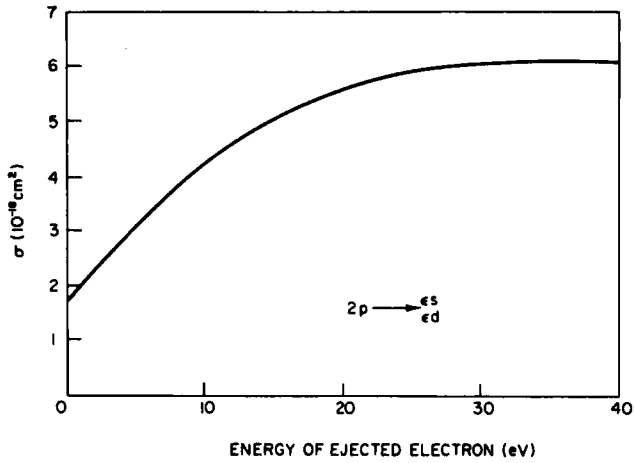

FIG. 30. Theoretical photoionization cross section of sodium for ejection of a 2*p* electron. Threshold $\simeq 325.8$ Å (after Boyd, 1964).

(Boyd, 1964). It should be noted that the predicted cross sections due to ionization of the inner shell electrons are about 100 times greater than for the outer 3*s* electron.

D. POTASSIUM (I.P. 2856.3 Å)

The absorption of radiation by potassium has been studied by a number of investigators. Mohler and Boeckner (1929) and Lawrence and Edlefsen (1929) used the space-charge amplification method. Ditchburn *et al.* (1943) measured the attenuation of the radiation passing through a column of potassium vapor using photographic plates as detectors. Hudson and Carter (1965b) have repeated the attenuation measurements using photoelectric detection and more recent vapor pressure data.

The various experimental results are in general agreement. The region of greatest disagreement being that of minimum absorption between 2500 and 2800 Å. Hudson and Carter find that their data between 2600 and 2750 Å lie sufficiently close to zero that this value actually falls within their experimental error and cannot be precluded as the actual value. The other experimental data give a value of 0.008 Mb at the minimum.

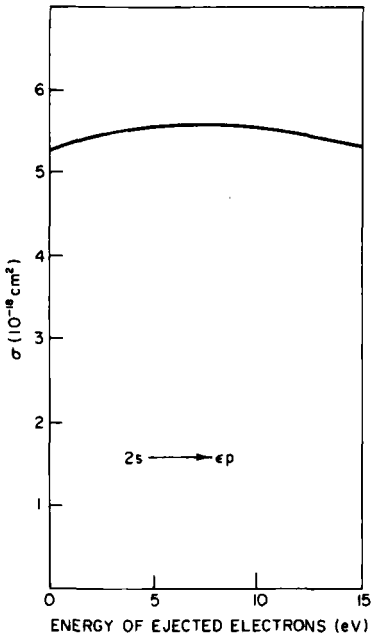

FIG. 31. Theoretical photoionization cross section of sodium for ejection of a 2*s* electron. Threshold ≃ 175.4 Å (after Boyd, 1964).

No accurate theoretical calculations exist for potassium; however, Bates (1946b) showed the need for taking into account the polarization of the core in any calculation. Treating the polarizability as an adjustable parameter he adjusted its value such that the cross section calculations fitted the experimental data of Ditchburn *et al.* (1943) at the spectral head. By so doing, his calculations predicted the general shape of the cross section curve from threshold to 2200 Å. The minimum value, however, was essentially zero. The polarizability was assumed to be 1.55×10^{-24} cm^3.

The experimental results of Hudson and Carter for atomic potassium are shown in Fig. 32, while their values for the molecular cross section are compared to those of Ditchburn *et al.* (1943) in Fig. 33.

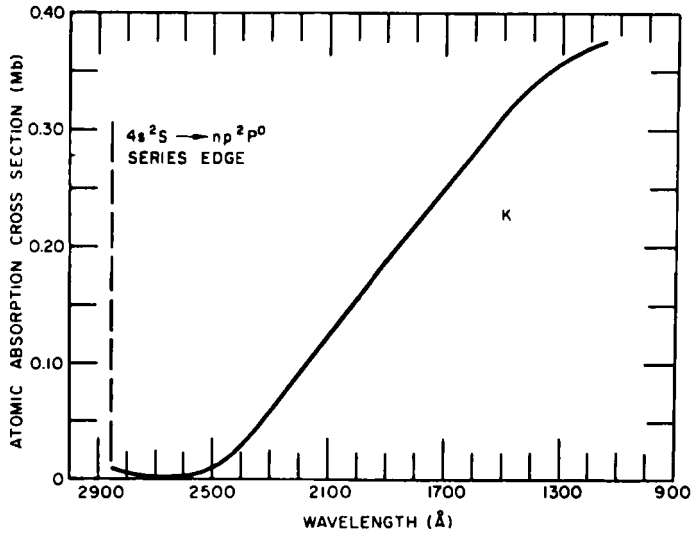

FIG. 32. Atomic potassium absorption cross section (after Hudson and Carter, 1965b).

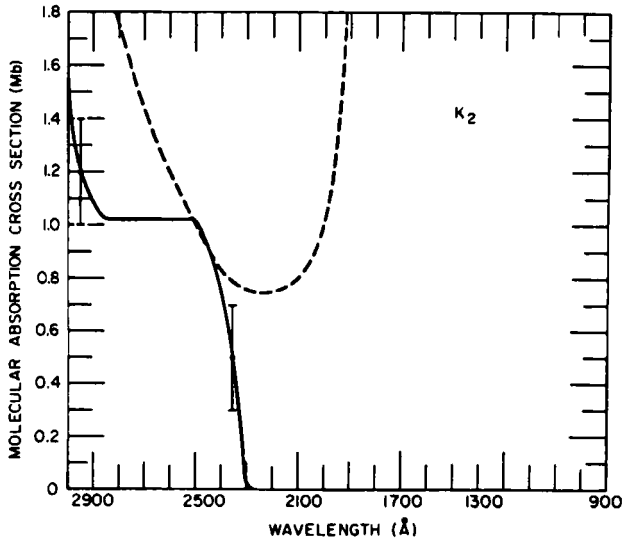

FIG. 33. Molecular potassium absorption cross section. Solid line with error bars represents data of Hudson and Carter (1965b). The broken curve represents the results of Ditchburn *et al.* (1943).

E. Rubidium (I.P. 2968.2 Å)

The only absolute photoionization cross section measurements of rubidium were made by Mohler and Boeckner (1929) using the space-charge amplification method in conjunction with a simple ionization chamber. Their results are reproduced in Fig. 34. It would appear that rubidium also exhibits a minimum cross section near the ionization threshold. The measured continuum oscillator strength from Fig. 34 is only ~0.00025 from threshold to 2500 Å, whereas the valence electron would be expected to contribute a total of 1.0 to the total oscillator strength. Thus, unless the discrete oscillator strengths for the resonance absorption lines are large, the continuum absorption cross sections will undoubtedly increase towards shorter wavelengths as in the case of sodium, potassium, and cesium.

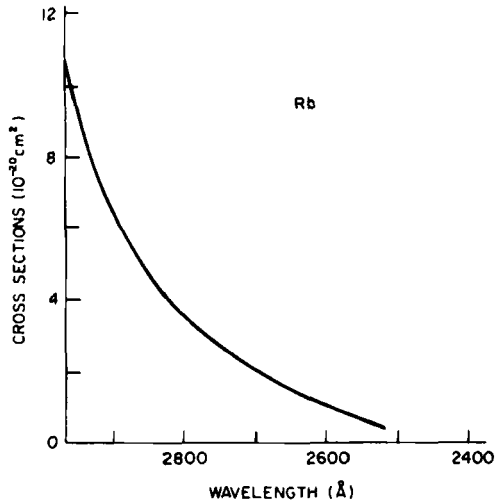

Fig. 34. Rubidium absorption cross section. Results of Mohler and Boeckner (1929).

Very little theoretical work exists for rubidium. Bates (1946b) estimates the cross section at the spectral head to be ~0.01 Mb and Seaton (1951b) estimates the minimum to be 0.004 Mb.

F. Cesium (I.P. 3184.0 Å)

The only available results for cesium are the early measurements by Braddick and Ditchburn (1935) and Mohler and Boeckner (1929). Their results are shown in Fig. 35. Again a low cross section at the spectral head is found

with a minimum cross section about 0.5 eV beyond the ionization threshold. The cross section then increases towards shorter wavelengths.

Judging from the great similarity in the spectral shape of the cross section curves for Na to Cs it would not be surprising if the minimum cross section for Cs were closer to zero. The theoretical estimate by Seaton (1951b) gives a value of 0.03 Mb for the minimum.

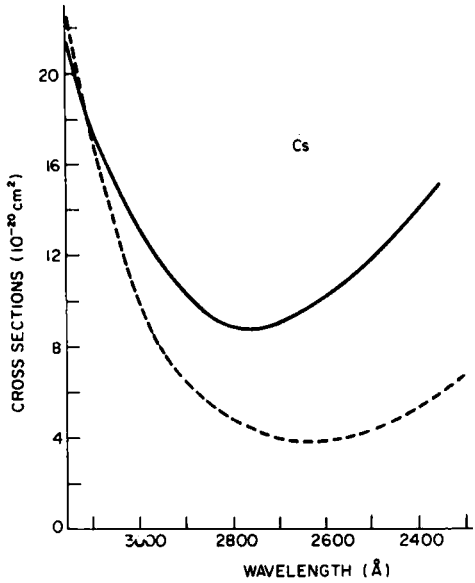

FIG. 35. Cesium absorption cross section. Results of Braddick and Ditchburn (1935), ——; and Mohler and Boeckner (1929), – – –.

A review of the vapor pressure data used by Mohler and Boeckner (1930) indicates that the present values quoted by Nesmeyanov are about 40% greater than those used by Mohler and Boeckner. Thus, assuming the more recent vapor pressure data to be correct, the data in Fig. 35 should be reduced by approximately a factor of 40%, giving a minimum cross section of 0.023 Mb.

Cesium and rubidium are particularly difficult elements to handle; both metals can burst into flame spontaneously in air. However, new measurements are currently underway by Marr and Hudson with the results being extended to shorter wavelengths.

The very low continuous absorption cross sections for the alkali metals, as shown in the preceding sections, perhaps can be explained if the single valence electron is assumed to contribute only one to the total oscillator strength. That is, for this electron $\Sigma f_{\text{line}} + f_c = 1$. The total oscillator strength for the resonance absorption series is, however, very close to one for the

alkali metals; thus, f_c must be very small. For example, the f values of the first sodium and lithium doublets have been calculated to be 0.945 and 0.75, respectively (Bates and Damgaard, 1949). The experimental values for the discrete lines have a considerable spread (Landolt and Börnstein, 1950; Corliss and Bozman, 1962), however, the average $\Sigma f_{\text{line}} \sim 0.95$ for the alkali metals. This leaves, on the above assumption, only 0.05 for the continuum oscillator strengths.

The continuum f value obtained from the theoretical cross section curve of sodium, for the ejection of the $3s$ electron (Fig. 29), was 0.032 when calculated from threshold to 165 Å. In the case of lithium the experimental value for f_c was ~ 0.11 for the region covered by Fig. 26. Thus, a consistent picture appears to be obtained by the assumption that a single valence electron should contribute a total of one to the oscillator strength.

V. Miscellaneous Atoms

The technique for measuring the absorption cross sections of the following atoms is the same as that used by Ditchburn *et al.* (1943) and is described in the last section.

A. Calcium (I.P. 2028.2 Å)

The absorption cross sections for calcium were first measured by Jutsum (1954) between 2028 and 1950 Å. Later, the measurements were extended down to 1100 Å by Ditchburn and Hudson (1960). This region includes two series of rather strongly autoionizing lines which were first observed by Kaiser (1960) and identified as transitions from the ground $4s^2(^1S_0)$ level to the doubly excited levels $3dnp$ ($^1P_1{}^0$, $^3P_1{}^0$), where $n = 5, 6, \ldots$, etc. The cross sections measured by Ditchburn and Hudson are reproduced in Figs. 36 and 37. Figure 36 shows the two autoionized series with limits at 1589.6 and 1586.9 Å. The absorption cross sections for the $5p\ ^1P_1$ and $6p\ ^1P_1$ lines (shown off scale in Fig. 36) are 30 and 70 Mb, respectively. The spectral head cross section is 0.45 ± 0.07 Mb as given by Ditchburn and Hudson. Seaton (1955) calculated the absorption cross section by a semiempirical method based on measurements of the quantum defect. However, this calculation, as indeed all the theoretical work on photoionization, does not take into account the possibility of autoionization. Thus, while the theoretical cross sections are in good agreement with the experimental results at threshold and a little beyond the agreement ends with the large autoionized line at 1890 Å.

Ditchburn and Hudson have measured the continuum oscillator strength, including the autoionized lines, from the ionization threshold to 1100 Å and

found it to be 0.047. They quote that the resonance series, $4snp\ ^1P_1$, contributes approximately 1.8 to the oscillator strength giving a total of 1.847 for the two s electrons.

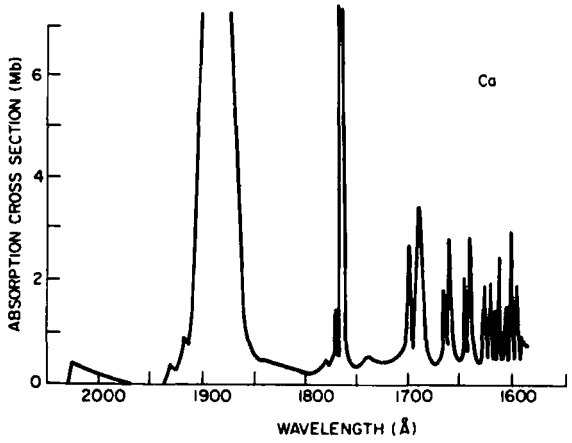

FIG. 36. Calcium absorption cross section between 2100 and 1600 Å (after Ditchburn and Hudson, 1960).

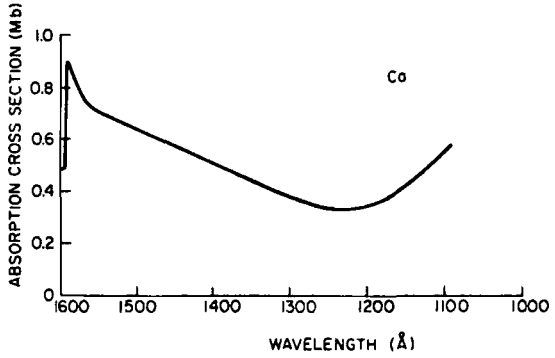

FIG. 37. Calcium absorption cross section between 1600 and 1080 Å (after Ditchburn and Hudson, 1960).

B. THALLIUM (I.P. 2029.9 Å)

The absorption spectrum for thallium presents another good example of autoionized lines as the prominent absorption feature in the ionization continuum. The absorption cross sections of the autoionized lines and underlying

continuum have been measured by Marr (1954a) between 2030 and 1450 Å. The value of the cross section at the spectral head was 4.5 ± 0.8 Mb. The experimental results are shown in Fig. 38. Three discrete absorption lines were observed at 2007, 1610, and 1490 Å representing transitions from the ground state to the $^4P_{3/2}$, $^2D_{3/2}$, and $^2P_{1/2}$ states, respectively. Each of these states lies above the first ionization threshold at 2030 Å; however, only the $^2D_{3/2}$ state is allowed completely to autoionize into the adjoining continuum. Over the region investigated it is the outstanding absorption feature having a peak absorption cross section of 150 Mb with a half-width of approximately 60 Å. The $^4P_{3/2}$ and $^2P_{1/2}$ states only partially satisfy the selection rules; however, they are slightly diffuse indicating that they partially autoionize. It is unlikely that these two states will have an ionization yield of exactly 100%; hence, the cross sections given for these two lines will not be exactly the photoionization cross sections.

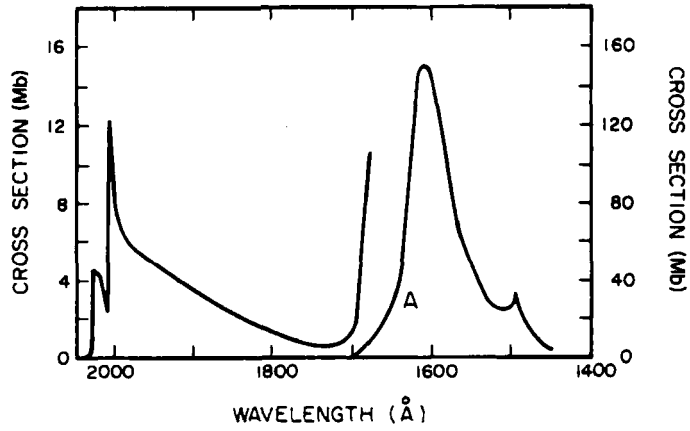

FIG. 38. Thallium absorption cross section. The ordinate scale for curve *A* is given on the right (after Marr, 1954a).

Marr reports an oscillator strength of 0.55 between 2030 and 1450 Å, with most of the contribution arising from autoionization processes. The contribution from the resonance series is 0.518 (Foster, 1964). Thus, the single $6p$ electron contributes a total of 1.07 to the oscillator strength over the range of the measurements. It is likely, therefore, that the absorption cross sections will continue to decrease at wavelengths shorter than 1450 Å until the threshold is reached for ejection of an inner s electron, namely, at 1013 Å.

A more complete discussion of the oscillator strengths for thallium is given by Foster (1964).

C. Indium (I.P. 2142.7 Å)

The absorption spectrum of indium was first observed by Garton (1950) using a short carbon absorption tube in a King furnace. No absolute cross sections were determined because of uncertainties in the effective pathlength of the absorbing column. However, a strong autoionized line was observed at 1758 Å with a furnace temperature of 950°C, while a temperature of 1400°C was required to observe the series limit.

Marr (1954b) was successful in measuring the peak cross section of the 1758-Å line finding a value ~100 Mb. Owing to the limitations of his furnace he was unable to produce a sufficiently absorbing column of indium vapor to observe the series limit. He used a pathlength of 150 cm with a maximum vapor pressure of 3 μ. Referring to Garton's data, Marr compares the relative absorption of the 1758-Å line with that at the series limit, then, using his measured value at 1758 Å, estimates the series limit (spectral head) absorption to be ~0.1 to 1.0 Mb.

D. Magnesium (I.P. 1621.6 Å) and Cadmium (I.P. 1318.6 Å)

Finally, the absorption cross sections for magnesium have been measured by Ditchburn and Marr (1953) while cadmium has been investigated by Ross and Marr (1965). Figures 39 and 40 show their respective cross sections as a

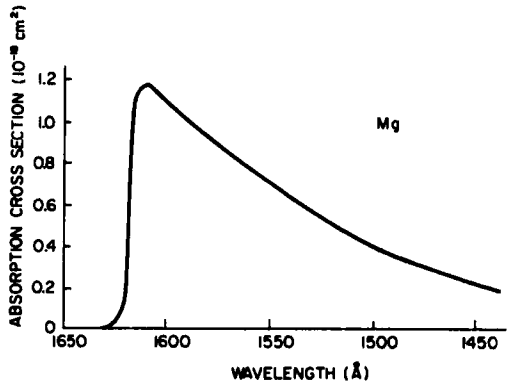

Fig. 39. Magnesium absorption cross section (after Ditchburn and Marr, 1953).

function of wavelength. No discrete structure has been observed in the ionization continuum for these two atoms. Both atoms show a characteristic decrease in absorption beyond the ionization threshold. The small value for the continuum f value over the region measured (0.0024 for cadmium)

suggests that the cross sections of both these atoms will increase towards shorter wavelengths.

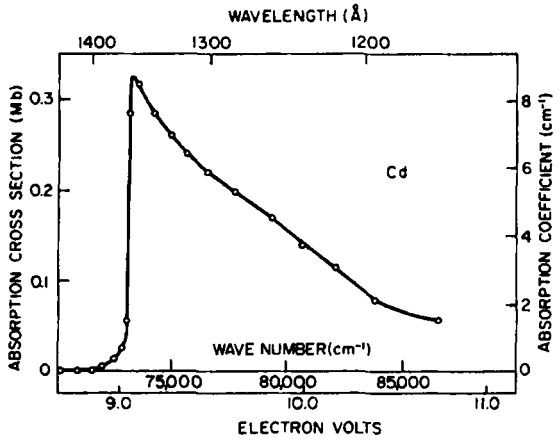

FIG. 40. Cadmium absorption cross section (after Ross and Marr, 1965).

It is expected that new measurements on cesium, rubidium, zinc, mercury, lead, and manganese will be available in the near future and that data on the alkali metals will be extended down to 600 Å.

GENERAL REFERENCES

Ditchburn, R. W., Jutsum, P. J., and Marr, G. V. (1953). *Proc. Roy. Soc.* **A219**, 89.
Ditchburn, R. W., and Öpik, U. (1962). *In* "Atomic and Molecular Processes" (D. R. Bates, ed.), Vol. I, pp. 79–99. Academic Press, New York.
Weissler, G. L. (1956). *In* "Handbuch der Physik" (S. Flugge, ed.), Vol. 21, pp. 304–382. Springer, Berlin.

REFERENCES

Allen, S. J. M. (1935). See Compton and Allison below.
Anderson, D. K., (1965). *Phys. Rev.* **137**, A21.
Astoin, N. D., and Kastler, M. A. (1964). *Compt. Rend.* **259**, 1493.
Axelrod, N., and Givens, M. P. (1959). *Phys. Rev.* **115**, 97.
Baker, D. J., Bedo, D. E., and Tomboulian, D. H. (1961). *Phys. Rev.* **124**, 1471.
Bates, D. R. (1939). *Monthly Notices Roy. Astron. Soc.* **100**, 25.
Bates, D. R. (1946a). *Monthly Notices Roy. Astron. Soc.* **106**, 423.

Bates, D. R. (1946b). *Monthly Notices Roy. Astron. Soc.* **106**, 432.
Bates, D. R., and Damgaard, A. (1949). *Phil. Trans. Roy. Soc.* (*London*) **A242**, 101.
Bates, D. R., and Seaton, M. J. (1949). *Monthly Notices Roy. Astron. Soc.* **109**, 698.
Bates, D. R., Buckingham, R. A., Massey, H. S. W., and Unwin, J. J. (1939). *Proc. Roy. Soc.* **A170**, 322.
Beutler, H. (1935). *Z. Physik* **93**, 177.
Beynon, J. D. E., and Cairns, R. B. (1964). *J. Sci. Instr.* **41**, 111.
Beynon, J. D. E., and Cairns, R. B. (1965). *Proc. Phys. Soc.* (*London*) (in press); see also *Nature* (1965) **207**, 405.
Blackwell, H. E., Bajwa, G. S., Shipp, G. S., and Weissler, G. L. (1964). *J. Quant. Spectry. & Radiative Transfer* **4**, 249.
Bott, J. (1939). *Ann. Physik.* [5] **35**, 314.
Boyd, A. E. (1964). *Planetary Space Sci.* **12**, 729.
Braddick, H. J. J., and Ditchburn, R. W. (1935). *Proc. Roy. Soc.* **A150**, 478.
Burgess, A., and Seaton, M. J. (1960). *Monthly Notices Roy. Astron. Soc.* **120**, 121.
Cairns, R. B., and Samson, J. A. R. (1965). *Phys. Rev.* **139**, A1403.
Cairns, R. B., and Weissler, G. L. (1962). *Bull. Am. Phys. Soc.* [2] **7**, 129.
Cauchois, Y. (1955). *J. Phys. Radium* **16**, 253.
Chandrasekhar, S., and Herzberg, G. (1955). *Phys. Rev.* **98**, 1050.
Codling, K., and Madden, R. P. (1964). *Phys. Rev. Letters* **12**, 106.
Codling, K., and Madden, R. P. (1965). *Natl. Bur. Std.* (*U.S.*) (private communication).
Comes, F., and Elzer, A. (1964). *Z. Naturforsch.* **19a**, 721.
Comes, F., and Lessman, W. (1961). *Z. Naturforsch.* **16a**, 1396.
Compton, A. H., and Allison, S. K. (1935). "X-Rays in Theory and Experiment", p. 799. Van Nostrand, Princeton, New Jersey.
Compton, K. T. (1922). *Rev. Sci. Instr.* **6**, 910.
Cook, D. B., and Danby, C. J. (1953). *J. Sci. Instr.* **30**, 238.
Cook, G. R., and Metzger, P. H. (1964). Aerospace Corporation, Los Angeles (private communication).
Cooper, J. W. (1962). *Phys. Rev.* **128**, 681.
Cooper, J. W. (1964). *Phys. Rev. Letters* **13**, 762.
Corliss, C. H., and Bozman, W. R. (1962). *Natl. Bur. Std.* (*U.S.*), *Monograph* **53**.
Coster, D., and Van der Tuuk, J. H. (1926). *Z. Physik* **37**, 367.
Dalgarno, A. (1952). *Proc. Phys. Soc.* (*London*) **65**, 663.
Dalgarno, A., and Lynn, N. (1957). *Proc. Phys. Soc.* (*London*) **70**, 802.
Dalgarno, A., and Parkinson, D. (1960). *J. Atmospheric Terrest. Phys.* **18**, 335.
Dalgarno, A., and Stewart, A. L. (1960). *Proc. Phys. Soc.* (*London*) **76**, 49.
Dalgarno, A., Henry, R. J. W., and Stewart, A. L. (1964). *Planetary Space Sci.* **12**, 235.
Ditchburn, R. W. (1960). *Proc. Phys. Soc.* (*London*) **75**, 461.
Ditchburn, R. W., and Hudson, R. D. (1960). *Proc. Roy. Soc.* **A256**, 53.
Ditchburn, R. W., and Marr, G. V. (1953). *Proc. Phys. Soc.* (*London*) **A66**, 655.
Ditchburn, R. W., Tunstead, J., and Yates, J. G. (1943). *Proc. Roy. Soc.* **A181**, 386.
Ditchburn, R. W., Jutsum, P. J., and Marr, G. V. (1953). *Proc. Roy. Soc.* **A219**, 89.
Duffendack, O. S. (1922). *Phys. Rev.* **20**, 665.
Ederer, D. L. (1964). *Phys. Rev. Letters* **13**, 760.
Ederer, D. L., and Tomboulian, D. H. (1964a). *Phys. Rev.* **133**, A1525.
Ederer, D. L., and Tomboulian, D. H. (1964b). Private communication.
Ehler, A. W., and Weissler, G. L. (1955). *J. Opt. Soc. Am.* **45**, 1035.
Fano, U. (1961). *Phys. Rev.* **124**, 1866.
Fano, U., and Cooper, J. W. (1965). *Phys. Rev.* **137**, A1364.

Foote, P. D., and Mohler, F. L. (1925). *Phys. Rev.* **26**, 195.
Foster, E. W. (1964). *Rept. Progr. Phys.* **27**, 469.
Garton, W. R. S. (1950). *Nature* **166**, 150.
Gaunt, J. A. (1930). *Phil. Trans. Roy. Soc. London* **A229**, 163.
Geiger, J. (1962). Thesis, Technical University of Berlin.
Gold, A., and Knox, R. S. (1959). *Phys. Rev.* **113**, 834.
Hargreaves, J. (1928–1929). *Proc. Cambridge Phil. Soc.* **25**, 91.
Hargreaves, J. (1929). *Proc. Cambridge Phil. Soc.* **25**, 75.
Harrison, G. R. (1924). *Phys. Rev.* **24**, 466.
Harteck, P. (1928). *Z. Physik. Chem.* **A139**, 98.
Harteck, P., Reeves, R. R., and Mannella, G. (1958). *J. Chem. Phys.* **29**, 608.
Henke, B. L. (1957). *J. Appl. Phys.* **28**, 98.
Herzberg, G. (1944). "Atomic Spectra and Atomic Structure," 2nd ed., p. 163. Dover, New York.
Herzberg, G. (1958). *Proc. Roy. Soc.* **A248**, 309.
Hill, R. D., Church, E. L., and Mihelich, J. W. (1952). *Rev. Sci. Instr.* **23**, 523.
Honig, R. E. (1957). *R C A Rev.* **18**, 195.
Honig, R. E. (1962). *R C A Rev.* **23**, 567.
Huang, S. (1948). *Astrophys. J.* **108**, 354.
Hudson, R. D. (1964). *Phys. Rev.* **135**, A1212.
Hudson, R. D. (1965). Aerospace Corporation, Los Angeles (private communication).
Hudson, R. D., and Carter, V. L. (1965a). *Phys. Rev.* **137**, A1648.
Hudson, R. D., and Carter, V. L. (1965b). *Phys. Rev.* **139**, A1426.
Huffman, R. E., Tanaka, Y., and Larrabee, J. E. (1963a). *J. Chem. Phys.* **39**, 902.
Huffman, R. E., Tanaka, Y., and Larrabee, J. C. (1963b). *Appl. Opt.* **2**, 947.
Hultgren, R., Orr, R. L., Anderson, P. D., and Kelley, K. K. (1963). "Selected Values of Thermodynamic Properties of Metals and Alloys." Wiley, New York.
Hylleraas, E. A. (1937). *Z. Physik* **106**, 395.
JANAF (1962). "Thermochemical Tables." The Dow Chemical Co., Midland, Michigan.
Jutsum, P. J. (1954). *Proc. Phys. Soc. (London)* **A67**, 190.
Kaiser, T. R. (1960). *Proc. Phys. Soc. (London)* **75**, 152.
Karzas, W. J., and Latter, R. (1961). *Astrophys. J. Suppl. Soc.* **6**, 167.
Kaufman, F. (1961). *In* "Progress in Reaction Kinetics" (G. Porter, ed.), Vol. I, pp. 3–39. Pergamon Press, Oxford.
Kistiakowsky, G. B., and Volpi, G. G. (1957). *J. Chem. Phys.* **27**, 1141.
Knox, R. S. (1958). *Phys. Rev.* **110**, 375.
Korolev, F. A., Odintsov, V. I., and Fursova, E. V. (1964). *Opt. Spectry. (USSR) (English Transl.)* **16**, 304.
Köwien, H. (1934). *Z. Physik* **91**, 1.
Kramers, H. A. (1923). *Phil. Mag.* [6] **46**, 836.
Lamb, W. E., and Retherford, R. C. (1950). *Phys. Rev.* **79**, 549.
Landolt, H. H., and Börnstein, R. (1950). "Zahlenwerte und Funktionen," Vol. 1, Part 1, p. 264. Springer, Berlin.
Lawrence, E. O., and Edlefson, N. E. (1929). *Phys. Rev.* **34**, 233 and 1056.
Lee, P., and Weissler, G. L. (1952). *J. Opt. Soc. Am.* **42**, 214; also *Proc. Roy. Soc.* **A219**, 71 (1953).
Lee, P., and Weissler, G. L. (1955). *Phys. Rev.* **99**, 540.
Lincke, R., and Griem, H. R. (1965). *Bull. Am. Phys. Soc.* [2] **10**, 202.
Lowry, J. F., Tomboulian, D. H., and Ederer, D. L. (1965). *Phys. Rev.* **137**, A1054.

Lukirskii, A. P., and Zimkina, T. M. (1963). *Bull. Acad. Sci. USSR, Phys. Ser.* (*English Transl.*) **27**, 808.
Lukirskii, A. P., Brytov, I. A., and Zimkina, T. M. (1964). *Opt. Spectry.* (*USSR*) (*English Transl.*) **17**, 234.
Madden, R. P., and Codling, K. (1963). *Phys. Rev. Letters* **10**, 516.
Madden, R. P., and Codling, K. (1964). *J. Opt. Soc. Am.* **54**, 268.
Madden, R. P., and Codling, K. (1965a). *Astrophys. J.* **141**, 364
Madden, R. P., and Codling, K. (1965b). Private communication.
Marr, G. V. (1954a). *Proc. Roy. Soc.* **A224**, 83.
Marr, G. V. (1954b). *Proc. Phys. Soc.* (*London*) **A67**, 196.
Marr, G. V. (1963). *Proc. Phys. Soc.* (*London*) **81**, 9.
Menzel, D. H., and Pekeris, C. L. (1935). *Monthly Notices Roy. Astron. Soc.* **96**, 77.
Mohler, F. L., and Boeckner, C. (1929). *J. Res. Natl. Bur. Std.* **3**, 303.
Mohler, F. L., and Boeckner, C. (1930). *J. Res. Natl. Bur. Std.* **5**, 51.
Moore, C. E. (1949). *Natl. Bur. Std.* (*U.S.*), *Circ.* **476**, Vol. 1; Vol. 2 (1952); Vol. 3 (1958).
Morse, F. A., and Kaufman, F. (1965). *J. Chem. Phys.* **42**, 1785.
Nesmeyanov, An. N. (1963). "Vapour Pressure of the Elements," p. 456. Academic Press, New York.
Parratt, L. G. (1939). *Phys. Rev.* **56**, 295.
Pery-Thorne, A., and Garton, W. R. S. (1960). *Proc. Phys. Soc.* (*London*) **76**, 833.
Ross, K. J., and Marr, G. V. (1965). *Proc. Phys. Soc.* (*London*) **85**, 193.
Rustgi, O. P. (1964). *J. Opt. Soc. Am.* **54**, 464.
Rustgi, O. P., Fisher, E. I., and Fuller, C. H. (1964). *J. Opt. Soc. Am.* **54**, 745.
Salpeter, E. E., and Zaidi, M. H. (1962). *Phys. Rev.* **125**, 248.
Samson, J. A. R. (1958). Dissertation, University of Southern California.
Samson, J. A. R. (1963). *Phys. Rev.* **132**, 2122.
Samson, J. A. R. (1964a). *J. Opt. Soc. Am.* **54**, 6.
Samson, J. A. R. (1964b). *J. Opt. Soc. Am.* **54**, 876.
Samson, J. A. R. (1964c). *J. Opt. Soc. Am.* **54**, 420.
Samson, J. A. R. (1964d). *Phys. Letters* **8**, 107.
Samson, J. A. R. (1964e). *J. Opt. Soc. Am.* **54**, 842.
Samson, J. A. R., and Cairns, R. B. (1965). *J. Opt. Soc. Am.* **55**, 1035.
Schönheit, E. (1961). *Z. Naturforsch.* **16a**, 1094.
Seaton, M. J. (1951a). *Proc. Roy. Soc.* **A208**, 408.
Seaton, M. J. (1951b). *Proc. Roy. Soc.* **A208**, 418.
Seaton, M. J. (1954). *Proc. Phys. Soc.* (*London*) **67**, 927.
Seaton, M. J. (1955). *Ann. Astrophys.* **18**, 206.
Sewell, K. G. (1965a). *Phys. Rev.* **137**, A418.
Sewell, K. G. (1965b). Private communication.
Shaw, C. H. (1940). *Phys. Rev.* **57**, 877.
Siegbahn, M. (1931). "Spektroscopie der Rontgenstrahlen," 2nd ed., pp. 346–349. Springer, Berlin.
Stacey, D. N., and Vaughan, J. M. (1964). *Phys. Letters* **11**, 105.
Stewart, A. L. (1954). *Proc. Phys. Soc.* (*London*) **A67**, 917.
Stewart, A. L., and Webb, T. G. (1963). *Proc. Phys. Soc.* (*London*) **82**, 532.
Stewart, A. L., and Wilkinson, W. J. (1960). *Proc. Phys. Soc.* (*London*) **75**, 796.
Sugiura, Y. (1927). *J. Phys. Radium* **8**, 113.
Tait, J. H. (1964). *Proc. 3rd Intern. Conf. Phys. Electron. At. Collisions, London*, 1963 p. 586. North-Holland Publ., Amsterdam.
Townsend, J. S. (1903). *Phil. Mag.* [6] **6**, 598.

Trefftz, E., Schulter, A., Dettmar, K. H., and Jorgens, K. (1957). *Z. Astrophys.* **44**, 1.
Trumpy, B. (1931). *Z. Physik* **71**, 720.
Tunstead, J. (1953). *Proc. Phys. Soc.* (*London*) **A66**, 304.
Victoreen, J. A. (1949). *J. Appl. Phys.* **20**, 1141.
Vinti, J. P. (1932). *Phys. Rev.* **42**, 632.
Vinti, J. P. (1933). *Phys. Rev.* **44**, 524.
Wainfan, N., Walker, W. C., and Weissler, G. L. (1955). *Phys. Rev.* **99**, 542.
Watanabe, K. (1964). University of Hawaii (private communication).
Watanabe, K. (1965). *Phys. Rev.* **137**, A1380.
Weissler, G. L. (1962). *J. Quant. Spectry. & Radiative Transfer* **2**, 383.
Weissler, G. L., and Lee, P. (1952). *J. Opt. Soc. Am.* **42**, 200.
Wheeler, J. A. (1933). *Phys. Rev.* **43**, 258.
White, T. N. (1934). *Phys. Rev.* **46**, 865.
Woo, Y. H., and Sun, C. P. (1937–1947). *Natl. Tsing Hua Univ. Sci. Rept.* **A4**, 398.
Wrede, E. (1928). *Z. Instrumentenk.* **48**, 201.